



<https://theses.gla.ac.uk/>

Theses Digitisation:

<https://www.gla.ac.uk/myglasgow/research/enlighten/theses/digitisation/>

This is a digitised version of the original print thesis.

Copyright and moral rights for this work are retained by the author

A copy can be downloaded for personal non-commercial research or study,  
without prior permission or charge

This work cannot be reproduced or quoted extensively from without first  
obtaining permission in writing from the author

The content must not be changed in any way or sold commercially in any  
format or medium without the formal permission of the author

When referring to this work, full bibliographic details including the author,  
title, awarding institution and date of the thesis must be given

Enlighten: Theses

<https://theses.gla.ac.uk/>  
[research-enlighten@glasgow.ac.uk](mailto:research-enlighten@glasgow.ac.uk)

**VIDEO PULSE WIDTH MODULATION FOR OPTICAL FIBER TRANSMISSION.**

**By**

**TAHAR BOUMERFEG**

**A Thesis Presented for the Degree of  
Master of Science in Electronics.**

**Department of Electronics and  
Electrical Engineering,  
University of Glasgow.**

**September 1988.**

ProQuest Number: 10998026

All rights reserved

INFORMATION TO ALL USERS

The quality of this reproduction is dependent upon the quality of the copy submitted.

In the unlikely event that the author did not send a complete manuscript and there are missing pages, these will be noted. Also, if material had to be removed, a note will indicate the deletion.



ProQuest 10998026

Published by ProQuest LLC (2018). Copyright of the Dissertation is held by the Author.

All rights reserved.

This work is protected against unauthorized copying under Title 17, United States Code  
Microform Edition © ProQuest LLC.

ProQuest LLC.  
789 East Eisenhower Parkway  
P.O. Box 1346  
Ann Arbor, MI 48106 – 1346

## ACKNOWLEDGEMENTS

The author wishes to thank Professor J. Lamb, head of the department of Electronics and Electrical Engineering at Glasgow University, for making the facilities available, and Doctor J. Arnold for his supervision of this project and for the valuable help he provided me with during the execution of this project.

The author would like to thank the computing staff, in particular Miss A. Mackinnon, for their help in solving the computing problems.

I give my special thanks to my parents, my wife, my friends and colleagues, and M. Pralong, for their support during the years spent here, in Glasgow.

My thanks are also extended to the Algerian Ministry of Higher Education for their financial support.

## SUMMARY

This thesis describes theoretically the feasibility of two pulse width modulation (PWM) systems for transmission through an optical fiber.

The first part of this work is devoted to the electronics of the two PWM systems. A comparison of the performance of each system is carried out. This comparison takes into account spectra, harmonic distortion, bandwidth requirement, system complexity and output signal to noise ratio (SNR). A comparison of PWM SNR and PCM SNR in the presence of intersymbol interference (ISI) is made.

The second part is devoted to the optical system. The choice of optoelectronic devices, link losses, power budget, signal to noise ratio, and rise time budget are discussed.

## CONTENTS

ACKNOWLEDGEMENTS	i
SUMMARY	ii
CONTENTS	iii
LIST OF ABBREVIATIONS AND SYMBOLS	vii
CHAPTER 1 INTRODUCTION	1
1.1 Optical fiber characteristics	1
1.2 Optical fiber modulation schemes	2
1.3 Previous work	4
CHAPTER 2 PULSE WIDTH MODULATION THEORY	6
2.1 Introduction	6
2.2 PAM signals with instantaneous sampling (IS)	6
2.2.1 Spectrum of PAM signals with IS	7
2.2.2 Demodulation of PAM signals with IS	12
2.3 Pulse Width Modulation	15
2.3.1 PWM with uniform sampling (US)	17
2.3.1.1 Spectrum of PWM signals with US	17
2.3.1.2 Demodulation of PWM signals with US	24
2.3.2 PWM with natural sampling (NS)	28
2.3.2.1 Spectrum of PWM signals with NS	28
2.3.2.2 Demodulation of PWM signals with NS	35
2.3.3 Bandwidth required for PWM transmission	37

2.4	Comparison of PWM and PCM SNRs	38
2.5	Conclusion	40
CHAPTER 3 PWM WITH US SYSTEM PERFORMANCE		41
3.1	Introduction	41
3.2	Bandwidth limitation distortion $D_k$	41
3.2.1	Dependence of $D_k$ on the slicing level	43
3.2.2	Dependence of $D_k$ on the receiver bandwidth	43
3.2.2.1	$D_k$ for a sinusoidal modul. signal	45
3.2.2.2	$D_k$ for a uniformly distributed R.V.	48
3.3	PWM output SNR	50
3.3.1	The output signal average power	50
3.3.2	The output noise average power	52
3.3.3	PWM carrier to noise ratio threshold level	53
3.3.4	PWM SNR improvement factor I for a sinusoidal modulating signal	54
3.3.5	PWM SNR improvement factor I for a uniformly distributed random variable	54
3.4	Bandwidth – modulation index relationship for given $D_k$	55
3.5	PCM SNR in the presence of ISI	58
3.6	Conclusion	64
CHAPTER 4 AN OVERVIEW OF OPTICAL FIBERS		65
4.1	Introduction	65
4.2	Fiber structure	66
4.2.1	Fiber types	66
4.2.2	Snell's law	66

4.3	Fiber dispersion	68
4.3.1	Intramodal dispersion	70
4.3.1.1	Material dispersion	70
4.3.1.2	Material dispersion	70
4.3.2	Intermodal dispersion	72
4.4	Fiber losses	74
4.4.1	Radiative losses	74
4.4.2	Scattering losses	75
4.4.3	Absorption losses	75
4.5	Optical sources	75
4.5.1	Light emitting diodes (LEDs) response time	77
4.5.2	Surface emitter LEDs	77
4.5.3	Edge emitter LEDs	79
4.6	Photodetectors	79
4.6.1	Photodetectors response time	79
4.6.2	Photodetectors quantum efficiency	81
4.6.3	Noises currents	81
4.7	Power coupled from an LED into a fiber	82
4.7.1	Power coupled into a step index fiber	82
4.7.2	Power coupled into a graded index fiber	83
4.7.3	Power lost due to NA	83
CHAPTER 5 THE PWM OPTICAL SYSTEM		85
5.1	Introduction	85
5.2	Choice of the optical system	85
5.2.1	Choice of a light source	85
5.2.2	Choice of a fiber	85
5.2.3	Choice of a photodetector	86
5.3	Schematic of the optical PWM system	86

5.4	Link losses	86
5.5	Power budget	88
5.6	Optical PWM system SNR	90
5.6.1	Signal current ms	90
5.6.2	Total noise current ms	90
5.7	Rise time budget	94
5.8	Conclusion	95
	<b>CONCLUSIONS</b>	<b>96</b>
	<b>LIST OF REFERENCES</b>	<b>99</b>
	<b>APPENDICES</b>	<b>101</b>
A1	Bandwidth requirement	102
A2	RC filter time response to a rectangular pulse	104
A3	One property of a $\delta$ function	106
A4	Some useful FTs	107
A5	Time constant - 3dB bandwidth relationship	109
A6	Signal average power - spectral density relationship	109
A7	Autocorrelation function of a periodic signal	110
A8	Spectral density of sampled noise	111
A9	Program giving PCM SNR in the presence of ISI	112

## LIST OF ABBREVIATIONS AND SYMBOLS

A	Modulating signal peak amplitude
$A_C$	Carrier peak amplitude
APD	Avalanche Photodiode
$\alpha$	Slicing level
$\alpha(\text{opt.})$	Profile parameter
B	Receiver Bandwidth
CNR	Carrier to Noise Ratio
$\gamma$	Receiver bandwidth to sampling rate ratio
$\delta$	Dirac impulse
$\Delta$	Index difference
$f_C$	Low pass filter cut off frequency
$f_m$	Modulating signal frequency
$f_s$	Sampling rate
FT	Fourier Transform
IS	Instantaneous Sampling
ISI	Intersymbol Interference
$\theta_{\parallel}$	Half power beam width in the plane $\parallel$ to the junction
$\theta_{\perp}$	Half power beam width in the plane $\perp$ to the junction
k	Duty cycle
LD	Laser Diode
LED	Light Emitting Diode
ms	Mean square value
M	Modulation index
n	Refractive index
NA	Numerical Aperture
NS	Natural Sampling
$P_e$	Probability of error
PAM	Pulse Amplitude Modulation

<b>PCM</b>	<b>Pulse Code Modulation</b>
<b>PPM</b>	<b>Pulse Position Modulation</b>
<b>PWM</b>	<b>Pulse Width Modulation</b>
<b>rms</b>	<b>Root mean square</b>
<b>S/H</b>	<b>Sample and Hold</b>
<b>SIR</b>	<b>Signal to Interference Ratio</b>
<b>SNR</b>	<b>Signal to Noise Ratio</b>
$\sigma$	<b>Noise rms</b>
<b>T</b>	<b>RC filter time constant</b>
$T_r$	<b>Rise time</b>
$T_s$	<b>Sampling period</b>
$\tau$	<b>Pulse width</b>
<b>US</b>	<b>Uniform Sampling</b>

### 1.1 OPTICAL FIBER CHARACTERISTICS

First of all it seems reasonable to motivate the use of optical fiber over other means of trunk routing of information, which are principally coaxial cables, microwave and satellite broadcasting. A brief examination of each of the previously mentioned means of communication reveals their characteristics.

- Coaxial cables present losses proportional to the square root of the bandwidth used and therefore limit transmission to a few hundred MHz at distances of the order of 1Km.
- Microwave transmission allows higher bandwidths to be used but they are subject to the problem of aerial alignment.
- Satellite communication could be applied to the distribution of wideband services direct from satellite to consumer, but each consumer would require a properly oriented aerial on a line of sight path to the satellite.

Optical fiber presents features that none of the previous systems does. Its advantages include the fact that since the link between source and detector is metal free, containing only glass, earth loop pick up problems can be eliminated. Optical fiber carries electromagnetic energy at optical wavelengths. Since glass is dielectric and since the fiber dimension is much smaller than the wavelength of the electromagnetic waves in the radio and microwave bands, it does not pick up such radiations. It is immune to electromagnetic interference. Furthermore, since the radiation from optical fiber is at optical frequencies it will not provoke interference at radio frequencies.

The fiber is a very wideband transmission medium with a bandwidth potential of several GHz over 1Km and hundreds of MHz over 10Km without intervening electronics. Dispersion values of several tens of ns/Km down to a few ps/Km are possible. The equivalent bandwidths are tens of MHz/Km to tens of GHz/Km. Since

an optical carrier is in the region  $10^{14}$  to  $10^{15}$ Hz, even a bandwidth of 10GHz is a small fractional bandwidth and would cause constant attenuation. Hence, for optical fiber systems, fiber offers constant attenuation for any operating bandwidth, this means that fewer repeaters are to be used and link lengths are longer so that the electronics can be confined to the terminal building only.

The small size of the fiber avoids the handling problems from which copper cables suffer. A 1-Km fiber weights about 50Kg whereas 1Km of copper weights much more.

Assuming an inexpensive modulation scheme can be developed for optical fiber transmission, the advantages of the fiber will overcome the co axial cable's ability to cope with the analogue modulation.

## 1.2 OPTICAL FIBER MODULATION SCHEMES

The modulation schemes that can be used for an optical fiber system are:

- Analogue intensity modulation (IM)
- Analogue pulse modulation (PWM, PPM, PFM)
- Digital modulation (PCM, ASK, FSK, PSK)

Analogue intensity modulation is carried out by making the drive current proportional to the baseband information signal (time varying signal). A requirement for this modulation scheme is that a linear relation should exist between the source input drive current and the output power. This type of modulation is attractive in that the receiver design would be relatively simple except for the fact that the receiver would be very sensitive to power fluctuations in the received signal. This would make the receiver susceptible to noise problems. This and the signal degradation resulting from nonlinearities, which are a consequence of the transient response characteristic of sources (LEDs and LDs), make the implementation of analogue intensity modulation not attractive.

PCM has no serious competitor, but coding and decoding techniques are not easily achieved and raise serious financial questions. Furthermore, the transmission bandwidth required in an 8-bit digital transmission, assuming that the modulating signal is sampled at the minimum Nyquist sampling rate, is  $8 \times 2 \times f_m$ . In T.V. transmission systems, for example, the sampling rate must be an exact multiple of the colour subcarrier (4.43MHz) in order to avoid the sampling rate beating with the colour subcarrier which results in a degradation of the reconstructed picture. For a composite signal bandwidth of 5.5MHz including sound, only frequencies in the series 13.34MHz ( $4.43 \times 3$ ), 17.7MHz ( $4.43 \times 4$ ), 22.2MHz ( $4.43 \times 5$ ) etc...must be used as the sampling rate. In the interest of minimum bandwidth, the sampling rate is chosen to be the colour subcarrier third harmonic, that is  $3 \times 4.43$ MHz. This means that the bit rate should be  $8 \times 3 \times 4.43$ bit/s which requires at least a bandwidth of 100MHz, making the constraint on the receiver more severe.

This leaves analogue pulse modulation such as PWM, PPM and PFM. PPM and PWM types of modulation are of considerable interest in optical communication systems, since it is relatively easy to modulate semiconductor sources by switching the drive current between high and low levels. Besides, analogue pulse modulation methods do not incur the electronic complexity of digital PCM, and modulation and demodulation are achieved with relatively simple electronics. One of the serious drawbacks of the analogue technique, whether PWM or PFM, is that it does not allow noise free regeneration of signals in case where repeaters are required.

For PWM the modulation displays a linear voltage to pulse width translation, for PFM a pulse repetition translation and for PPM a pulse position translation. Intensity modulation (IM) with direct detection conveys the pulse train on the optical carrier to the receiver. The performance of an analogue receiver is measured in terms of the output SNR. If we define the SNR improvement factor  $I$  as the difference (in dB) between the SNR and the CNR, ref.13 shows that PFM displays the greatest  $I$ , namely 19.2dB, whereas PPM and PWM display 4.2 and 1.6dB

respectively. The 3dB difference between PPM and PWM I is a consequence of the necessity to detect both edges of PWM pulses. The SNR, however, is not the only consideration in choosing one or other scheme. Accepting that multi-channel transmission is a necessary feature, the question of multiplexing must be examined. Leaving aside the possibility of optical wavelength multiplexing, two electrical domains remain, frequency and time multiplexing. PFM requires that individual channels must be first multiplexed in the frequency domain then presented to the modulator as a single baseband signal. Such an operation places a high demand on pulse repetition frequencies and modulation indices. PPM and PWM produce regularly periodic pulse trains and so lend themselves to multiplexing in the time domain. PPM modulation being synchronous, however, requires a clocked stage to generate the clock timing to serve as reference for demodulation. In contrast PWM is self clocking, that is the clock timing is directly present in the modulated signal.

### 1.3 PREVIOUS WORK

A colour T.V. broadcast system using PWM with uniform sampling over 1Km of multimode graded index fiber has been experimentally demonstrated by ref.14. This system used a combination of a surface emitter LED at the optical transmitter and a PIN photodiode at the receiver. SNRs of 40 to 50dB have been achieved for modulation indices in the range  $0.1 < M < 0.5$ . The overall rise time achieved was 15ns which limited M to 0.6. It was concluded that PWM is indeed an attractive and viable technique of modulation for low cost and acceptable quality of video transmission. However, the theoretical analysis of the system has been neglected, and this project aims to investigate the feasibility of two PWM systems for optical fiber transmission. Throughout this investigation, all the calculations will be carried out with respect to video transmission specifications. For video systems a convenient sampling rate is  $3 \times 4.43\text{MHz}$  i.e. 13.34MHz which gives a usable time slot of about 75ns. If the circuitry used allows rise and fall times of 12ns each, which correspond to a transmission bandwidth  $B = 40\text{MHz}$ , the usable time slot would be only 51ns which allows a modulation index  $M = 0.67$  to be used. Therefore, faster

components are required to permit higher M to be used. The advantage of having a large M is an increase in the output SNR.

Ref.14 quotes the signal to interference ratio (SIR) as being 36dB at the end of the video receiver chain, and this must be seen as the difference between the signal fundamental power and the highest interference component power in the video band.

## 2.1 INTRODUCTION

In this chapter we will review the theory of pulse width modulation (PWM). Techniques of modulation and demodulation, spectra and transmission bandwidth required will be discussed. As we will see later on, PWM with uniform sampling (US) is generated when the modulating signal is first converted to a sample and hold (S/H) signal, which is a PAM signal with instantaneous sampling (IS) and with duty cycle  $k \approx 1$ . Therefore, it is instructive to review first the theory of PAM with IS.

## 2.2 PAM SIGNALS WITH INSTANTANEOUS SAMPLING

To convert analogue band limited data to a sampled form we should first sample it at least at Nyquist sampling rate. The latter is the frequency at which an analogue signal should be sampled in order that the recovery of the modulating signal will be possible. The minimum Nyquist sampling rate is twice the highest frequency component in the input signal. The sampled values of the analogue signal carry the original intelligence. A system transmitting these sampled values is called a PAM system. To achieve this modulation, a switching function representing the unmodulated pulse carrier is needed. The period of this carrier is called the time slot or sampling interval, its frequency is called the sampling rate and the time at which a sample is taken is called the sampling instant.

There are two types of PAM signals: PAM with instantaneous sampling (IS) and PAM with natural sampling (NS). In the former the sampling instant is not small compared to the time slot, and the sample consists of a narrow section of the modulating signal. In the latter the sampling instant is very small (approaching 0) and the sample represents exactly the value of the modulating signal at the sampling instant. This kind of sampling is, very often, called ideal sampling. A simplified block diagram of a PAM system with IS is given in Fig.2.1.

An impulse train  $c_\delta(t)$  and the modulating signal  $s(t)$  are multiplied in an ideal multiplier, yielding  $x_\delta(t)$ . These impulses are then filtered by a holding filter whose impulse response is the basic pulse  $p(t)$ , to yield an output pulse train  $x(t)$  with equally spaced pulses of identical shape but varying amplitudes. Fig.2.2 gives a plot of the waveforms of interest. For S/H signals the holding period  $\tau$  is almost equal to the time slot  $T_S$ , therefore,

$$k = \tau/T_S \approx 1 \quad (2.1)$$

$P(f)$  serves to hold the values of the instantaneous samples  $s(kT_S)$  for a period determined by the duration of the basic pulse  $p(t)$  i.e  $\tau$ . The multiplier with an impulse train is regarded as a device that samples the signal at the sampling points  $kT_S$ . With reference to Fig.2.1, the multiplier output is,

$$x_\delta(t) = s(t)c_\delta(t) = s(t)\sum_{-\infty}^{+\infty} \delta(t-kT_S) \quad (2.2)$$

The holding filter output, taking into account a proportionality constant  $M$  (modulation index) due to the circuitry used, is

$$\begin{aligned} x(t) &= M p(t)*x_\delta(t) = M \int_{-\infty}^{+\infty} p(t)x_\delta(t-t')dt' \\ &= M \sum_{-\infty}^{+\infty} \int_{-\infty}^{+\infty} p(t')s(t-t')\delta(t-t'-kT_S)dt' \\ &= M \sum_{-\infty}^{+\infty} s(kT_S)p(t-kT_S) \end{aligned} \quad (2.3)$$

Eq.(2.3) is the equation representing PAM signals with IS.

### 2.2.1 Spectra of PAM signals with IS

We assume a cosinusoidal modulating signal given by,

$$s(t) = A \cos(2\pi f_m t) \quad (2.4)$$

and a rectangular pulse  $p(t)$  of width  $\tau$  and amplitude  $p(0) = 1$ . Eq.(2.3) becomes,

$$x(t) = M p(t)*[s(t)c_\delta(t)] \quad (2.5)$$

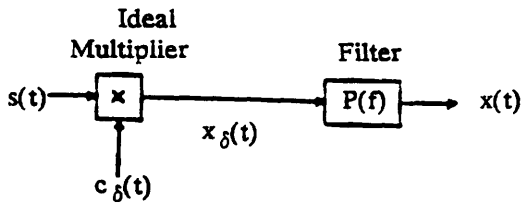


Fig.2.1 Block Diagram Of A PAM System With Instantaneous Sampling.

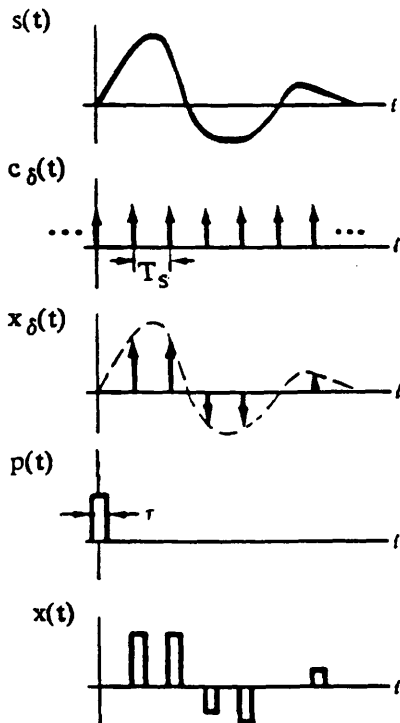


Fig.2.2 PAM Signal With Instantaneous Sampling.

The FT of eq.(2.5), making use of eqs.(A4.5) and (A4.6), is

$$X(f) = (M/T_S) \sum_{-\infty}^{+\infty} P(f)S(f-nf_S) \quad (2.6)$$

We know that the FT of a cosinusoidal signal is,

$$S(f) = (A/2) [\delta(f+f_m) + \delta(f-f_m)] \quad (2.7)$$

Sustituting eq.(2.7) into eq.(2.6) we get,

$$\begin{aligned} X(f) &= (MA/2T_S) \sum_{-\infty}^{+\infty} P(f) [\delta(f-nf_S-f_m) + \delta(f-nf_S+f_m)] \\ &= (MA/2T_S) \sum_{-\infty}^{+\infty} P(nf_S+f_m) \delta(f-nf_S-f_m) + \\ &\quad (MA/2T_S) \sum_{-\infty}^{+\infty} P(nf_S-f_m) \delta(f-nf_S+f_m) \end{aligned} \quad (2.8)$$

Upon making an index change in the  $\delta$  functions and summing up the appropriate terms, eq.(2.8) becomes,

$$\begin{aligned} X(f) &= (MA/2T_S) \sum_{-\infty}^{-1} P(nf_S+f_m) [\delta(f-f_m-nf_S) + \delta(f+f_m+nf_S)] + \\ &\quad (MA/2T_S) \sum_1^{+\infty} P(nf_S+f_m) [\delta(f-f_m-nf_S) + \delta(f+f_m+nf_S)] + \\ &\quad (MA/2T_S) P(f_m) [\delta(f-f_m) + \delta(f+f_m)] \\ &= (MA/2T_S) \sum_{-\infty}^{+\infty} P(nf_S+f_m) [\delta(f-f_m-nf_S) + \delta(f+f_m+nf_S)] \end{aligned} \quad (2.9)$$

Taking the inverse FT of eq.(2.9) we get,

$$\begin{aligned} x(t) &= (MA/T_S) \sum_{-\infty}^{+\infty} P(nf_S+f_m) \cos 2\pi(f_m+nf_S)t \\ &= MAk \sum_{-\infty}^{+\infty} \frac{\text{sinc} \pi(f_m/f_S+n)}{k\pi(f_m/f_S+n)} \cos 2\pi(f_m+nf_S)t \end{aligned} \quad (2.10)$$

Where  $k$  is the duty cycle given by eq.(2.1). Let,

$$S_n = MA \frac{\sin \pi(f_m/f_S+n)}{\pi(f_m/f_S+n)} \quad (2.11)$$

The signal fundamental is obtained by substituting  $n = 0$  into eq.(2.11),

$$S_0 = MA \frac{\sin(\pi f_m/f_s)}{\pi f_m/f_s}$$

The clock fundamental first sidetones are obtained by substituting  $n = \pm 1$  into eq.(2.11),

$$S_1 = MA \frac{\sin\pi(f_m/f_s+1)}{\pi(f_m/f_s+1)}$$

$$S_{-1} = MA \frac{\sin\pi(f_m/f_s-1)}{\pi(f_m/f_s-1)}$$

These components are computed for various  $M$  for a modulating signal input frequency  $f_m = 2\text{MHz}$  and a sampling rate  $f_s = 13.34\text{MHz}$ . The relative powers of these components have to be calculated against a reference level. A suitable level is the amplitude of the signal fundamental with  $M = 1$ .

$$\begin{aligned} P_{\text{rel}}(\text{dB}) &= 10 \log\left[\frac{S_n}{S_0(M=1)}\right]^2 \\ &= 20 \log(S_n) + 0.32\text{dB} \end{aligned} \quad (2.12)$$

The components' relative powers are given in Tab.2.1 and sketched in Fig.2.3.

$M$	0.1	0.25	0.5
$S_0$ (dB)	-20.0	-12.0	-6.0
$S_1$ (dB)	-37.7	-29.7	-23.7
$S_{-1}$ (dB)	-35.1	-27.1	-21.1

**Tab.2.1 Relative powers of the spectrum components of a PAM signal with IS for  $k = 1$ .**

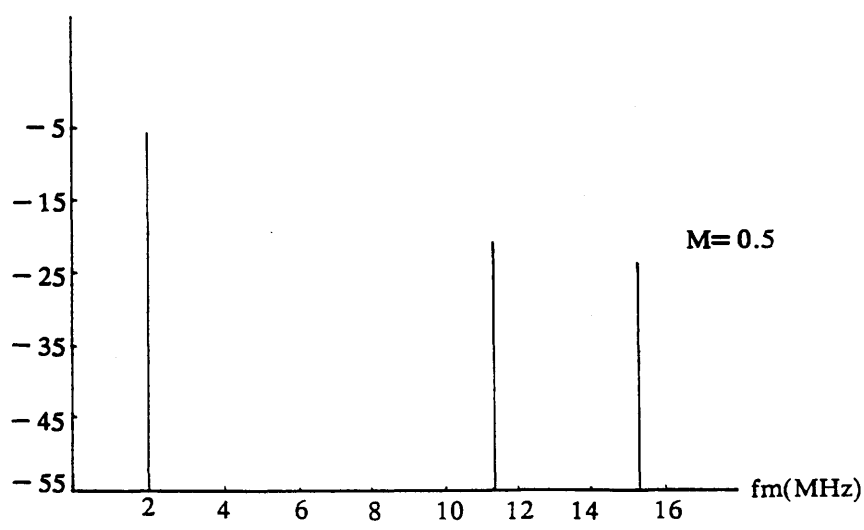
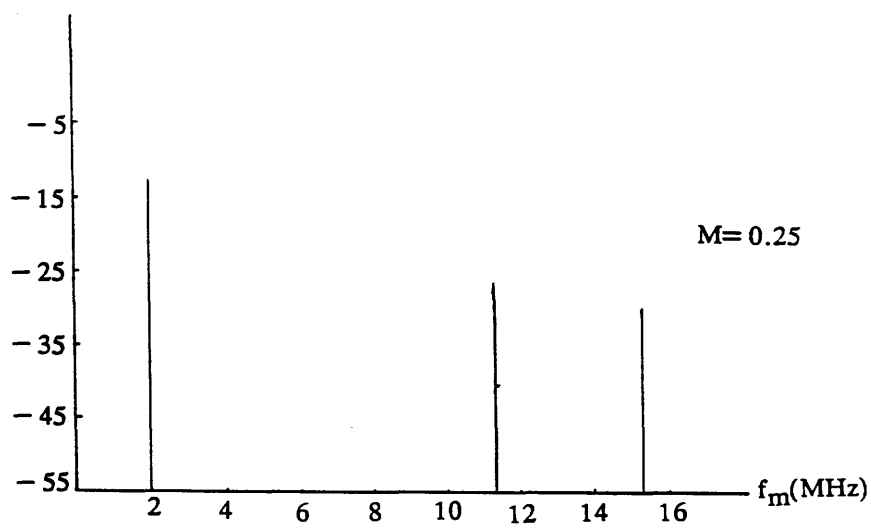
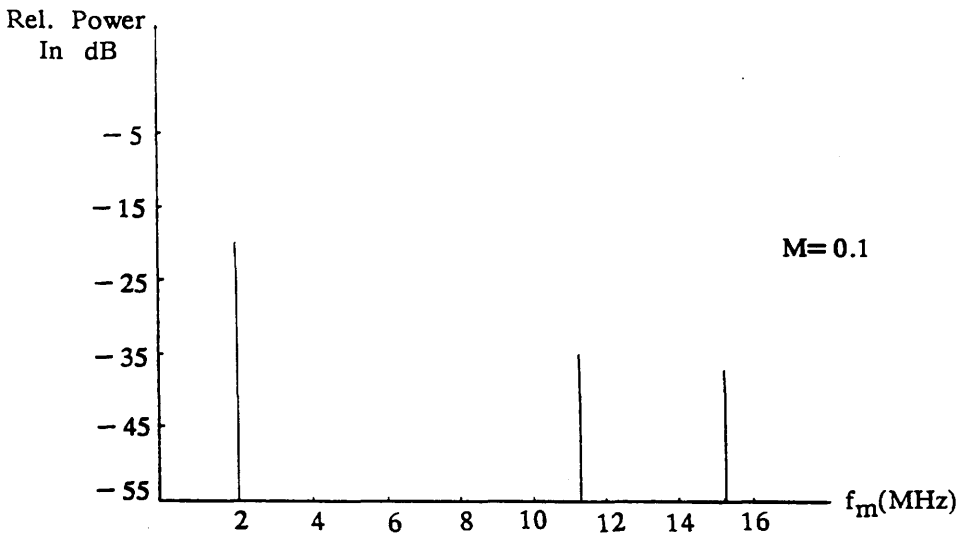


Fig.2.3 Spectra Of A PAM Signal With Instantaneous Sampling.

## 2.2.2 Demodulation of PAM signals with IS

The sidebands of the spectrum of a PAM signal with IS have different shapes i.e they are distorted. As a result low pass filtering alone is not sufficient. To recover the original modulating signal  $s(t)$  from its sample values without distortion, the incoming PAM signal must be itself instantaneously sampled and the resulting signal passed through the ideal low pass filter of eq.(2.13), namely

$$H(f) = \begin{cases} T_s & |f| \leq f_s/2 \\ 0 & |f| > f_s/2 \end{cases} \quad (2.13)$$

The block diagram of such a demodulator is given in Fig.2.4. With reference to this figure, the multiplier (sampler) output is,

$$\begin{aligned} y_\delta(t) &= x(t) \sum_{-\infty}^{+\infty} \delta(t-kT_s) = \sum_{-\infty}^{+\infty} x(kT_s) \delta(t-kT_s) \\ &= M \sum_{-\infty}^{+\infty} s(kT_s) p(t-kT_s) \delta(t-kT_s) \\ &= Mp(0) \sum_{-\infty}^{+\infty} s(kT_s) \delta(t-kT_s) \end{aligned} \quad (2.14)$$

The FT of the filter output is,

$$\begin{aligned} Y(f) &= H(f)Y_\delta(f) = (Mp(0)/T_s) H(f) \sum_{-\infty}^{+\infty} S(f-kf_s) \\ &= Mp(0) S(f) \end{aligned} \quad (2.15)$$

Eq.(2.15) shows that the filter output is the original modulating signal multiplied by a constant that can be eliminated through the amplification process. If the receiver is simply a low pass filter acting on the incoming PAM signals without subjecting them first to IS, the output signal will be,

$$y(t) = p(t)*s(t) \quad (2.16)$$

which is the modulating signal convolved with the basic pulse  $p(t)$ . If  $p(t)$  is rectangular and its width  $\tau$  is made smaller, with reference to eq.(A4.6), the  $P(f)$  first zero crossing moves to higher frequencies and  $P(f)$  tends to be more flat within the signal fundamental sidebands, see Fig.2.5. Ref.4 quotes that as long as,

$$\tau \leq 0.1 \times T_s \quad \text{i.e.} \quad 1/\tau \geq 10 \times f_s \quad (2.17)$$

demodulation can be achieved by using merely a low pass filter, otherwise IS or

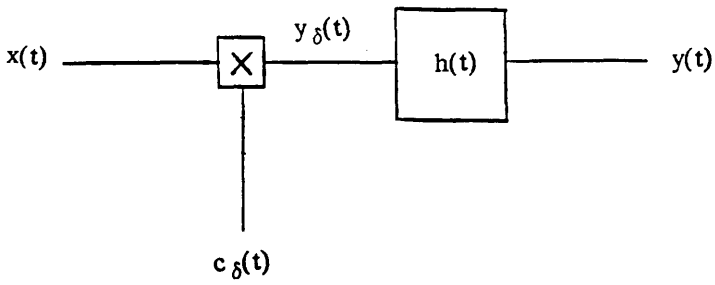


**Fig.2.4 Block Diagram Of PAM Signals With Instantaneous Sampling Demodulator.**

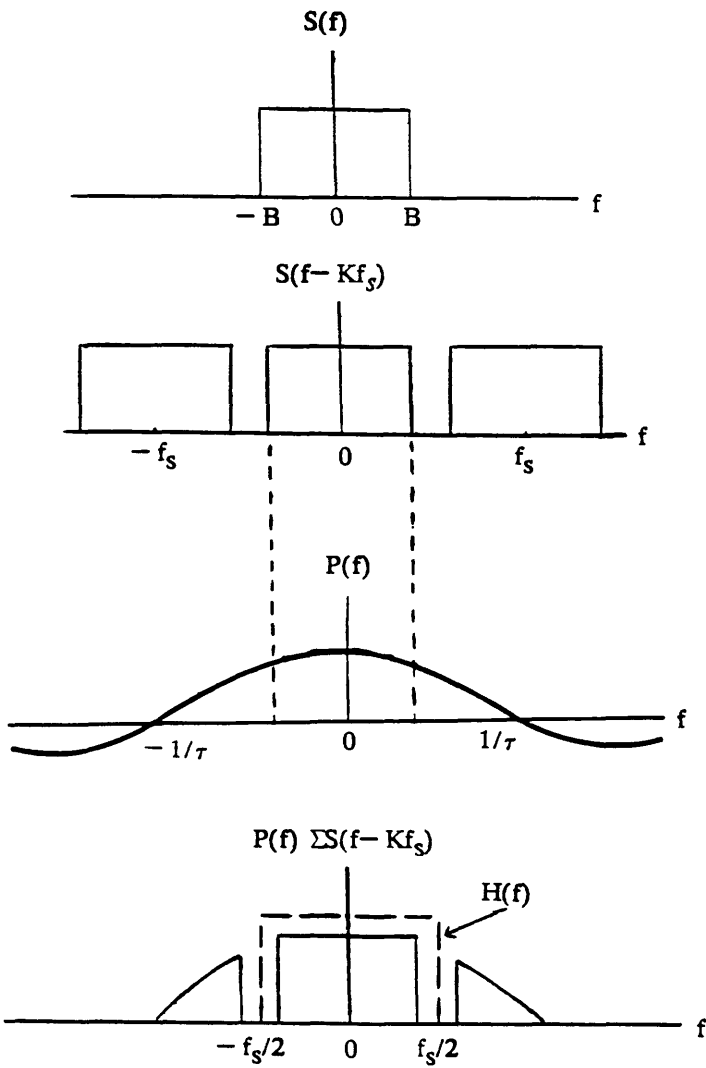


**Fig.2.5 Demodulating A PAM Signal Using Simply A Low pass Filter.**

equalisation and low pass filtering are required for demodulation.

In the case of a S/H signal the holding period is almost equal to the time slot, therefore, equalisation is required if only a low pass filter is used for demodulation.

The transfer function of the equalising filter is the inverse of  $P(f)$  namely,

$$Q(f) = 1/P(f) \quad (2.18)$$

Fig.2.3 shows that, if a low pass filter is to be used for demodulation, even if  $f_m$  increases to 5.5MHz the only component that falls within the filter passband is the signal fundamental.

## 2.3 PULSE WIDTH MODULATION

PWM is generated when the analogue modulating signal is sampled and the variations in amplitude of these samples cause a variation in width of the carrier pulses which are transmitted at constant rate. There are three types of PWM signals:

- PWM with trailing edge modulation: where the position of the leading edge is fixed and the trailing edge modulated.
- PWM with leading edge modulation: where the position of the trailing edge is fixed and the leading edge modulated.
- PWM with leading and trailing edge modulation: where both edges are modulated.

Generation of PWM commonly employs various combinations of a S/H circuit, a precision ramp generator and a comparator. As in many other forms of pulse modulation, the analogue signal must be sampled at regular intervals to obtain samples to assign to each pulse. To derive the mathematical equations representing PWM signals we assume a trailing edge modulation with non zero rise time pulses ( $a \neq 0$ ). Fig.2.6 gives the graphical derivation of a PWM pulse with trailing edge modulation.

To avoid the overlapping between the different edges, the modulation  $s_k$  must satisfy the following condition,

$$|s_k|_{\max} \leq T_s/2 - a \quad (2.19)$$

where  $a$  is the pulse rise time.

A PWM signal with trailing edge modulation can be represented by,

$$l(t) = \sum_{-\infty}^{+\infty} q(s_k, t - kT_s) \quad (2.20)$$

If uniform sampling is used, then

$$s_k = s(kT_s) \quad (2.21)$$

If natural sampling is used, then

$$s_k = s(t_k) \quad (2.22)$$

where,

$$t_k = kT_s + s(t_k) \quad (2.23)$$

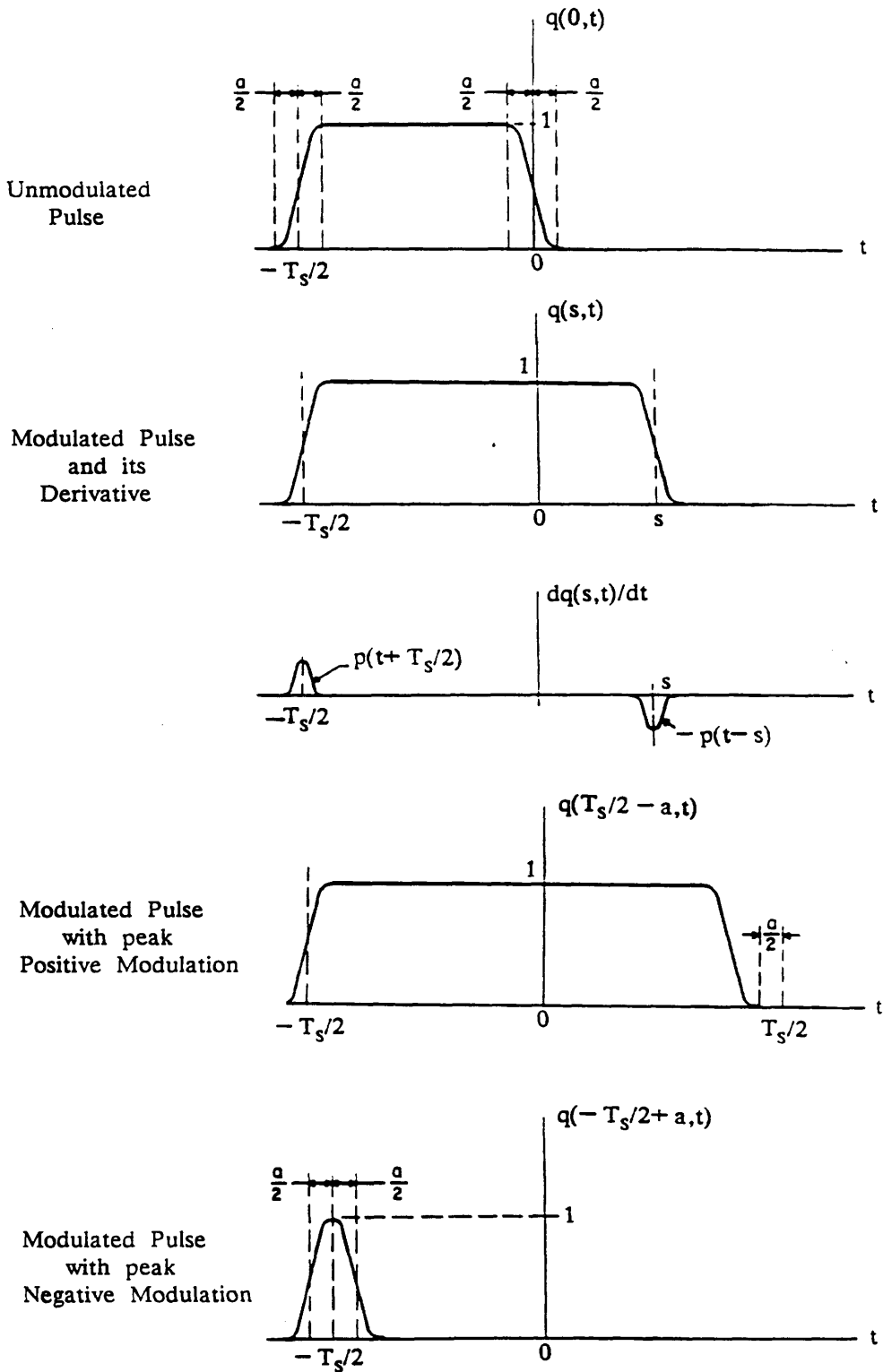


Fig.2.6 A PWM Pulse with Trailing Edge Modulation.

From Fig.2.6 we have the following equation,

$$dq(s, t)/dt = p(t+T_s/2) - p(t-s) \quad (2.24)$$

For an infinity of pulses eq.(2.24) becomes,

$$\begin{aligned} \sum_{-\infty}^{+\infty} dq(s_k, t-kT_s)/dt &= \sum_{-\infty}^{+\infty} p(t-kT_s+T_s/2) - \sum_{-\infty}^{+\infty} p(t-kT_s-s_k) \\ &= dl(t)/dt \end{aligned} \quad (2.25)$$

If pulses with zero rise times are used, instead of obtaining pulses  $p(t)$  we obtain impulses and eq.(2.25) becomes,

$$\begin{aligned} dl(t)/dt &= \sum_{-\infty}^{+\infty} \delta(t-kT_s+T_s/2) - \sum_{-\infty}^{+\infty} \delta(t-kT_s-s_k) \\ &= c_\delta(t+T_s/2) - x_\delta(t) \end{aligned} \quad (2.26)$$

For PWM there are two types of sampling: uniform and natural.

### 2.3.1 PWM with uniform sampling

In PWM with uniform sampling (US), a S/H circuit is used. The input signal is sampled and held at the sampling rate before being compared to the ramp voltage. Thus, the ramp voltage is compared to the value of the input modulating signal at uniform sampling instants. The block diagram of a popular PWM system with US is given in Fig.2.7(a). Fig.2.7(b) shows the generation of a PWM signal with US and with trailing edge modulation. Details on how this system works will be given in paragraph 2.3.2. The resulting PWM signal is a train of pulses whose trailing edges are governed by the sample values of the input signal.

#### 2.3.1.1 Spectrum of PWM signals with US

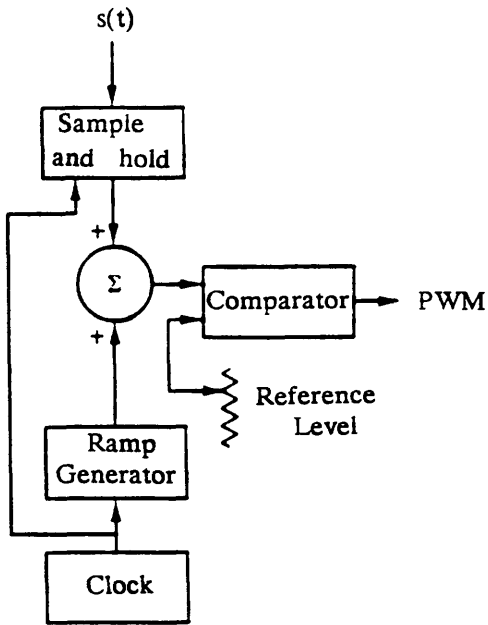
To compute the spectrum of PWM signals with US we assume a cosinusoidal modulating signal, ideal pulses with zero rise times and a trailing edge modulation.

$$s(t) = A \cos(2\pi f_m t) \quad (2.27)$$

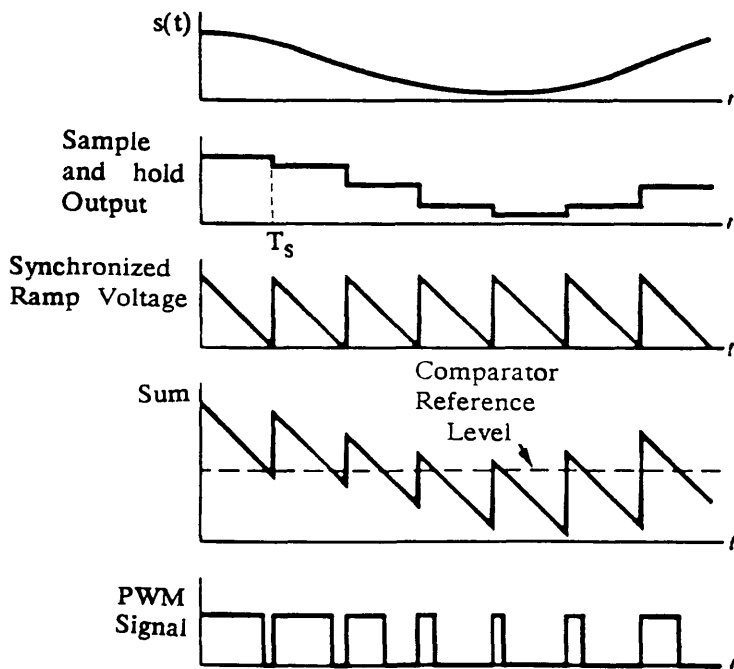
where the amplitude  $A$  must satisfy the condition given by eq.(2.19) namely,

$$A < T_s/2 \quad \text{i.e.} \quad M < 1 \quad (2.28)$$

where  $M$  is the modulation index which will be defined later on.



(a)



(b)

**Fig.2.7 (a) A Uniformly Sampled PWM System And (b) The Waveforms Of Interest.**

Eq.(A4.5) gives the expansion of  $c_\delta(t)$  into Fourier series,

$$c_\delta(t) = (1/T_S) \sum_{-\infty}^{+\infty} e^{2\pi j n f_S t} \quad (2.29)$$

Therefore,

$$c_\delta(t+T_S/2) = (1/T_S) \sum_{-\infty}^{+\infty} (-1)^n e^{2\pi j n f_S t} \quad (2.30)$$

Substituting eqs.(2.21) and (2.27) into  $x_\delta(t)$  we get,

$$x_\delta(t) = \sum_{-\infty}^{+\infty} \delta[ t - kT_S - A \cos(2\pi f_m k T_S) ] \quad (2.31)$$

To determine the spectrum of  $x_\delta(t)$ , we should make use of Bennett's double Fourier series which has been applied by him to determine the spectra of PWM and PPM signals. The details of this method are very well developed in ref.5.

A periodic function  $g(y,z)$  of two independent variables  $y$  and  $z$  has to be found for  $x_\delta(t)$  is periodic in two variables  $f_s$  and  $f_m$ . Let,

$$y = f_s t \quad (2.32)$$

$$z = f_m t \quad (2.33)$$

Then,

$$x_\delta(t) = g(f_s t, f_m t) = g(y, z) = \sum_{-\infty}^{+\infty} \delta[ t - kT_S - A \cos(2\pi f_m k T_S) ] \quad (2.34)$$

The function  $g(y,z)$  can be expanded in a double Fourier series,

$$x_\delta(t) = g(y, z) = \sum_{-\infty}^{+\infty} g_{mn} e^{2\pi j (my+nz)} \quad (2.35)$$

where the Fourier coefficient  $g_{mn}$  are given by,

$$g_{mn} = \int_0^1 \int_0^1 g(y, z) e^{-2\pi j (my+nz)} dy dz \quad (2.36)$$

The coefficients  $g_{mn}$  have been found in ref.5, and are given by,

$$g_{mn} = [ (-j)^n / T_S ] J_n [ 2\pi A (m f_s + n f_m) ] \quad (2.37)$$

where  $J_n$  is the Bessel function of the first kind of order  $n$  given by,

$$J_n(\beta) = (1/2\pi) \int_{-\pi}^{+\pi} e^{j(\beta \sin u - nu)} du$$

$$= [(-j)^{-n/2\pi}] \int_{-\pi}^{+\pi} e^{j(\beta \cos u - nu)} du \quad (2.38)$$

Substituting eq.(2.37) into eq.(2.35) we get,

$$x_\delta(t) = (1/T_S) \sum_{-\infty}^{+\infty} (-j)^n J_n[2\pi A(mf_S + nf_m)] e^{2\pi j(mf_S + nf_m)t} \quad (2.39)$$

Substituting eqs.(2.30) and (2.39) into eq.(2.26) we get,

$$dI(t)/dt = (1/T_S) \left[ \sum_{-\infty}^{+\infty} (-1)^n e^{2\pi jnf_S t} - \sum_{-\infty}^{+\infty} (-j)^n J_n[2\pi A(mf_S + nf_m)] e^{2\pi j(mf_S + nf_m)t} \right] \quad (2.40)$$

The term corresponding to  $n = 0$  of the first summation is equal to the term of the second summation corresponding to  $m = n = 0$ , therefore they can be subtracted. After integration we get,

$$I(t) = - (1/T_S) \sum_{\substack{+\infty \\ |m|+|n| \neq 0}} J_n[2\pi A(mf_S + nf_m)] \frac{e^{2\pi j(mf_S + nf_m)t}}{2\pi j(mf_S + nf_m)} + (1/T_S) \sum_{\substack{+\infty \\ n \neq 0}} (-1)^n \frac{e^{2\pi jnf_S t}}{2\pi jnf_S} + C \quad (2.41)$$

where  $C$  is an integration constant.

The modulating signal amplitude  $A$  is made proportional to  $T_S/2$ , the constant of proportionality is the modulation index  $M$  which is the ratio of the peak to peak amplitude of the modulating signal to the amplitude of the ramp generator output.

$$A = MT_S/2 \quad (2.42)$$

Substituting eq.(2.42) into eq.(2.41) and expanding the latter we get,

$$I(t) = \sum_{\substack{+\infty \\ n \neq 0}} (-1)^n \frac{e^{2\pi jnf_S t}}{2\pi jn} - \sum_{\substack{+\infty \\ m \neq 0}} \frac{J_0(\pi m M)}{2\pi jm} e^{2\pi jmf_S t} - \sum_{\substack{+\infty \\ m, n \neq 0}} (-j)^n \frac{J_n[\pi MT_S(mf_S + nf_m)]}{2\pi jT_S(mf_S + nf_m)} e^{2\pi j(mf_S + nf_m)t} + C = \sum_{\substack{+\infty \\ n \neq 0}} \frac{(-1)^{n-J_0(\pi n M)}}{2\pi jn} e^{2\pi jnf_S t} -$$

$$\sum_{\substack{n=-\infty \\ m, n \neq 0}}^{+\infty} (-j)^n \frac{J_n[\pi M(m+nf_m/f_s)]}{2\pi j(m+nf_m/f_s)} e^{2\pi j(mf_s+nf_m)t} + C \quad (2.43)$$

Let,

$$C_n = \frac{(-1)^n J_0(n\pi M)}{n\pi} \quad (2.44)$$

and,

$$S_{m,n} = \frac{J_n[\pi M(m+nf_m/f_s)]}{\pi(m+nf_m/f_s)} \quad (2.45)$$

The clock fundamental is,

$$C_1 = \frac{1+J_0(\pi M)}{\pi}$$

The signal fundamental is,

$$S_{0,1} = \frac{J_1(\pi M f_m/f_s)}{\pi f_m/f_s}$$

The signal second harmonic is,

$$S_{0,2} = \frac{J_2(2\pi M f_m/f_s)}{2\pi f_m/f_s}$$

The signal third harmonic is,

$$S_{0,3} = \frac{J_3(3\pi M f_m/f_s)}{3\pi f_m/f_s}$$

The clock fundamental first sidetones are,

$$S_{1,1} = \frac{J_1[\pi M(1+f_m/f_s)]}{\pi(1+f_m/f_s)}$$

$$S_{1,-1} = \frac{J_{-1}[\pi M(1-f_m/f_s)]}{\pi(1-f_m/f_s)}$$

The clock fundamental second sidetones are,

$$S_{1,2} = \frac{J_2[\pi M(1+2f_m/f_s)]}{\pi(1+2f_m/f_s)}$$

$$S_{1,-2} = \frac{J_{-2}[\pi M(1-2f_m/f_s)]}{\pi(1-2f_m/f_s)}$$

The clock fundamental third sidetones are,

$$S_{1,3} = \frac{J_3[\pi M(1+3f_m/f_s)]}{\pi(1+3f_m/f_s)}$$

$$S_{1,-3} = \frac{J_{-3}[\pi M(1-3f_m/f_s)]}{\pi(1-3f_m/f_s)}$$

These components are computed for a modulating signal input frequency

$f_m = 2\text{MHz}$  and a sampling rate  $f_s = 13.34\text{MHz}$  for various  $M$ . The computation is done against a reference level which is the amplitude of the signal fundamental with  $M = 1$ . The relative powers of the components are calculated through eq.(2.46) namely,

$$P_{rel} = 10 \log\left[\frac{\text{component's amplitude}^2}{S_0(M=1)}\right]$$

$$= 20 \log(\text{component's amplitude}) + 6\text{dB} \quad (2.46)$$

The results are given in Tab.2.2 and a plot of these components is given in Fig.2.8.

M	0.1	0.25	0.5
C <sub>1</sub>	2.0	1.4	-0.6
S <sub>0,1</sub>	-20.0	-12.0	-6.0
S <sub>0,2</sub>	-53.3	-36	-25.1
S <sub>0,3</sub>	-81.3	-57.8	-40.1
S <sub>1,1</sub>	-20.1	-13.0	-9.8
S <sub>1,-1</sub>	-20.1	-12.5	-8.1
S <sub>1,2</sub>	-39.7	-24.7	-15.0
S <sub>1,-2</sub>	-45.3	-30.8	-18.0
S <sub>1,3</sub>	-62.0	-38.3	-22.2
S <sub>1,-3</sub>	-77.3	-54.0	-36.2

Tab.2.2 The relative powers of the spectrum of a PWM signal with US.

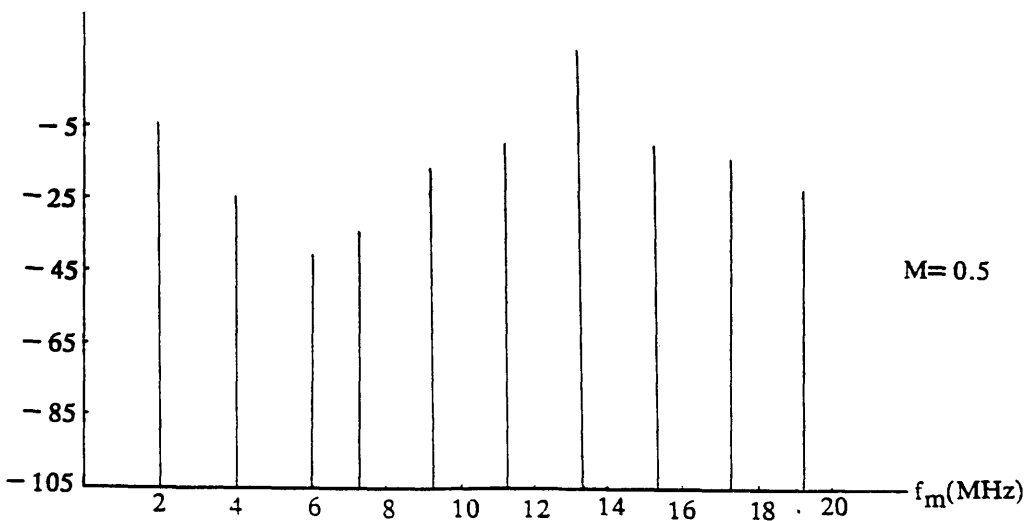
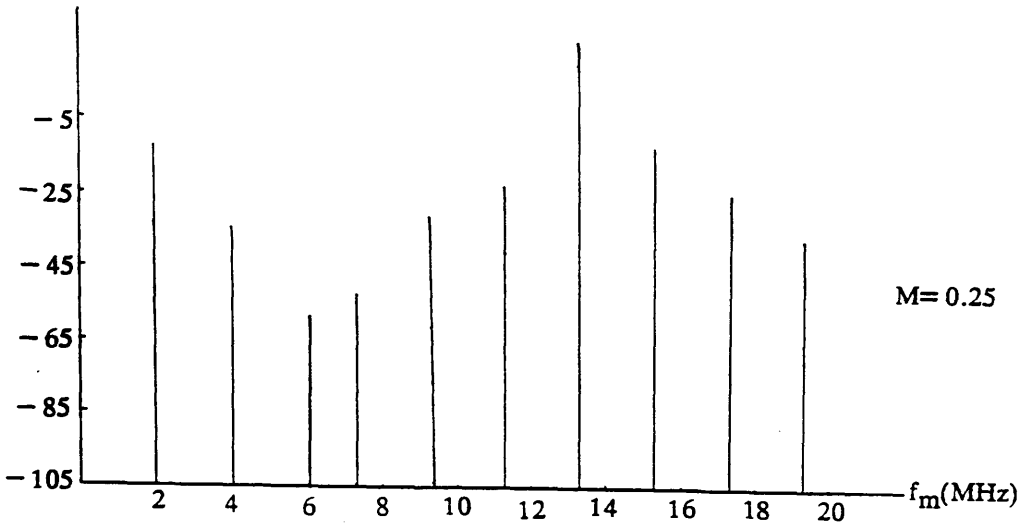
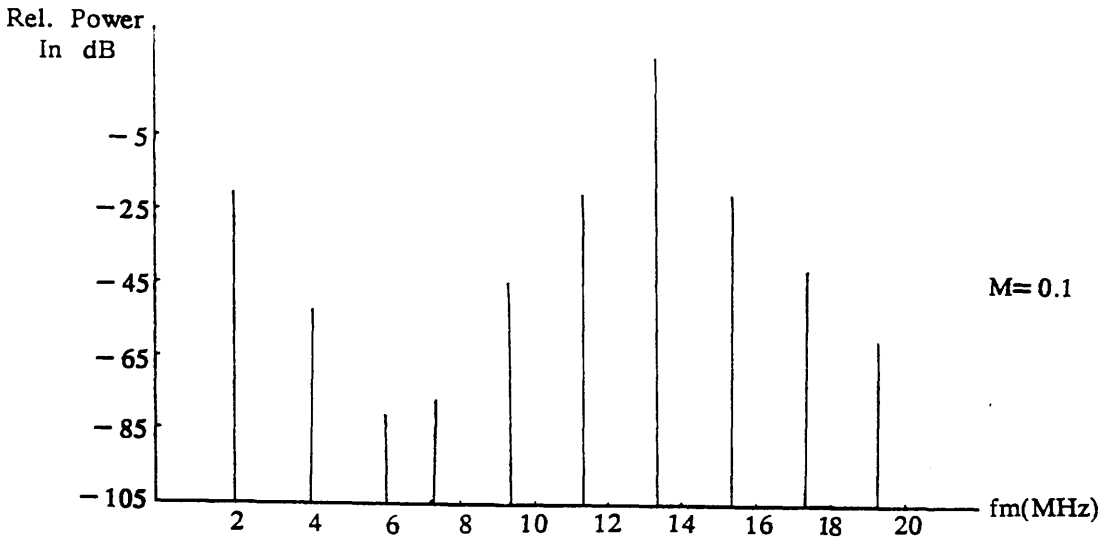


Fig.2.8 Spectra Of A PWM signal With Uniform Sampling.

### 2.3.1.2 Demodulation of PWM signals with US

The PWM demodulator comprises a non linear device called a slicer. The latter removes as much noise as possible from the incoming PWM signals. The slicer output pulses are rectangular and can be represented by,

$$l(t) = \sum_{-\infty}^{+\infty} q(s_k, t - kT_s) \quad (2.47)$$

Next, the slicer output is integrated by a device giving the area of each pulse. This can be achieved by passing a current proportional to the PWM pulses width into a capacitor that is discharged at the beginning of each pulse. The output of the integrator is sampled at a uniform rate to yield a S/H signal (PAM signal with IS and  $k \approx 1$ ), this detector is called a S/H detector. Finally, the original modulating signal may be recovered without distortion as indicated in paragraph 2.4.

The block diagram of such a detector is given in Fig.2.9. The pulses arriving at the input port of the detector are distorted and noise is superimposed upon them. The slicer output consists of rectangular pulses whose widths are different from the actual widths, an illustration being given in Fig.2.10.

The integrator output is,

$$v(t) = g(t) * l(t) = \int_{-\infty}^{+\infty} g(t') l(t-t') dt' \quad (2.48)$$

The integrator can be seen as a linear filter whose impulse response is,

$$g(t) = \begin{cases} 1 & |t| \leq T_s/2 \\ 0 & |t| > T_s/2 \end{cases} \quad (2.49)$$

In practice, we must sample and hold the signal issued from the integrator and then subject it to IS, but in theory the overall effect is as if the integrator output has been only instantaneously sampled. The sampler output is therefore,

$$u_\delta(t) = v(t) \sum_{-\infty}^{+\infty} \delta(t - kT_s) = \sum_{-\infty}^{+\infty} v(kT_s) \delta(t - kT_s) \quad (2.50)$$

For the  $k^{\text{th}}$  pulse, and making use of eq.(2.48),  $v(kT_s)$  is,

$$v(kT_s) = \int_{(k-1/2)T_s + d_k}^{s_k + kT_s - d_k} g(t') l(kT_s - t') dt'$$

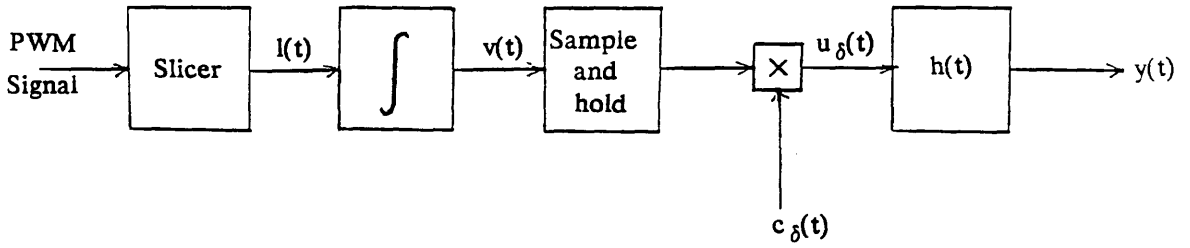


**Fig.2.9 Block Diagram Of Uniformly Sampled PWM Signals Demodulator.**

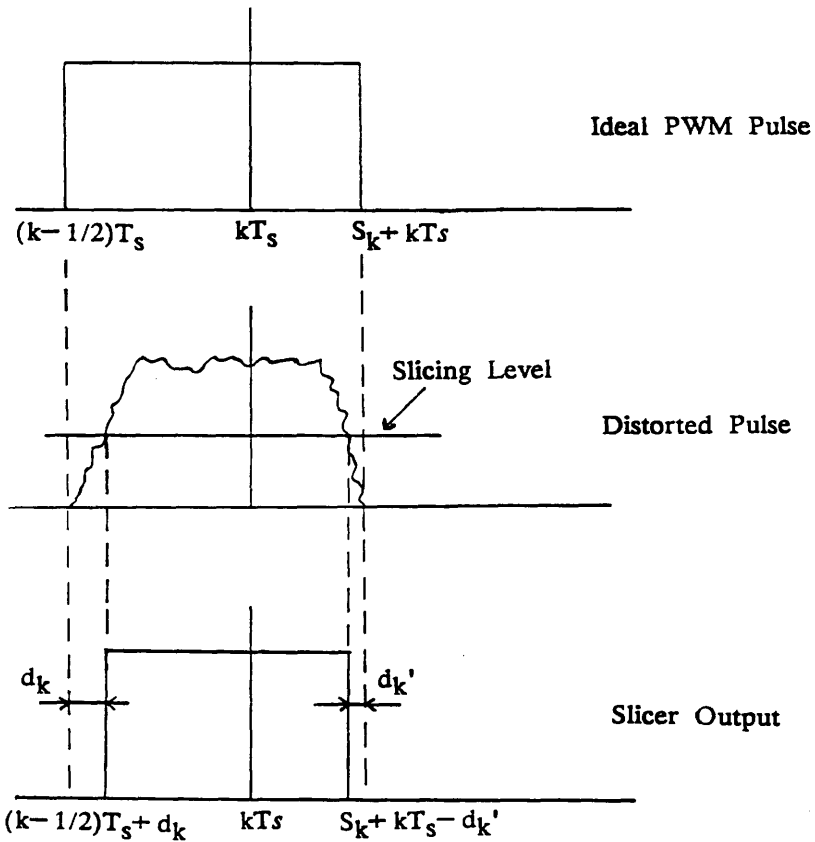


**Fig.2.10 Slicing Operation.**

$$\begin{aligned}
&= \int_{(k-1/2)T_s+d_k}^{kT_s} dt' + \int_{kT_s}^{s_k+kT_s-d_k'} \frac{dt'}{kT_s} = s_k + T_s/2 - (d_k+d_k') \\
&= s(kT_s) + T_s/2 - (d_k+d_k') \tag{2.51}
\end{aligned}$$

Substituting eq.(2.51) into eq.(2.50) we get,

$$\begin{aligned}
u_\delta(t) &= \sum_{-\infty}^{+\infty} [s(kT_s) + T_s/2 - (d_k+d_k')] \delta(t-kT_s) \\
&= \sum_{-\infty}^{+\infty} s(kT_s) \delta(t-kT_s) + (T_s/2) \sum_{-\infty}^{+\infty} \delta(t-kT_s) - \\
&\quad \sum_{-\infty}^{+\infty} (d_k+d_k') \delta(t-kT_s) \tag{2.52}
\end{aligned}$$

Taking the FT of eq.(2.52) we get,

$$\begin{aligned}
U_\delta(f) &= (1/T_s) \sum_{-\infty}^{+\infty} S(f-kf_s) + (1/2) \sum_{-\infty}^{+\infty} \delta(f-kf_s) - \\
&\quad \text{FT} \left[ \sum_{-\infty}^{+\infty} (d_k+d_k') \delta(t-kT_s) \right] \tag{2.53}
\end{aligned}$$

The signal given by eq.(2.53) passes through the ideal low pass filter of eq.(2.13) to yield,

$$\begin{aligned}
Y(f) &= H(f)U_\delta(f) = \begin{cases} U_\delta(f) & |f| \leq f_s/2 \\ 0 & |f| > f_s/2 \end{cases} \\
&= S(f) + (T_s/2) \delta(f) - H(f) \text{FT} \left[ \sum_{-\infty}^{+\infty} (d_k+d_k') \delta(t-kT_s) \right] \tag{2.54}
\end{aligned}$$

The inverse FT of eq.(2.54) is,

$$y(t) = s(t) + T_s/2 - h(t) * \left[ \sum_{-\infty}^{+\infty} (d_k+d_k') \delta(t-kT_s) \right] \tag{2.55}$$

where  $h(t)$  is the ideal low pass filter impulse response given by,

$$h(t) = \frac{\sin \pi f_s t}{\pi f_s t} \tag{2.56}$$

Finally, the detector output is,

$$y(t) = T_s/2 + s(t) - \sum_{-\infty}^{+\infty} (d_k + d_k') \frac{\sin \pi(t - kT_s) f_s}{\pi(t - kT_s) f_s} \quad (2.57)$$

The detector output comprises a DC component  $T_s/2$ , the original modulating signal  $s(t)$  and a band limited noise term, of sample value  $(d_k + d_k')$ , that we shall call  $y_n(t)$ . Neglecting the noise term of eq.(2.57) we have,

$$\begin{aligned} u_\delta(t) &= \sum_{-\infty}^{+\infty} s(kT_s) \delta(t - kT_s) + (T_s/2) \sum_{-\infty}^{+\infty} \delta(t - kT_s) \\ &= s(t) \sum_{-\infty}^{+\infty} \delta(t - kT_s) + (T_s/2) \sum_{-\infty}^{+\infty} \delta(t - kT_s) \end{aligned} \quad (2.58)$$

The FT of eq.(2.58) is,

$$U_\delta(f) = (1/T_s) \sum_{-\infty}^{+\infty} S(f - nf_s) + (1/2) \sum_{-\infty}^{+\infty} \delta(f - nf_s) \quad (2.59)$$

If  $s(t)$  is cosinusoidal its FT is given by eq.(2.7), and eq.(2.59) becomes,

$$\begin{aligned} U_\delta(f) &= (A/2T_s) \sum_{-\infty}^{+\infty} [ \delta(f - nf_s + f_m) + \delta(f - nf_s - f_m) ] + \\ & \quad (1/2) \sum_{-\infty}^{+\infty} \delta(f - nf_s) \end{aligned} \quad (2.60)$$

Upon making a change of index in the  $\delta$  functions we get,

$$\begin{aligned} U_\delta(f) &= (A/2T_s) \sum_{-\infty}^{+\infty} [ \delta(f + f_m + nf_s) + \delta(f - f_m - nf_s) ] + \\ & \quad (1/2) \sum_{-\infty}^{+\infty} \delta(f - nf_s) \end{aligned} \quad (2.61)$$

Upon taking the inverse FT of eq.(2.61) and making use of eq.(2.42) we get,

$$u_\delta(t) = (M/2) \sum_{-\infty}^{+\infty} \cos 2\pi(f_m + nf_s)t + (1/2) \sum_{-\infty}^{+\infty} \delta(t - kT_s) \quad (2.62)$$

Eq.(2.62) gives the output signal prior to low pass filtering. It shows that for any  $M < 1$  and for  $f_m$  up to 5.5MHz the only component that falls within the filter

passband is the signal fundamental. This means that a combination of a PWM with US transmitter and a S/H receiver has no limitation on M ( $M < 1$ ) and this for frequencies covering the whole video band.

### 2.3.2 PWM with natural sampling

In PWM with natural sampling (NS) although the sampling rate is fixed the sampling instant can vary anywhere within the time slot due to the amplitude of the modulating signal being compared directly with the ramp voltage. The block diagram of a typical system generating PWM signals with NS along with the waveforms of interest are given in Fig.2.11. The ramp generator produces a ramp voltage which has a peak to peak amplitude slightly larger than the maximum amplitude range of the input signal. The comparator is a high gain amplifier intended for two-state operation. If the input signal is higher than a preset reference level, the comparator output is held in one state. Whenever the input signal is less than the reference level the output is held in the other state. In this circuit the first crossing of the reference level indicates the clock timing and the second one generates the variable trailing edge. The constant amplitude of the output pulses is determined by the output voltage of the comparator.

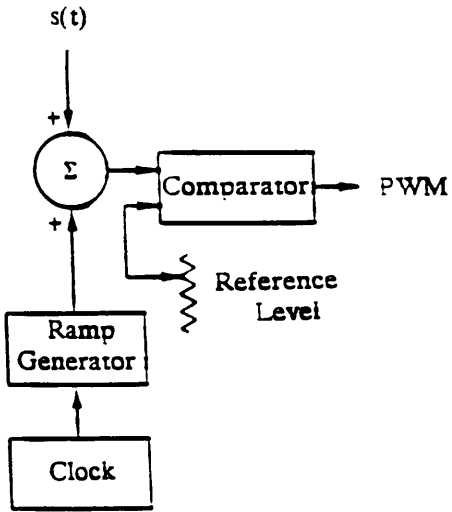
#### 2.3.2.1 Spectrum of PWM signals with NS

As before, we assume a cosinusoidal modulating signal  $s(t)$  given by eq.(2.27), and a trailing edge modulation. A should satisfy the condition given by eq.(2.28). To be able to use the property given by eq.(A3.6) we should have in addition to the previous condition the following one as well,

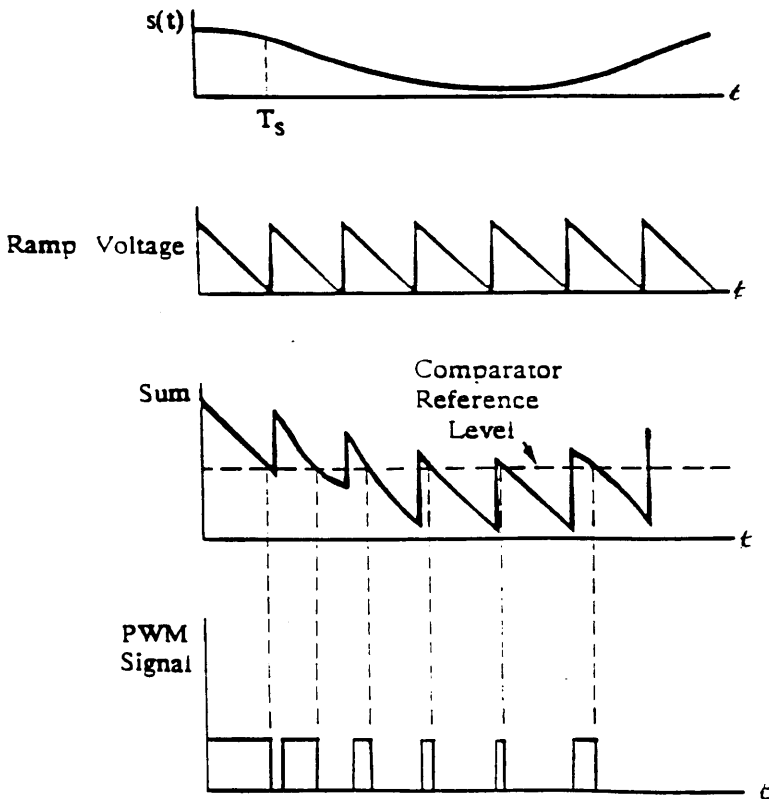
$$|s'(t)|_{\max} < 1 \quad \text{i.e.} \quad A < 1/2\pi f_m \quad \text{or} \quad M < f_s/\pi f_m \quad (2.63)$$

Substituting eq.(2.27) into eq.(2.26), which gives the analytical expression of a PWM signal with zero rise time, and making use of the property given by eq.(A3.6) we find,

$$dl(t)/dt = c_\delta(t+T_s/2) - x_\delta(t)$$



(a)



(b)

Fig.2.11 (a) A Naturally Sampled PWM System And (b) The Waveforms Of Interest.

$$\begin{aligned}
&= (1/T_S) \sum_{-\infty}^{+\infty} (-1)^n e^{2\pi j n f_S t} - \sum_{-\infty}^{+\infty} \delta[t - kT_S - s(t_k)] \\
&= (1/T_S) \sum_{-\infty}^{+\infty} (-1)^n e^{2\pi j n f_S t} - [1 - s'(t)] \sum_{-\infty}^{+\infty} \delta[t - kT_S - s(t_k)] \\
&= - [1 + 2\pi A f_m \sin(2\pi f_m t)] \sum_{-\infty}^{+\infty} \delta[t - kT_S - A \cos(2\pi f_m t_k)] + \\
&\quad (1/T_S) \sum_{-\infty}^{+\infty} (-1)^n e^{2\pi j n f_S t} \tag{2.64}
\end{aligned}$$

As we did before, we expand  $x_\delta(t)$  into a double Fourier series,

$$x_\delta(t) = \sum_{-\infty}^{+\infty} g_{mn} e^{2\pi j (m f_S + n f_m) t} \tag{2.65}$$

The Fourier coefficients  $g_{mn}$  were determined in ref.5, to be,

$$\begin{aligned}
g_{mn} &= (1/2\pi T_S) \int_{-\pi}^{+\pi} e^{2\pi j m A f_S \cos \theta} e^{-j n \theta} d\theta + \\
&\quad A f_m f_S \int_{-\pi}^{+\pi} e^{-2\pi j m A f_S \cos \theta} \sin \theta e^{-j n \theta} d\theta \tag{2.66}
\end{aligned}$$

The second term of eq.(2.66) may be integrated by parts to yield an integral having the same form as that of the first term when  $m \neq 0$ . Upon combining these terms we obtain for  $m \neq 0$ ,

$$\begin{aligned}
g_{mn} &= \frac{m f_S + n f_m}{m} (1/2\pi) \int_{-\pi}^{+\pi} e^{-2\pi j m A f_S \cos \theta} e^{-j n \theta} d\theta \\
&= \frac{m f_S + n f_m}{m} (-j)^n J_n(2\pi A m f_S) \tag{2.67}
\end{aligned}$$

For the  $m = 0$  case, we have directly from eq.(2.66),

$$g_{0n} = (f_S/2\pi) \int_{-\pi}^{+\pi} e^{-j n \theta} d\theta + A f_m f_S \int_{-\pi}^{+\pi} \sin \theta e^{-j n \theta} d\theta \tag{2.68}$$

Therefore,

$$\begin{aligned}
g_{00} &= f_S \\
g_{01} &= -j\pi A f_S f_m \\
g_{0,-1} &= j\pi A f_S f_m
\end{aligned}$$

$$g_{0n} = 0 \quad \text{for} \quad |n| \geq 2$$

Expanding the terms of the double summation of eq.(2.65) we get,

$$x_{\delta}(t) = \sum_{\substack{+\infty \\ m \neq 0 \\ -\infty}} g_{mn} e^{2\pi j(mf_s + nf_m)t} + g_{00} + g_{01} e^{2\pi j f_m t} + g_{0,-1} e^{-2\pi j f_m t} \quad (2.69)$$

Substituting eqs.(2.67) and (2.68) into eq.(2.69) we get,

$$\begin{aligned} x_{\delta}(t) &= f_s + j\pi A f_s f_m e^{-2\pi j f_m t} - j\pi f_m f_s e^{2\pi j f_m t} + \\ &\sum_{\substack{+\infty \\ m \neq 0 \\ -\infty}} \frac{mf_s + nf_m}{m} (-j)^n J_n(2\pi A m f_s) e^{2\pi j(mf_s + nf_m)t} \\ &- \sum_{\substack{+\infty \\ m \neq 0 \\ -\infty}} \frac{mf_s + nf_m}{m} (-j)^n J_n(2\pi A m f_s) e^{2\pi j(mf_s + nf_m)t} + f_s \\ &+ 2\pi A f_s f_m \sin(2\pi f_m t) \end{aligned} \quad (2.70)$$

Substituting eq.(2.70) into eq.(2.64) and integrating the latter we get,

$$\begin{aligned} l(t) &= s(t)/T_s + (1/T_s) \sum_{\substack{+\infty \\ n \neq 0 \\ -\infty}} (-1)^n \frac{e^{2\pi j n f_s t}}{2\pi j n f_s} - \\ &\sum_{\substack{+\infty \\ m \neq 0 \\ -\infty}} \frac{mf_s + nf_m}{m} (-j)^n J_n(2\pi A m f_s) \frac{e^{2\pi j(mf_s + nf_m)t}}{2\pi j(mf_s + nf_m)} + C \end{aligned} \quad (2.71)$$

where C is an integration constant.

Taking apart the term corresponding to  $n = 0$  from the double summation we get,

$$\begin{aligned} l(t) &= s(t)/T_s + (1/T_s) \sum_{\substack{+\infty \\ n \neq 0 \\ -\infty}} (-1)^n \frac{e^{2\pi j n f_s t}}{2\pi j n f_s} - (1/T_s) \sum_{\substack{+\infty \\ m \neq 0 \\ -\infty}} J_0(2\pi A m f_s) \\ &\frac{e^{2\pi j m f_s t}}{2\pi j m f_s} - \sum_{\substack{+\infty \\ m \neq 0 \\ -\infty \\ n \neq 0}} \frac{mf_s + nf_m}{m} (-j)^n J_n(2\pi A m f_s) \frac{e^{2\pi j(mf_s + nf_m)t}}{2\pi j(mf_s + nf_m)} + C \\ &- s(t)/T_s + (1/T_s) \sum_{\substack{+\infty \\ n \neq 0 \\ -\infty}} \frac{(-1)^{n-J_0(2\pi A n f_s)}}{2\pi j n f_s} e^{2\pi j n f_s t} - \\ &\sum_{\substack{+\infty \\ m, n \neq 0 \\ -\infty}} (-j)^n \frac{mf_s + nf_m}{m} J_n(2\pi A m f_s) \frac{e^{2\pi j(mf_s + nf_m)t}}{2\pi j(mf_s + nf_m)} + C \end{aligned} \quad (2.72)$$

Substituting eq.(2.42) into eq.(2.72) we get finally,

$$l(t) = (M/2) \cos(2\pi f_m t) + \sum_{-\infty}^{+\infty} \frac{(-1)^n J_0(\pi n M)}{2\pi n} e^{2\pi j f_s t} - \sum_{\substack{+\infty \\ m, n \neq 0 \\ -\infty}} (-j)^n \frac{J_n(m\pi M)}{2\pi j m} e^{2\pi j (m f_s + n f_m) t} + C \quad (2.73)$$

Let ,

$$C_n = \frac{(-1)^n J_0(\pi n M)}{\pi n} \quad (2.74)$$

$$C_{m, n} = \frac{J_n(\pi m M)}{\pi m} \quad (2.75)$$

The clock fundamental is,

$$C_1 = \frac{1 + J_0(\pi M)}{\pi}$$

The clock fundamental first sidetones are,

$$C_{1, 1} = \frac{J_1(\pi M)}{\pi}$$

$$C_{1, -1} = -\frac{J_1(\pi M)}{\pi}$$

The clock fundamental second sidetones are,

$$C_{1, 2} = \frac{J_2(\pi M)}{\pi}$$

$$C_{1, -2} = -\frac{J_2(\pi M)}{\pi}$$

The clock fundamental third sidetones are,

$$C_{1, 3} = \frac{J_3(\pi M)}{\pi}$$

$$C_{1, -3} = -\frac{J_3(\pi M)}{\pi}$$

The clock fundamental fourth sidetones are

$$C_{1,4} = \frac{J_4(\pi M)}{\pi}$$

$$C_{1,-4} = -\frac{J_4(\pi M)}{\pi}$$

The signal fundamental is,

$$S_0 = M/2$$

These components are computed, as before, for  $f_m = 2\text{MHz}$  and  $f_s = 13.34\text{MHz}$ .

The computation is done against a reference level which is the amplitude of the signal fundamental with  $M = 1$ . The relative powers of these components are calculated through eq.(2.76) namely,

$$\begin{aligned} P_{\text{rel}}(\text{dB}) &= 10 \log\left[\frac{\text{component's amplitude}^2}{S_0(M=1)}\right] \\ &= 20 \log(\text{comp. ampl.}) + 6\text{dB} \end{aligned} \quad (2.76)$$

The results are given in Tab.2.3 and a sketch of the spectrum is given in Fig.2.12 for various  $M$ .

$M$	0.1	0.25	0.5
$S_0$	-20.0	-12.0	-6.0
$C_1$	2.0	1.4	-0.6
$C_{1,1}$	-20.1	-12.8	-8.8
$C_{1,2}$	-42.4	-26.8	-16.0
$C_{1,3}$	-68.1	-44.4	-27.1
$C_{1,4}$	-96.3	-64.6	-41.0

**Tab.2.3** The relative powers of the spectrum of a PWM signal with NS.

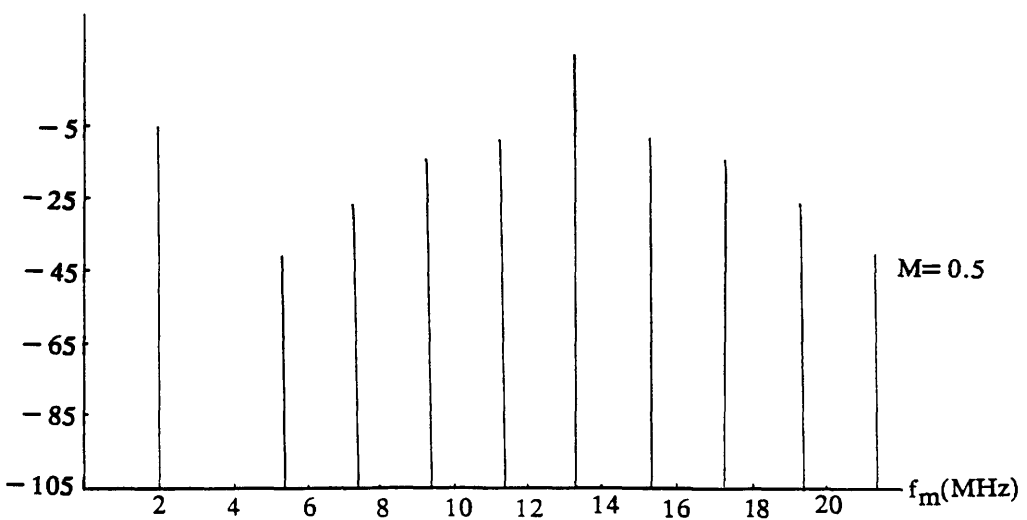
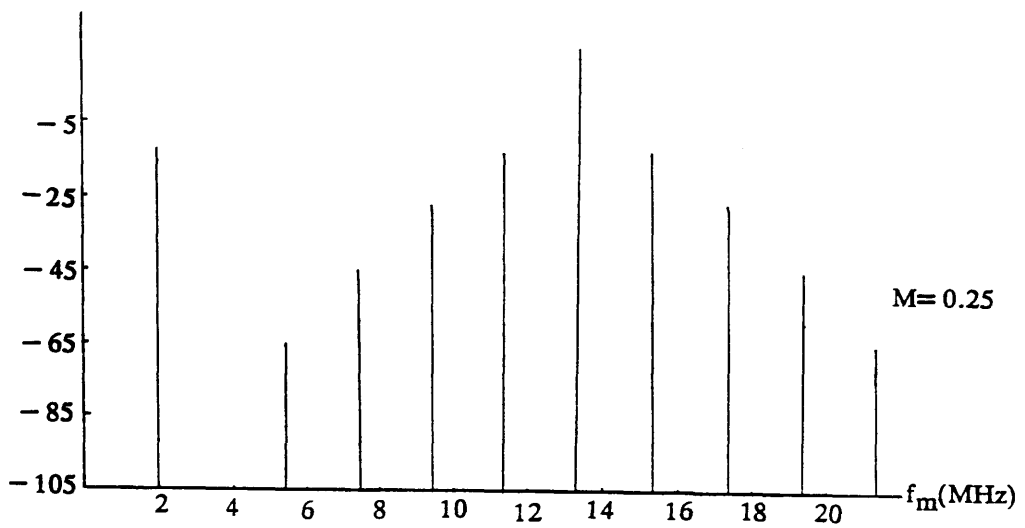
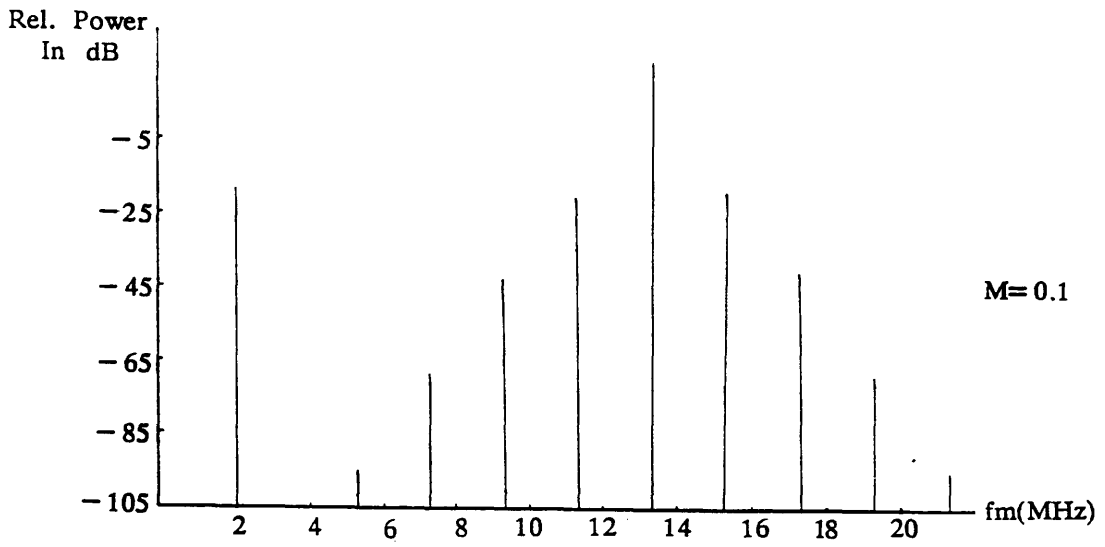


Fig.2.12 Spectra Of A PWM Signal With Natural Sampling.

### 2.3.2.2 Demodulation of PWM signals with NS

From eq.(2.73) or alternatively from the spectra of PWM signals with NS given in Fig.2.12 it can be seen that there is no signal second harmonic, and that the isolation between the signal fundamental and the distortion components is large enough, therefore, low pass filtering alone is enough for demodulation. Even for large values of M the isolation is considerable and one still can use a low pass filter for demodulation, this when  $f_m = 2\text{MHz}$ . If  $f_m$  increases to cover the high video frequencies (4 to 5.5MHz) more clock sidetones fall within the filter passband. The relative powers of the highest component falling into the low pass filter passband, whose cut off frequency is  $f_c = 6\text{MHz}$ , are computed through eq.(2.76). The results are given in Tab.2.4.

		$0 < f_m < 2.6\text{MHz}$	$2.6 < f_m < 4\text{MHz}$	$4 < f_m < 6\text{MHz}$
M	$S_0$	$S_{1,4}$	$S_{1,3}$	$S_{1,2}$
0.1	-20.0	-96.3	-68.1	-42.4
0.25	-12.0	-64.6	-44.4	-26.8
0.5	-6.0	-41.0	-27.1	-16.0

Tab.2.4 Relative powers of the highest component falling into the filter passband.

A sketch of these components is given in Fig.2.13. The upper curves of Fig.2.13 represent the signal fundamental relative powers for different M. The lower curves represent the highest other component that falls into the filter passband. Examination of Fig.2.13 shows that even with M as low as 0.1 we have an SIR of only 23dB for the range of frequencies 4 to 5.5MHz. This is due to the clock fundamental second sidetones whose effect comes at the critical part of the video band where the colour and high frequency information are carried. A relaxation of the limitation on M can be obtained by increasing  $f_s$ . However, the increase in the sampling rate is accompanied by an increase in the transmission bandwidth which can be seen as a

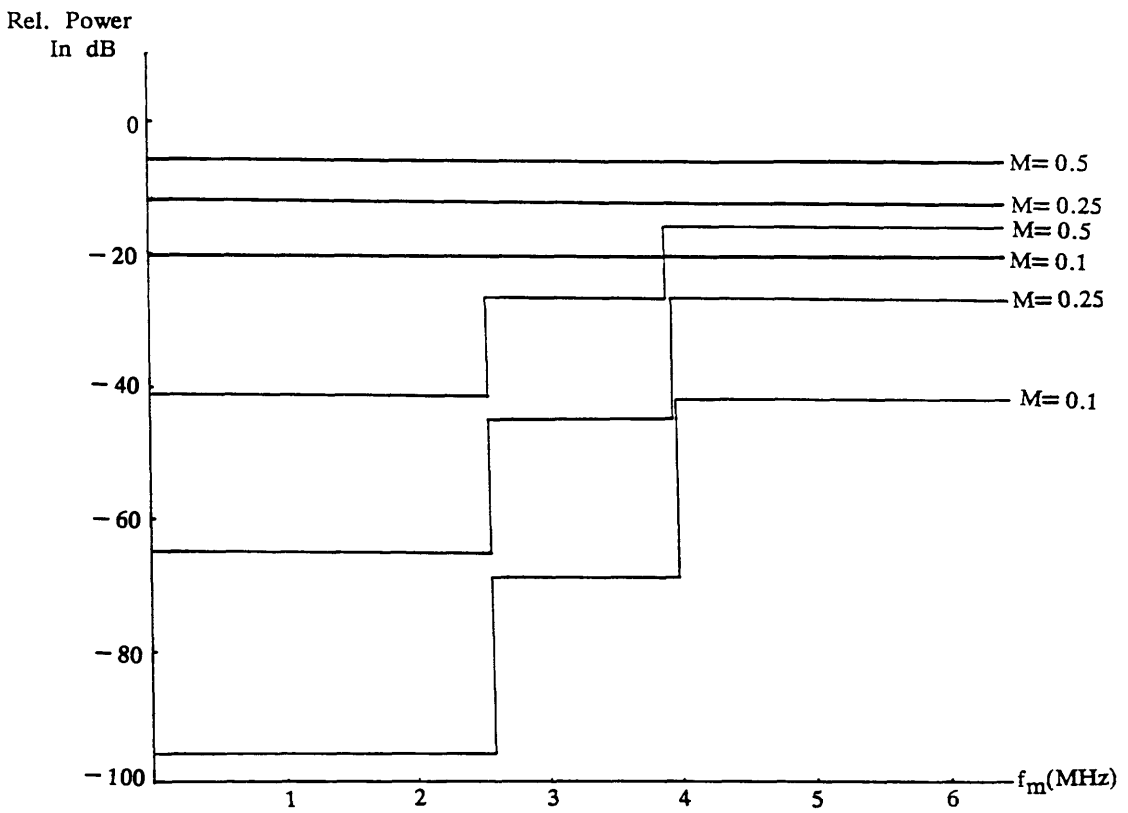


**Fig.2.13 Highest Component Falling Into The Filter Passband Versus Modulating Signal Frequencies.**

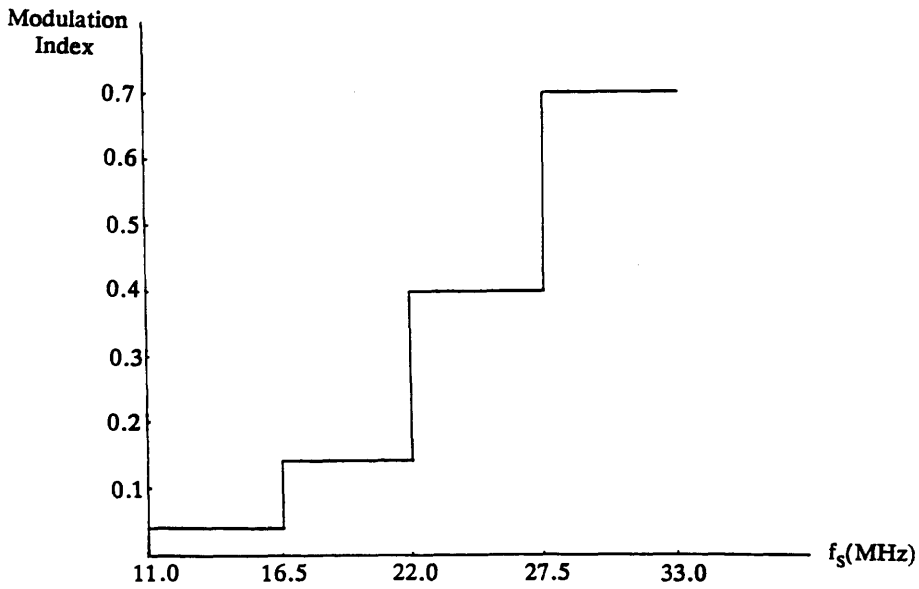


**Fig.2.14 Permissible Modulation Indices Versus Sampling Rates To Get An SIR>36dB For Frequencies Covering The Video Band.**

waste of bandwidth. Fig.2.14 gives the allowable range of  $M$  in terms of  $f_s$  in order to get an SIR > 36dB.

### 2.3.3 Bandwidth required for the transmission of PWM signals

In the detection of PWM signals fidelity is required and the bandwidth must be determined by rise time consideration. In the case of an ideal low pass filter channel this bandwidth is given by eq.(A1.4) namely,

$$B_{req} = 0.5/T_r \quad (2.77)$$

where  $T_r$  is the allowable rise time.

## 2.4 COMPARISON OF PCM AND PWM SNRS

We assume a binary PCM signal in the presence of white gaussian noise, thermal noise for example. The expression giving the PCM SNR in terms of the probability of error  $P_e$  and the number of bits used,  $n$ , is derived by ref.4. This is,

$$(S_0/N_0) = \frac{2^{2n} - 1}{1 + 4 P_e (2^{2n} - 1)} \quad (2.78)$$

The probability of error  $P_e$ , in the absence of ISI, is given in the same ref.4,

$$P_e = 1/2 \operatorname{erfc}(A_c/2\sigma\sqrt{2}) \quad (2.79)$$

where  $\operatorname{erfc}(x)$  is the complementary error function given by,

$$\operatorname{erfc}(x) = 1 - \operatorname{erf}(x) = 1 - (2/\sqrt{\pi}) \int_0^x e^{-u^2} du \quad (2.80)$$

$A_c$  the carrier peak amplitude, and  $\sigma$  the gaussian noise rms.

Substituting eq.(2.79) into eq.(2.78) we get,

$$(S_0/N_0) = \frac{2^{2n} - 1}{1 + 2 \operatorname{erfc}(A_c/2\sigma\sqrt{2}) (2^{2n} - 1)} \quad (2.81)$$

If  $S_c$  designates the carrier peak power  $A_c^2$ , and  $N_c$  the noise average power  $\sigma^2$ , then eq.(2.81) becomes,

$$(S_0/N_0) = \frac{2^{2n} - 1}{1 + 2 \operatorname{erfc}(S_c/2N_c\sqrt{2}) (2^{2n} - 1)} \quad (2.82)$$

The PWM output SNR will be derived in chapter 3. For a sinusoidal modulating signal this SNR is,

$$(S_0/N_0) = (\pi^2/16) M^2 (B/f_s)^2 (S_c/N_c) \quad (2.83)$$

Plots of eq.(2.82) in terms of the CNR  $S_c/N_c$  for  $n = 4, 6, 8$ , and eq.(2.83) for a receiver bandwidth  $B = 40\text{MHz}$ , a sampling rate  $f_s = 13.34\text{MHz}$ , and  $M = 1$  are given in Fig.2.15. As it can be seen from this figure, when the receiver bandwidth  $B$  is  $n \times f_s$ , PCM presents far better SNR performance than PWM and this even for the most favorable PWM case i.e  $M = 1$ .

If the allowable  $B$  is less than that required (i.e.  $n \times f_s$ ) then the PCM pulses will overlap and give rise to ISI. This will deteriorate the PCM SNR. The computation of this SNR in presence of ISI will be carried out in the next chapter.

PCM  
Output  
SNR  
vs  
Input  
SNR

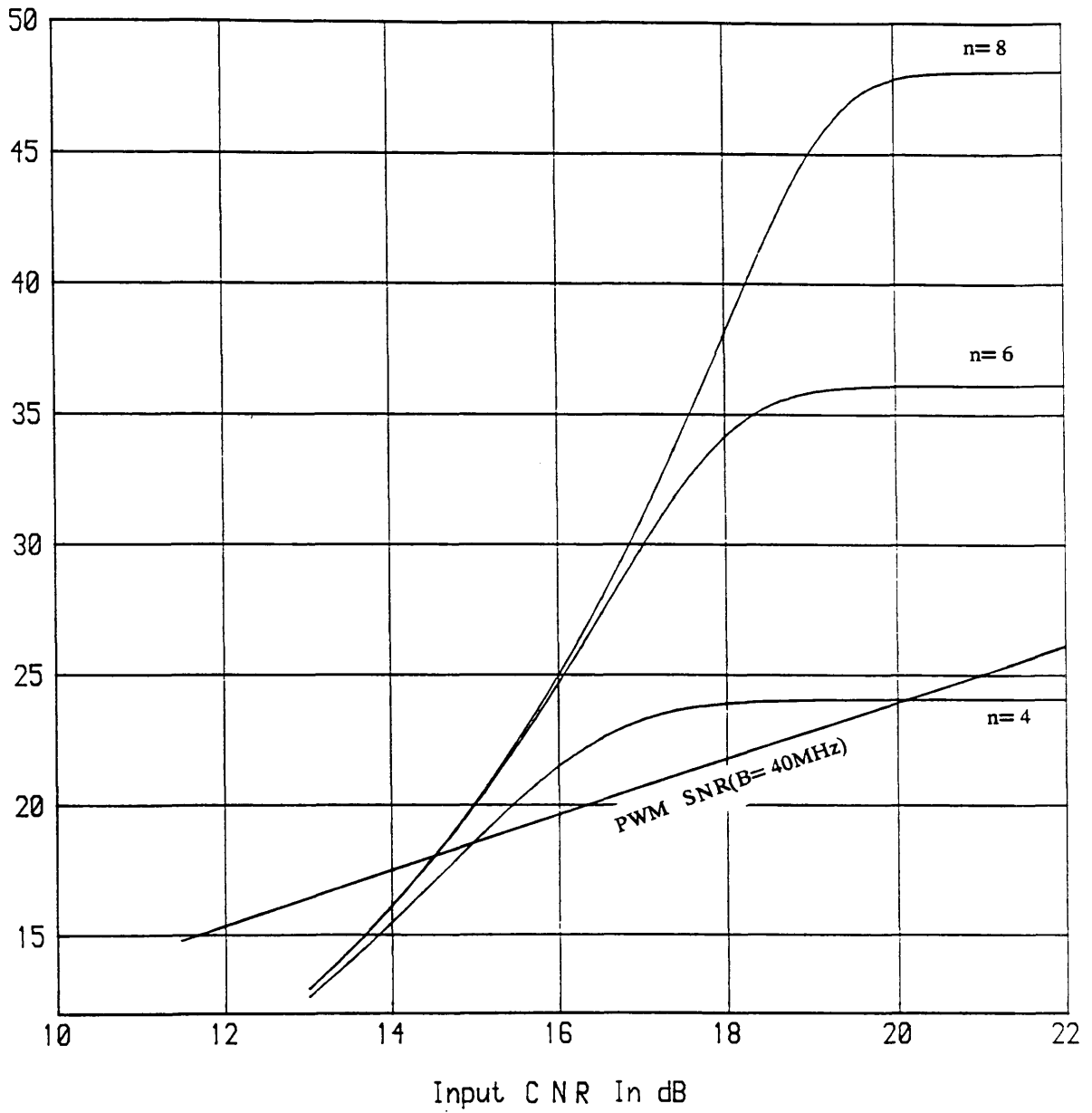


Fig.2.15 PCM Output SNR Versus Input CNR In Presence Of White Gaussian Noise.

## 2.5 CONCLUSION

We have treated, in this chapter, the theory of PWM with US and NS. We showed how easily modulation and demodulation can be achieved. In the case of PWM with NS, the demodulator consisted only of a low pass filter. But, there was a limitation on  $M$  ( $M < 0.1$ ) in order to respond to video specification ( $SIR > 36\text{dB}$ ). This will deteriorate the output SNR since the latter is proportional to the square of  $M$ . The constraint on  $M$  can be relaxed by increasing  $f_s$ , we showed that for  $f_s > 28\text{MHz}$  the allowable  $M$  can be as high as 0.7. However, an increase in  $f_s$  is accompanied by an increase in  $B$ . The latter is determined by the reciprocal of the rise time permitted by the electronics used. For  $f_s = 28\text{MHz}$ , the usable time slot is 35ns. If  $M = 0.7$  then, 25ns are used for modulation and 10ns for rise and fall times which corresponds to  $B = 100\text{MHz}$ . We should point out that components that allow  $T_r = 5\text{ns}$  are very expensive and this defeats one of the most important criteria of choosing PWM as a modulation technique which is cost. We concluded the chapter by showing that PCM SNR is far better than PWM SNR when ISI is absent.

3.1 INTRODUCTION

In this chapter we seek to examine the effect of finite channel bandwidths on the detection of PWM signals with US. The simplest channel model that we can adopt is that of an RC filter followed by a threshold detector. Because of the limited channel bandwidth imposed by the components R and C, pulse distortion will be introduced. The latter is computed in terms of M and the channel bandwidth B. The output SNR will be determined as well, and a comparison between this SNR and PCM SNR in presence of ISI will be carried out as well.

3.2 BANDWIDTH LIMITATION DISTORTION

In what follows, we assume a PWM signal with US and trailing edge modulation,

$$l(t) = \sum_{-\infty}^{+\infty} q(s_k, t - kT_s) \quad (3.1)$$

where,

$$q(s_k, t - kT_s) = \begin{cases} 1 & s_k < t < T_s/2 \\ 0 & t > s_k \end{cases} \quad (3.2)$$

If  $|s(kT_s)|_{\max} < T_s/2$ ,

$$s_k = M s(kT_s) \quad (3.3a)$$

For a normalised modulating signal  $sn(t)$  ( $sn(t) = s(t)/A$ ), if  $|sn(kT_s)| < 1$ ,

$$s_k = (MT_s/2) sn(kT_s) \quad (3.3b)$$

An example of a PWM signal with US is given in Fig.3.1. Because of the finite bandwidth, the circuit output signal will be distorted i.e. the actual width of any pulse k will be different from the detected width. Fig.3.3 gives an illustration of the difference between the pulses widths. The PWM signal passes through the RC filter and the threshold detector as shown in Fig.3.2.

The RC filter time response to a rectangular pulse is derived in appendix A2 and given by eq.(A2.7). Upon changing the integration limits, eq.(A2.7) becomes,

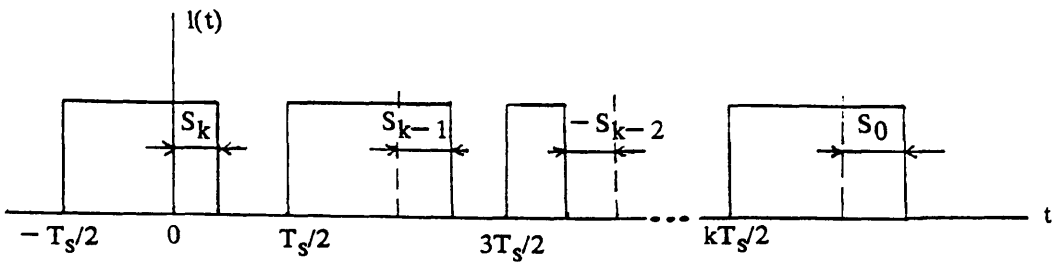


Fig.3.1 Uniformly Sampled PWM Signal With Trailing Edge Modulation.

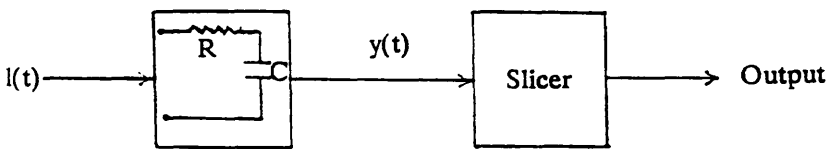


Fig.3.2 PWM Receiver Model.

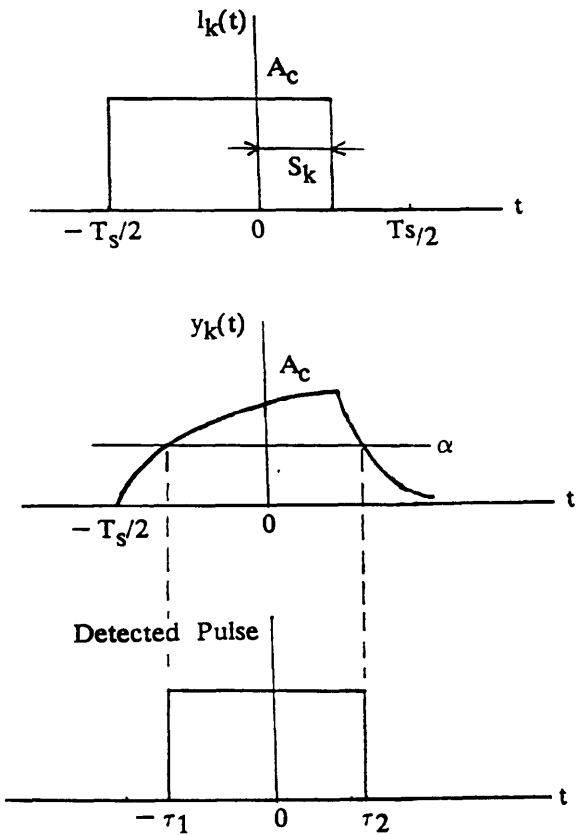


Fig.3.3 Detection Of The \$k^{th}\$ Pulse.

$$y_k(t) = \begin{cases} v_1(t) = A_c [1 - e^{-(t+T_s/2)/T}] & -T_s/2 < t < s_k \\ v_2(t) = A_c [1 - e^{-(s_k+T_s/2)/T}] e^{-(t-s_k)/T} & s_k < t < T_s/2 \end{cases} \quad (3.4)$$

where  $T$  is the time constant ( $T = RC$ ).

The rising edge  $v_1(t)$  reaches the slicing level  $\alpha$  at  $t = -\tau_1$ ,

$$\tau_1 = T_s/2 + T \ln(1-\alpha/A_c) \quad (3.5)$$

The falling edge  $v_2(t)$  reaches the slicing level  $\alpha$  at  $t = \tau_2$ ,

$$\tau_2 = s_k - T \ln(\alpha/A_c) + T \ln[1 - e^{-(s_k+T_s/2)/T}] \quad (3.6)$$

The detected pulse width is therefore,

$$\tau_1 + \tau_2 = s_k + T_s/2 + T \ln(A_c/\alpha - 1) + T \ln[1 - e^{-(s_k+T_s/2)/T}] \quad (3.7)$$

Distortion is the difference between the actual and detected pulse widths,

$$D_k = T \ln(A_c/\alpha - 1) + T \ln[1 - e^{-(s_k+T_s/2)/T}] \quad (3.8)$$

The expression given by eq.(3.8) depends on the slicing level  $\alpha$ , on the modulation index  $M$ , and on the channel bandwidth  $B$ .

### 3.2.1 Dependence of distortion on $\alpha$

To see whether or not there is a value of  $\alpha$  for which  $D_k$  is minimum, we should take the derivative of  $D_k$  with respect to  $\alpha$  for a given  $T$ ,

$$dD_k/d\alpha = -\frac{A_c}{\alpha(A_c - \alpha)} \neq 0 \quad (3.9)$$

Since eq.(3.9) is always different from 0, there is no specific value for which  $D_k$  is minimum. Examination of eq.(3.8) shows that the term on the right is always negative, therefore, to keep  $D_k$  low we should have

$$\ln(A_c/\alpha - 1) \geq 0 \quad \text{i.e.} \quad \alpha \leq A_c/2 \quad (3.10)$$

### 3.2.2 Dependence of distortion on $B$

We have seen that to keep  $D_k$  low we should take the slicing level  $\alpha$  less or equal to  $A_c/2$ . We assume that the latter is equal to half the carrier peak amplitude,

$$\alpha = A_c/2 \quad (3.11)$$

Substituting the value of  $\alpha$  given by eq.(3.11) into eq.(3.8) we get,

$$D_k = T \text{Ln}[1 - e^{-(s_k + T_s/2)/T}] \quad (3.12)$$

Let,

$$y = e^{-(s_k + T_s/2)/T} \quad (3.13)$$

The expansion of  $\text{Ln}(1-y)$  into Taylor series is,

$$\text{Ln}(1-y) = -(y + y^2/2 + y^3/3 + \dots + y^n/n) \quad (3.14)$$

If,

$$y < 1/e \quad \text{i.e.} \quad (s_k + T_s/2) > 1 \quad (3.15)$$

then, eq.(3.14) becomes,

$$\text{Ln}(1-y) \approx -(y + y^2/2 + y^3/3) \quad (3.16)$$

with an absolute error of less than 0.6%.

Substituting  $s_k$  by its value given by eq.(3.3b) into eq.(3.15) we get,

$$M \text{sn}(kT_s) > 2(T/T_s) - 1 \quad (3.17)$$

Substituting  $T$  by its value given by eq.(A5.3) we get,

$$M \text{sn}(kT_s) > 2(f_s/2\pi B) - 1 \quad (3.18)$$

Let  $\gamma$  be the ratio of the channel bandwidth to the sampling rate,

$$\gamma = B/f_s \quad (3.19)$$

Eq.(3.18) becomes then,

$$M \text{sn}(kT_s) > (1/\pi\gamma) - 1 \quad (3.20)$$

In the case of peak positive modulation i.e.  $\text{sn}(kT_s) = +1$ , eq.(3.20) becomes,

$$M > (1/\pi\gamma) - 1 \quad (3.21)$$

This condition is satisfied for any  $M$  ( $M < 1$ ) for all practical values of

$\gamma$  (1.0 to 3.0). In the case of peak negative modulation i.e.  $\text{sn}(kT_s) = -1$ , eq.(3.20) becomes,

$$M < 1 - 1/(\pi\gamma) \quad (3.22)$$

Making use of eqs.(3.16), (3.3), (A5,3) and (3.19), eq.(3.12) becomes,

$$D_k = T [e^{-\pi\gamma} e^{-M\pi\gamma \text{sn}(kT_s)} + (1/2) e^{-2\pi\gamma} e^{-2\pi\gamma M \text{sn}(kT_s)} + (1/3) e^{-3\pi\gamma} e^{-3\pi\gamma M \text{sn}(kT_s)}] \quad (3.23)$$

Because  $D_k$  depends on the sample values of the modulating signal, we should take its average value,

$$\begin{aligned} \langle D_k/T_s \rangle = & (1/2\pi\gamma) [ e^{-\pi\gamma} \langle e^{-M\pi\gamma} \text{sn}(kT_s) \rangle + \\ & (1/2) e^{-2\pi\gamma} \langle e^{-2\pi\gamma M} \text{sn}(kT_s) \rangle + \\ & (1/3) e^{-3\pi\gamma} \langle e^{-3\pi\gamma M} \text{sn}(kT_s) \rangle ] \end{aligned} \quad (3.24)$$

Eq.(3.24) is computed for two types of modulating signals: a sinusoidal signal and a uniformly distributed random variable.

### 3.2.2.1 The average distortion for a sinusoidal modulating signal

We assume a normalised sinusoidal signal,

$$\text{sn}(t) = \sin(\omega_m t) \quad (3.25)$$

Eq.(3.24) becomes then,

$$\begin{aligned} \langle D_k/T_s \rangle = & (1/2\pi\gamma) [ e^{-\pi\gamma} \langle e^{-\pi\gamma M} \sin(\omega_m kT_s) \rangle + \\ & (1/2) e^{-2\pi\gamma} \langle e^{-2\pi\gamma M} \sin(\omega_m kT_s) \rangle + \\ & (1/3) e^{-3\pi\gamma} \langle e^{-3\pi\gamma M} \sin(\omega_m kT_s) \rangle ] \end{aligned} \quad (3.26)$$

We know from Fourier analysis that,

$$e^{jz\sin(\omega_m t)} = \sum_{-\infty}^{+\infty} C_n e^{jn\omega_m t} \quad (3.27)$$

where the Fourier coefficient  $C_n$  are given by,

$$C_n = (1/T) \int_0^T e^{j[z\sin(\omega_m t) - n\omega_m t]} dt \quad (3.28)$$

Let,

$$\theta = \omega_m t \quad (3.29)$$

Substituting eq.(3.29) into eq.(3.28) we get,

$$C_n = (1/2\pi) \int_0^{2\pi} e^{jz\sin\theta - jn\theta} d\theta = J_n(z) \quad (3.30)$$

The above integral is a standard one known as the  $n^{\text{th}}$  order Bessel function in  $z$ .

Substituting eq.(3.30) into eq.(3.27) we get,

$$e^{jz\sin(\omega_m t)} = \sum_{-\infty}^{+\infty} J_n(z) e^{jn\omega_m t} \quad (3.31)$$

Let,

$$x = -jz$$

Eq.(3.31) becomes then,

$$e^{-x \sin(\omega_m t)} = \sum_{-\infty}^{+\infty} J_n(jx) e^{jn\omega_m t} \quad (3.32)$$

Making use of the following bessel function property,

$$J_n(jx) = (j)^n I_n(x) \quad (3.33)$$

where  $I_n(x)$  is the  $n^{\text{th}}$  order modified Bessel function, eq.(3.32) becomes,

$$e^{-x \sin(\omega_m t)} = \sum_{-\infty}^{+\infty} (j)^n I_n(x) e^{jn\omega_m t} \quad (3.34)$$

The same result applies if  $t$  takes on discrete values  $kT_s$ .

$$e^{-x \sin(\omega_m kT_s)} = \sum_{-\infty}^{+\infty} (j)^n I_n(x) e^{jn\omega_m kT_s} \quad (3.35)$$

We know that,

$$\langle e^{jn\omega_m t} \rangle = \begin{cases} 1 & n = 0 \\ 0 & n \neq 0 \end{cases} \quad (3.36)$$

The same result applies when  $t$  takes on discrete values  $kT_s$ ,

$$\langle e^{jn\omega_m kT_s} \rangle = \begin{cases} 1 & n = 0 \\ 0 & n \neq 0 \end{cases} \quad (3.37)$$

Making use of eq.(3.37), the average value of eq.(3.35) is then,

$$\langle e^{-x \sin(\omega_m kT_s)} \rangle = \sum_{-\infty}^{+\infty} (j)^n I_n(x) \langle e^{jn\omega_m kT_s} \rangle = I_0(x) \quad (3.38)$$

Finally, the average distortion for a sinusoidal modulating signal is,

$$\langle D_k/T_s \rangle = (1/2\pi\gamma) \left[ e^{-\pi\gamma} I_0(\pi M\gamma) + (1/2) e^{-2\pi\gamma} I_0(2\pi M\gamma) + (1/3) e^{-3\pi\gamma} I_0(3\pi M\gamma) \right] \quad (3.39)$$

As can be seen from eq.(3.39), the average distortion depends on  $M$  and on  $B$  (since  $\gamma$  is proportional to  $B$ ). A plot of eq.(3.39) in terms of  $M$  for typical values of  $\gamma$  is given in Fig.3.4.

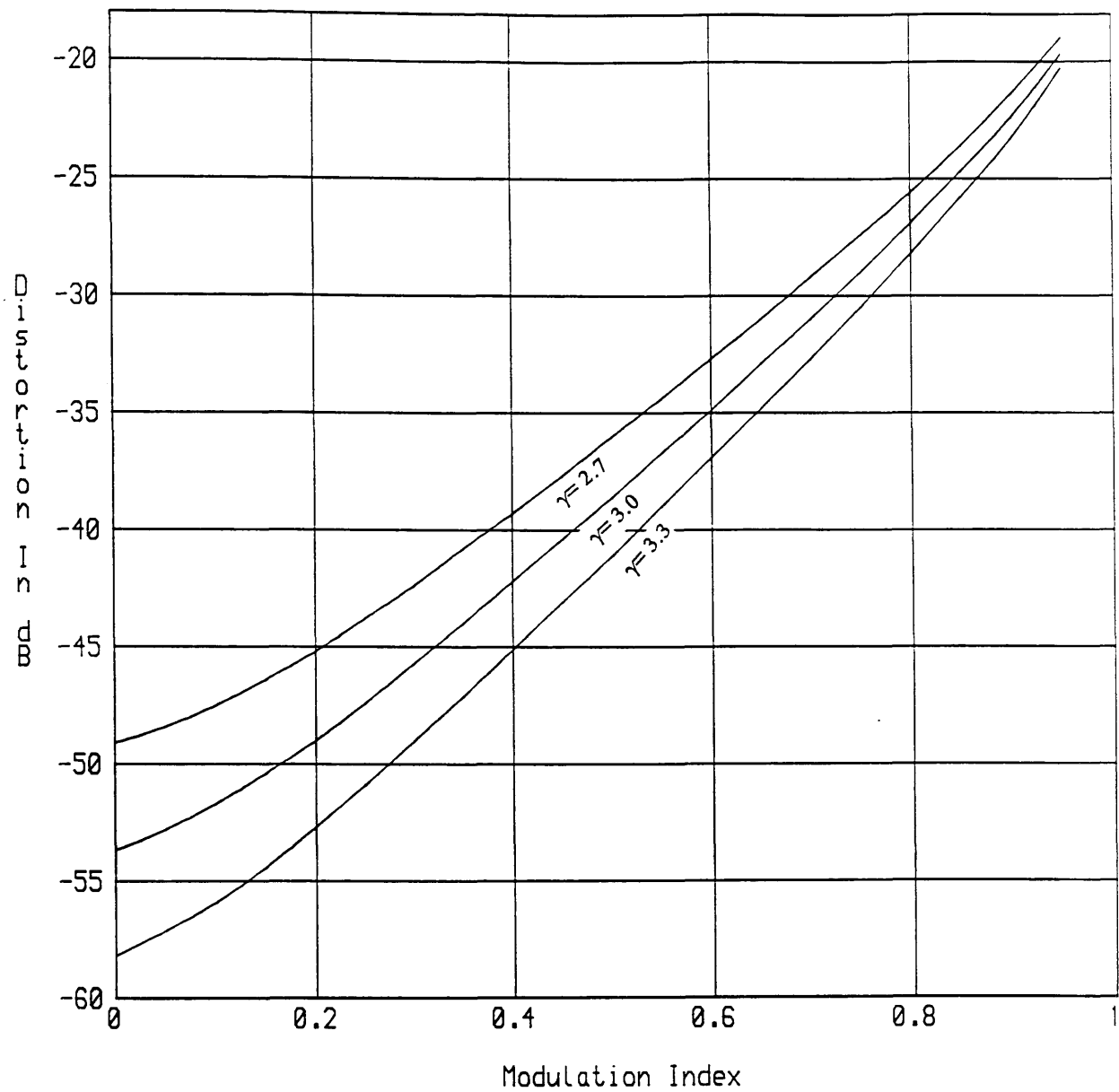


**Fig.3.4 Distortion Versus Modulation Index For A Sinusoidal Modulating Signal.**

### 3.2.2.2 The average distortion for a uniformly distributed random variable

The average distortion is computed this time for a uniformly distributed random variable  $sn$  of constant probability density function  $f(sn)$ . We know from probability theory that if  $f(sn)$  is a p.d.f then,

$$\int_{-\infty}^{+\infty} f(sn) dsn = 1 \quad (3.40)$$

Since,

$$|sn(kT_s)|_{\max} < 1 \quad \text{i.e.} \quad -1 < sn < 1 \quad (3.41)$$

eq.(3.40) becomes,

$$\int_{-1}^{+1} f(sn) dsn = f(sn) \int_{-1}^{+1} dsn = 2 f(sn) = 1 \quad (3.42)$$

Therefore,

$$f(sn) = 1/2 \quad (3.43)$$

The value of the p.d.f  $f(sn)$  being found we can compute the different averages for the determination of the average distortion given by eq.(3.24),

$$\begin{aligned} \langle e^{-\pi M \gamma sn} \rangle &= \int_{-\infty}^{+\infty} e^{-\pi M \gamma sn} f(sn) dsn = (1/2) \int_{-1}^{+1} e^{-\pi M \gamma sn} dsn \\ &= (1/\pi M \gamma) \sinh(\pi M \gamma) \end{aligned} \quad (3.44)$$

The computation of the other averages follows in the same maner, and eq.(3.24) becomes,

$$\begin{aligned} \langle D_{k/T_s} \rangle &= \frac{e^{-\pi \gamma}}{4\pi^2 M \gamma^2} [2 \sinh(\pi \gamma M) + (1/2) e^{-\pi \gamma} \sinh(2\pi \gamma M) + \\ &\quad (2/9) e^{-2\pi \gamma} \sinh(3\pi \gamma M)] \end{aligned} \quad (3.45)$$

If  $M = 0$  (i.e. for an unmodulated pulse), eq.(3.45) becomes,

$$\langle D_{k/T_s} \rangle = (e^{-\pi \gamma} / 2\pi \gamma) [1 + (1/2) e^{-\pi \gamma} + (1/3) e^{-2\pi \gamma}] \quad (3.46)$$

A plot of eq.(3.45) in terms of  $M$  for typical values of  $\gamma$  is given in Fig.3.5. The curves of this figure exhibit the same features as those of the preceding figure: distortion increases for increasing  $M$  and decreases for increasing  $\gamma$ . To get low distortion levels we should have either small  $M$  or large  $\gamma$ . Small  $M$  causes a degradation in the output SNR, large  $\gamma$  (i.e. large  $B$  or short  $T_p$ ) necessitates the

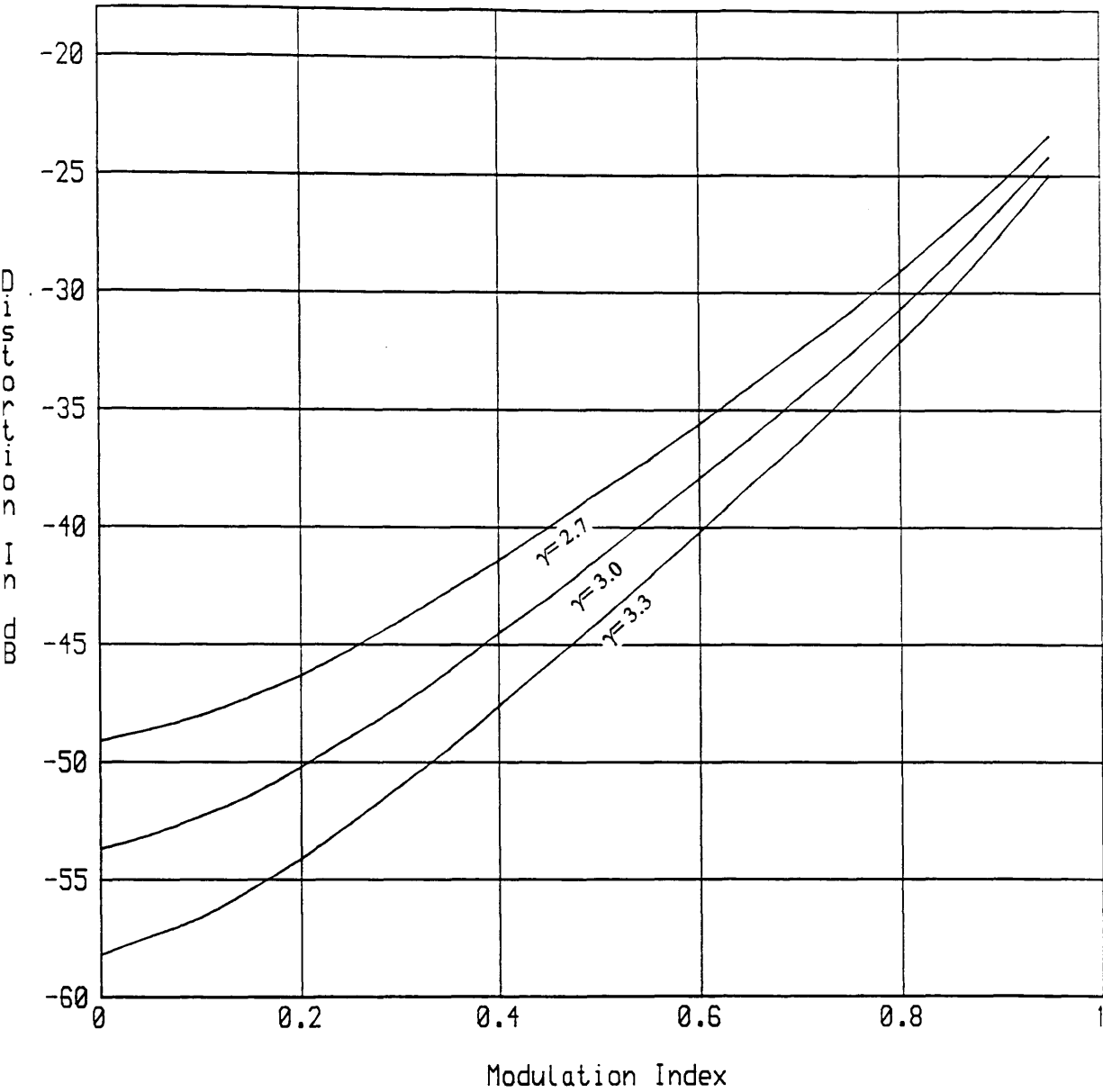


**Fig.3.5 Distortion Versus Modulation Index For A Uniformly Distributed Random Variable.**

use of fast components and these are unaffordable since they are expensive. It is therefore instructive to plot  $\gamma$  in terms of  $M$  for different distortion levels and SNR improvement factors  $I$ . The intersection of the first set of curves with the second determines the values of interest for both  $M$  and  $\gamma$  for given  $I$ . Before doing so we should first find the PWM SNR.

### 3.3 PWM OUTPUT SNR

The effect of noise is to modify the instants at which the incoming pulses cross the slicing level. Because the slicer is a non linear device, an exact analysis is not possible. However, a good approximate analysis is readily obtained for small noise magnitudes. The pulses arriving at the receiver input port are distorted. A part of this distortion comes from the transmission medium and the other is caused by the circuitry used. To render the subsequent analysis exact, we assume that the overall effect is reduced to that of an RC filter. The block diagram of such a model is given in Fig.3.6. The waveforms of interest for the  $k^{\text{th}}$  pulse are given in Fig.3.7.

#### 3.3.1 The output signal average power

The PWM with US detector output was derived in chapter 2. It was given by eq.(2.57) namely,

$$y(t) = T_s/2 + s(t) - \sum_{-\infty}^{+\infty} (d_k + d_k') \frac{\sin \pi f_s (t - kT_s)}{\pi f_s (t - kT_s)} \quad (3.47)$$

The DC component can be neglected and the signal average power in the absence of noise is,

$$S_0 = \langle s^2(t) \rangle \quad (3.48)$$

For a normalised modulating signal  $sn(t)$  and using eq.(3.3b), eq.(3.48) becomes

$$S_0 = (MT_s/2)^2 \langle sn^2(t) \rangle = (MT_s/2)^2 S_i \quad (3.49)$$

where  $S_i$  is the normalised modulating signal average power.

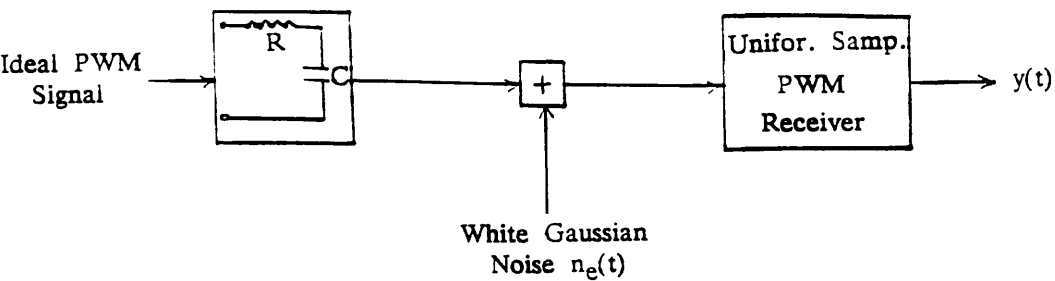


Fig.3.6 A Model Of A PWM System.

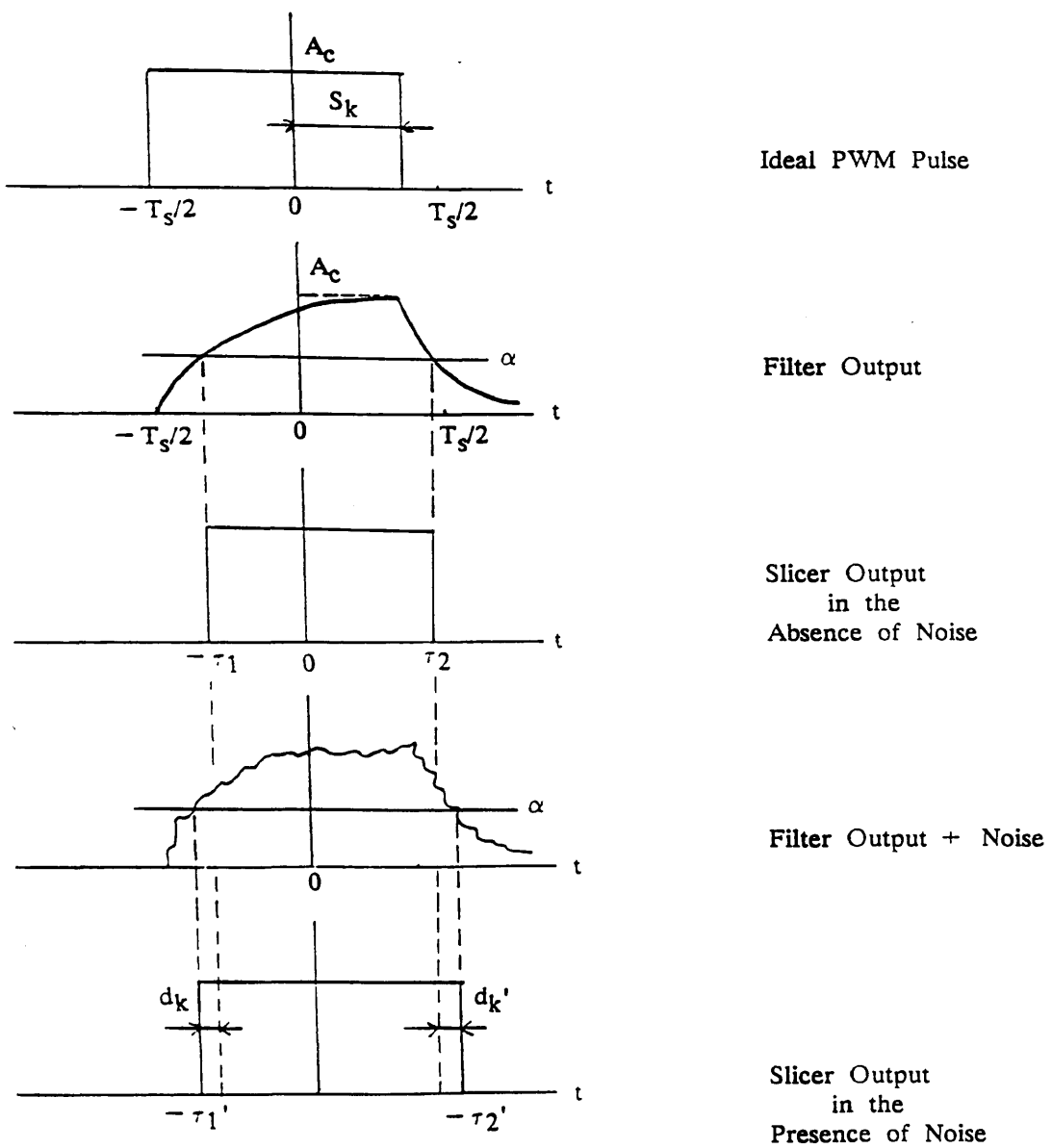


Fig.3.7 System Waveforms Of Interest.

### 3.3.2 The output noise average power

For simplicity's sake we assume that the noise power associated with the displacement  $d_k$  is equal to that associated with the displacement  $d_k'$ . We are therefore led to consider the noise associated with one of 'the two edges only. We consider for example the leading edge displacement  $d_k$  and try to find its statistics in terms of the input noise  $n_e(t)$ . When noise is absent, the pulse  $k$  crosses the slicing level  $\alpha$  at  $t = \tau_1$  that can be determined from eq.(3.4),

$$\tau_1 = T \ln(1-\alpha/A_C) + T_S/2 \quad (3.50)$$

When noise is present, the instant at which the pulse crosses  $\alpha$  is  $t = -\tau'_1$ ,

$$\tau'_1 = T \ln(1-\alpha/A_C) + T \ln\left(1 + \frac{n_e}{A_C - \alpha}\right) + T_S/2 \quad (3.51)$$

If we assume that,

$$n_e \ll A_C - \alpha \quad (3.52)$$

then,

$$\ln\left(1 + \frac{n_e}{A_C - \alpha}\right) \approx \frac{n_e}{A_C - \alpha} \quad (3.53)$$

Substituting eq.(3.53) into eq.(3.51) we get,

$$\tau'_1 = T \ln(1-\alpha/A_C) + T \frac{n_e}{A_C - \alpha} + T_S/2 \quad (3.54)$$

The displacement  $d_k$  is then,

$$d_k = \tau'_1 - \tau_1 = T \frac{n_e}{A_C - \alpha} \quad (3.55)$$

As we did before, we assume that  $\alpha$  is equal to half the carrier peak amplitude,

$$\alpha = A_C/2 \quad (3.56)$$

Substituting eq.(3.56) into eq.(3.55) we get,

$$d_k = (2T n_e)/A_C \quad (3.57)$$

Substituting eq.(3.57) into the detector band limited noise term of eq.(3.47) we get,

$$y_N(t) = \sum_{-\infty}^{+\infty} d_k \frac{\sin \pi f_S(t-kT_S)}{\pi f_S(t-kT_S)} = (2T/A_C) \sum_{-\infty}^{+\infty} n_e \frac{\sin \pi f_S(t-kT_S)}{\pi f_S(t-kT_S)} \quad (3.58)$$

The spectral density of  $y_n(t)$ , making use of appendix A8, is

$$G_{y_n}(f) = \begin{cases} (2T/A_c)^2 \sum_{-\infty}^{+\infty} G_{n_e}(f-nf_s) & |f_s| < f_s/2 \\ 0 & |f_s| > f_s/2 \end{cases} \quad (3.59)$$

The total noise average power, using eq.(A6.3), is

$$\begin{aligned} N_0 &= 2 \langle y_n^2(t) \rangle = 2 \int_{-\infty}^{+\infty} G_{y_n}(f) df = (8T^2/A_c^2) \sum_{-\infty}^{+\infty} \int_{-f_s/2}^{f_s/2} G_{n_e}(f-nf_s) df \\ &= (8T^2/A_c^2) \int_{-\infty}^{+\infty} G_{n_e}(f) df = (8T^2/A_c^2) \langle n_e^2(t) \rangle \\ &= (8T^2 N_i)/A_c^2 \end{aligned} \quad (3.60)$$

where  $N_i$  is the input white gaussian noise average power.

Substituting T by its value given by eq.(A5.3) we get,

$$N_0 = \frac{2N_i}{\pi^2 B^2 A_c^2} \quad (3.61)$$

This expression shows that  $N_0$  increases when B decreases and decreases when the peak carrier power  $A_c^2$  increases. Therefore, increasing B enables a smaller carrier power to be used.

Denoting  $A_c^2$  as  $S_c$ ,  $N_i$  as  $N_c$  and making use of eq.(3.49) we get the PWM SNR,

$$\begin{aligned} (S_o/N_o) &= (\pi^2 M^2/8)(B/f_s)^2 S_i (S_c/N_c) \\ &= (\pi^2 M^2/8) \gamma^2 S_i (S_c/N_c) \end{aligned} \quad (3.62)$$

This equation shows the improvement in SNR possible in PWM systems by widening the channel bandwidth B. However, common to all systems that exchange bandwidth for noise improvement, PWM has a threshold level below which there is no SNR improvement. This threshold level is determined in what follows.

### 3.3.3 PWM CNR threshold level

When we determined PWM SNR we assumed that,

$$n_e \ll A_c/2 \quad (3.63)$$

The mean square of  $n_e$  is,

$$\langle n_e^2 \rangle \ll A_c^2/4 \quad (3.64)$$

Substituting  $A^2_c$  by  $S_c$  and  $\langle n^2_e \rangle$  by  $N_c$  we get,

$$(S_c/N_c) \gg 4 \quad (3.65)$$

Hence, to expect an SNR improvement in PWM systems the CNR should be much greater than 6dB.

### 3.3.4 PWM SNR improvement for a sinusoidal modulating signal

We assume a normalised modulating signal  $sn(t)$ ,

$$sn(t) = \sin(\omega_m t) \quad (3.66)$$

Its average power is,

$$S_i = \langle sn^2(t) \rangle = 1/2 \quad (3.67)$$

substituting eq.(3.67) into eq.(3.62) we get,

$$(S_o/N_o) = (\pi^2 M^2 / 16) \gamma^2 (S_c/N_c) \quad (3.68)$$

The SNR improvement factor  $I$  is defined as the SNR to CNR ratio

$$I = \frac{(S_o/N_o)}{(S_c/N_c)} = \pi^2 M^2 \gamma^2 / 16 \quad (3.69)$$

Eq.(3.69) can be written as follows,

$$\gamma = (4\sqrt{I})/\pi M \quad (3.70)$$

This equation is plotted in Fig.3.8 for  $I = 0.8, 2.3, 3.5\text{dB}$ .

### 3.3.5 PWM SNR improvement for a uniformly distributed random variable

We have seen that the p.d.f of the normalised random variable  $sn$  was,

$$f(sn) = 1/2 \quad (3.71)$$

Its average power is,

$$S_i = \langle sn^2 \rangle = \int_{-1}^{+1} sn^2 f(sn) dsn = 1/3 \quad (3.72)$$

Substituting eq.(3.72) into eq.(3.62) we get,

$$\gamma = (\sqrt{24 I})/\pi M \quad (3.73)$$

A plot of eq.(3.73) is given in Fig.3.9 for  $I = 0.8, 2.3, 3.5\text{dB}$ .

### 3.4 BANDWIDTH - MODULATION INDEX RELATIONSHIP FOR GIVEN $D_x$

To plot  $\gamma$  in terms of  $M$  for given distortion levels, eq.(3.74) for a sinusoidal modulating signal,

$$D_1 = (e^{-\pi\gamma}/2\pi\gamma) [ I_0(M\pi\gamma) + (1/2) e^{-\pi\gamma} I_0(2M\pi\gamma) + (1/3) e^{-2\pi\gamma} I_0(3M\pi\gamma) ] \quad (3.74)$$

and eq.(3.75) for a uniformly distributed random variable,

$$D_2 = (e^{-\pi\gamma}/4\pi^2\gamma^2) [ 2 \sinh(\pi\gamma M) + (1/2) e^{-\pi\gamma} \sinh(2\pi\gamma M) + (2/9) e^{-2\pi\gamma} \sinh(3\pi\gamma M) ] \quad (3.75)$$

must be solved for given  $D_1$  and  $D_2$ . Since these equations are non linear a numerical computation is unavoidable. Each of the preceding equations has been solved for  $D_1$  and  $D_2$  equal to  $-25.0$ ,  $-27.5$ ,  $-30.0$ dB. Plots of eqs.(3.74) and (3.75) are given in Figs.3.8 and 3.9 respectively.

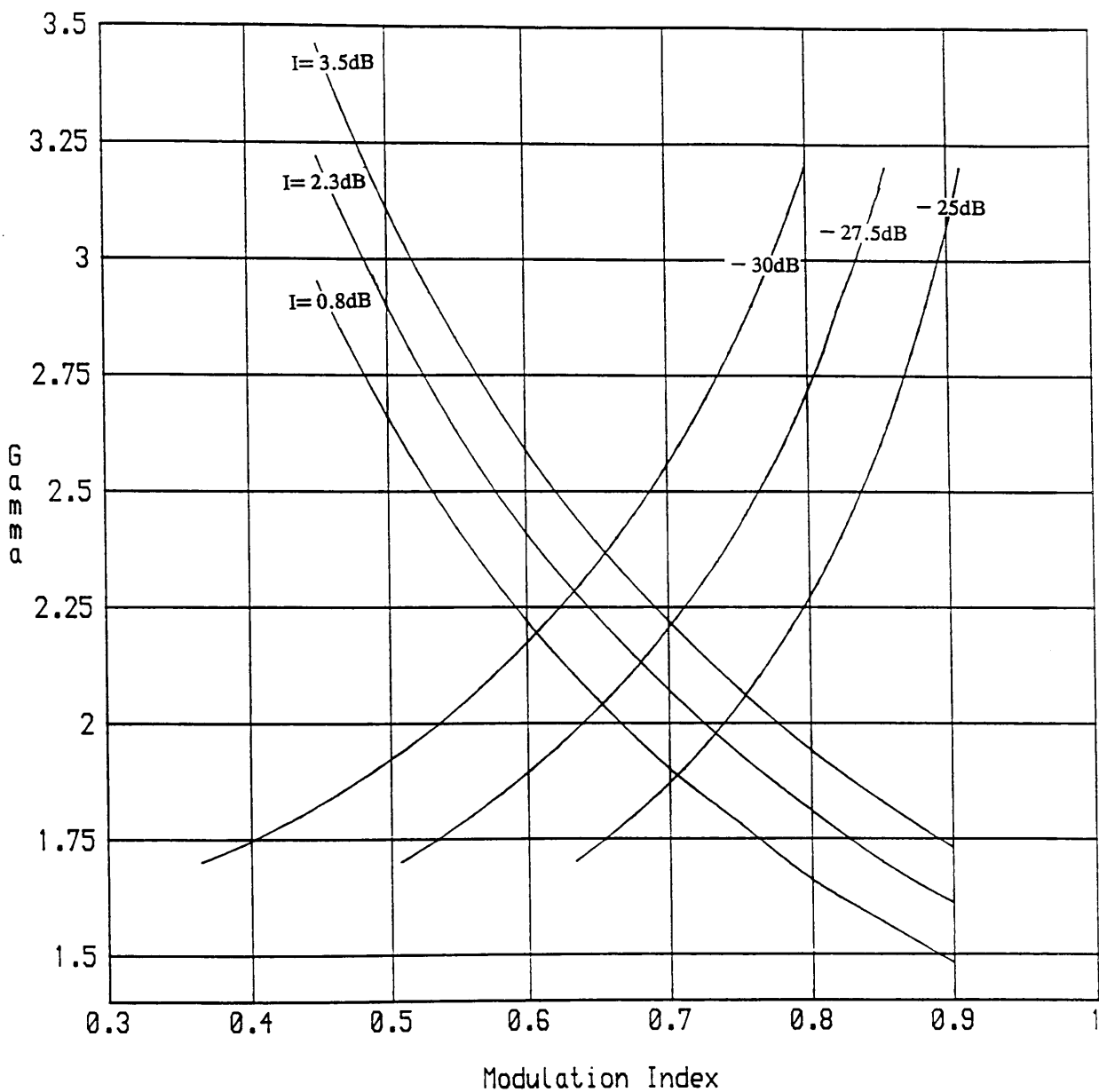


**Fig.3.8 Bandwidth Versus Modulation Index For A Sinusoidal Modulating Signal.**

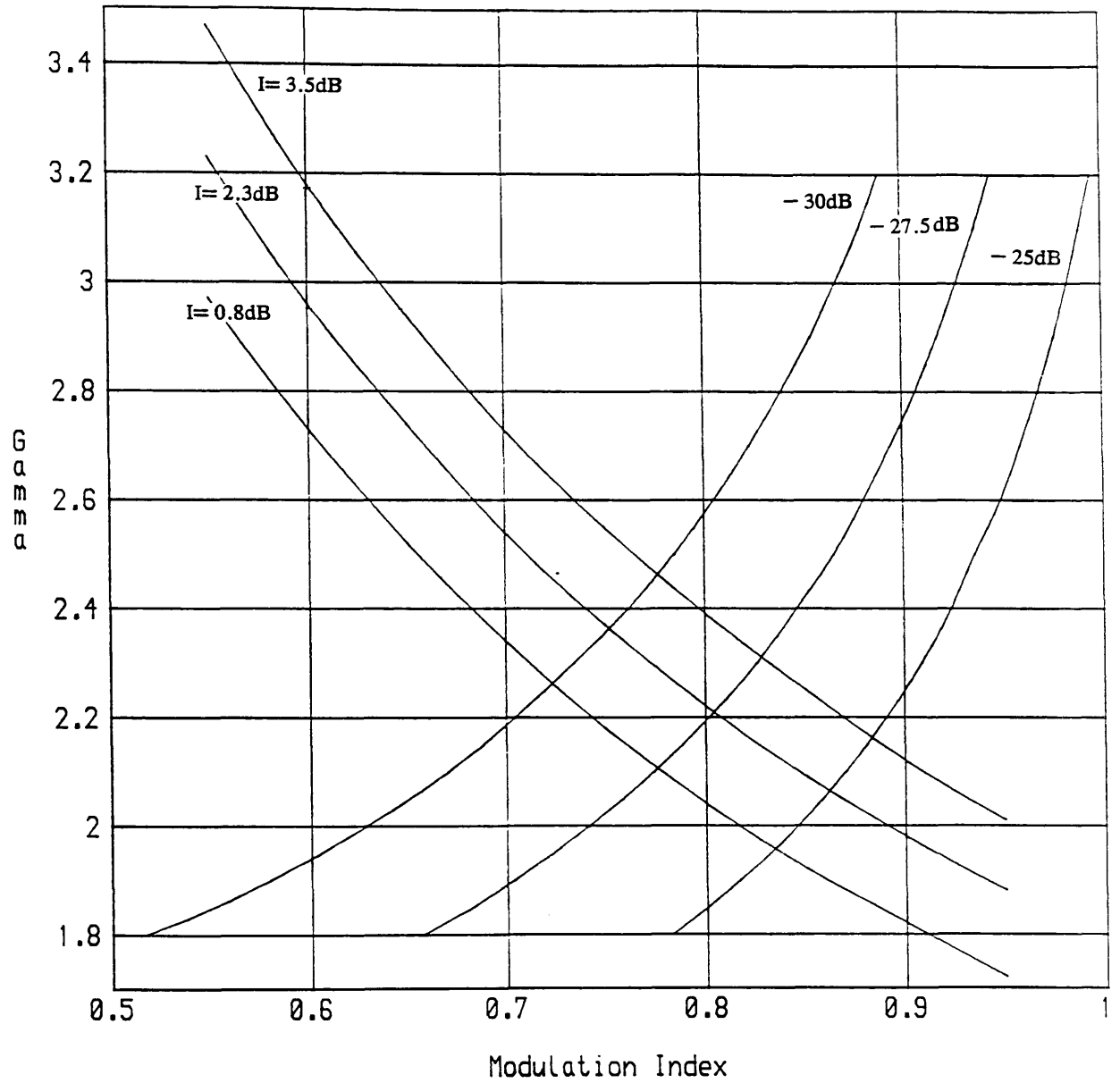


**Fig.3.9 Bandwidth Versus Modulation Index For A Uniformly Distributed Random Variable.**

### 3.5 PCM SNR IN THE PRESENCE OF ISI

In this paragraph we will determine the PCM SNR in the presence of white gaussian noise and ISI due to the channel bandwidth limitation. This SNR is given in terms of  $P_e$  (probability of error). The exhaustive method calculates  $P_e$  by taking into account all the possible states of the received binary PCM signal using an  $N$  sample approximation. This method is too time consuming because the computation involved grows exponentially with  $N$  ( $2^N$  states of  $N$  truncated pulse train). In ref.7, a method giving  $P_e$  in terms of the first  $2k$  moments of the ISI is considered. As before, to be able to carry out the computation, we assume that the receiver overall characteristic is reduced to that of an RC filter. The block diagram of such a receiver is given in Fig.3.10.

We assume a non return to zero (NRZ) PCM binary signal at the input of the RC filter,

$$s(t) = \sum_{-\infty}^{+\infty} a_m \text{rec}(t-mT_0) \quad (3.76)$$

where  $\text{rec}(t)$  is a rectangular pulse of width  $T_0$  and amplitude  $A_c/2$ , and  $a_m$  a sequence of binary bipolar random variables equal to  $\pm 1$  and satisfying,

$$P(a_m=+1) = P(a_m=-1) = 1/2 \quad (\text{i.e. equiprobable events}) \quad (3.77)$$

The RC low pass filter output signal  $y(t)$  is,

$$y(t) = \sum_{-\infty}^{+\infty} a_m r(t-mT_0) + n_0(t) \quad (3.78)$$

where  $n_0(t)$  is the filter output noise and,

$$r(t) = \text{rec}(t)*h(t) \quad (3.79)$$

$h(t)$  is the RC filter impulse response given by eq.(A2.4) namely,

$$h(t) = (1/RC) e^{-t/RC} u(t) = (1/T) e^{-t/T} u(t) \quad (3.80)$$

The filter input and output signals are sketched in Fig.3.11.

At the sampling instant  $t_s$  the filter output is,

$$y(t_s) = a_{N-1} r(t_s) + \sum_{m=0}^{N-2} a_m r(t_s-mT_0) + n_0(t_s) \quad (3.81)$$

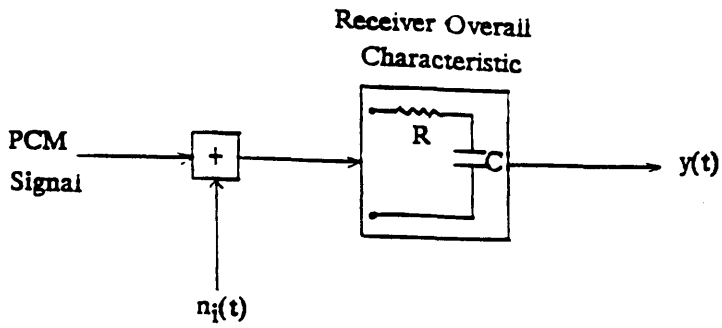


Fig.3.10 A PCM Receiver Model.

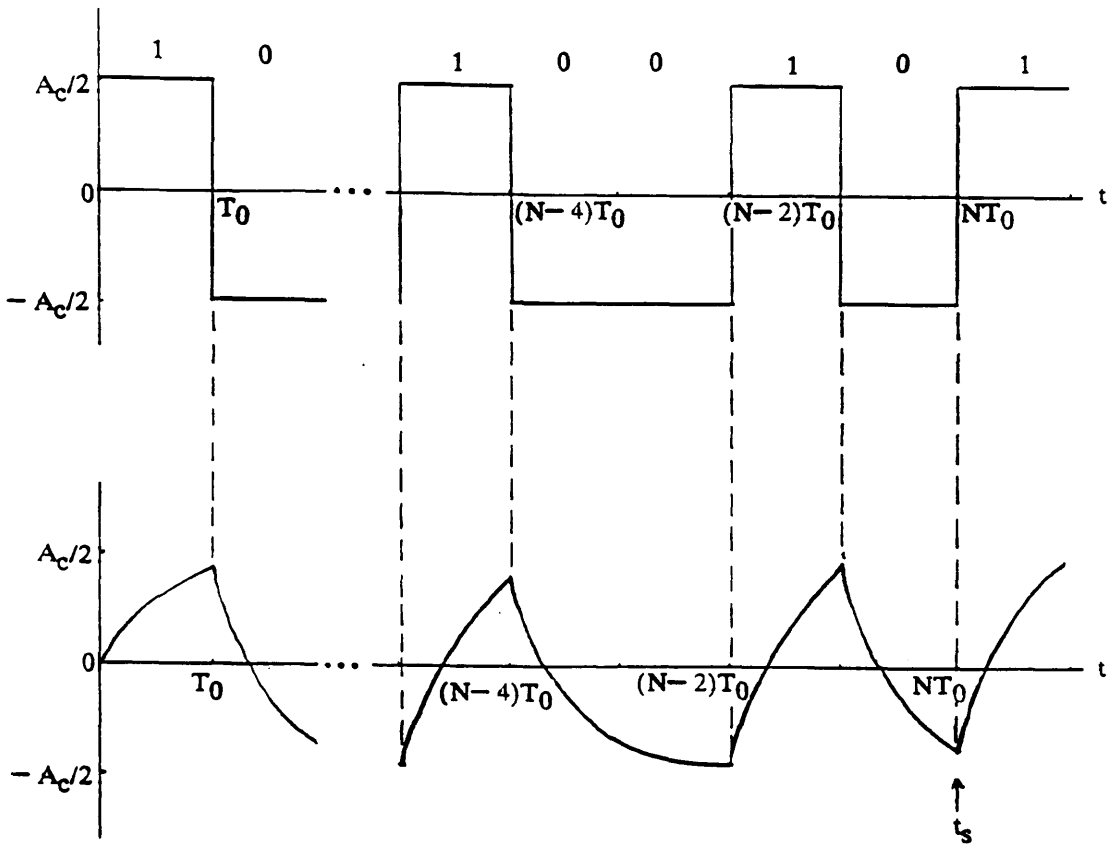


Fig.3.11 An Example Of A PCM Signal And Its Corresponding Filter Output.

The first term of eq.(3.81) is the desired signal while the second and the third are the ISI and white gaussian noise respectively.

The signal  $r(t)$  can be written as follows,

$$r(t) = \text{rec}(t) * h(t) = \int_{-\infty}^{+\infty} h(t') \text{rec}(t-t') dt' \quad (3.82)$$

The rectangular pulse  $\text{rec}(t)$  can be decomposed into two step functions,

$$\text{rec}(t) = (A_C/2) u(t) - A_C u(t-T_0) \quad (3.83)$$

Since the RC filter is a realistic one, the integration limits are from 0 to  $\infty$ .

Substituting eq.(3.84) into eq.(3.83) we get,

$$r(t) = -A_C/2 + A_C [1 - (1/2) e^{-T_0/T}] e^{-(t-T_0)/T} \quad (3.84)$$

The ISI caused by the 1<sup>st</sup> pulse at the sampling instant  $t_s$  is

$$I(t_s) = r(t_s) + A_C/2 = A_C [1 - (1/2) e^{-T_0/T}] e^{-(t_s-T_0)/T} \quad (3.85)$$

The even moments of the total ISI, at the sampling instant  $t_s$ , are given by ref.7, these are,

$$M_{2k} = \sum_{i=1}^k (-1)^{i+1} \binom{2k-1}{2i-1} M_{2(k-i)} \frac{2^{2i} (2^{2i}-1)}{2^i} |B_{2i}|$$

$$\sum_{m=0}^{N-2} I^{2i}(t_s - mT_0) \quad (3.86)$$

where  $B_{2i}$  are the Bernoulli numbers given in ref.8, and

$$\binom{2k-1}{2i-1} = \frac{(2k-1)!}{(2k-2i)!(2i-1)!} \quad (3.87)$$

Since the  $a_m$  are independently distributed random variables with 0 mean,

$$M_{2k+1} = 0 \quad \text{for } k = 0, 1, 2, 3, \dots, N \quad (3.88)$$

To find the even moments we should first compute the following summation,

$$S = \sum_{m=0}^{N-2} I^{2i}(t_s - mT_0) \quad (3.89)$$

Substituting eq.(3.85) into eq.(3.89) we get,

$$S = \sum_{m=0}^{N-2} I^{2i}(t_s - mT_0)$$

$$\begin{aligned}
&= A^{2i} c [1 - (1/2) e^{-T_0/T}]^{2i} \sum_{m=0} e^{-2i[t_s - (m+1)T_0]/T} \\
&= A^{2i} c [1 - (1/2) e^{-T_0/T}]^{2i} [e^{-2i(t_s - T_0)/T} + e^{-2i(t_s - 2T_0)/T} \\
&\quad + \dots + e^{-2i(t_s - (N-1)T_0)/T}] \quad (3.90)
\end{aligned}$$

Substituting  $t_s$  by  $NT_0$  eq.(3.90) becomes,

$$\begin{aligned}
S &= A^{2i} c [1 - (1/2) e^{-T_0/T}]^{2i} [e^{-2iT_0/T} + e^{-4iT_0/T} + e^{-6iT_0/T} \\
&\quad + \dots + e^{-2i(N-1)T_0/T}] \quad (3.91)
\end{aligned}$$

The expression between brackets is a geometric progression of reason  $e^{-2iT_0/T}$ , therefore, eq.(3.91) can be written as,

$$S = A^{2i} c [1 - (1/2) e^{-T_0/T}]^{2i} \frac{e^{-2iT_0/T}}{1 - e^{-2iT_0/T}} \quad (3.92)$$

Substituting eq.(3.92) into eq.(3.86) we find,

$$\begin{aligned}
M_{2k} &= \sum_{i=1}^k (-1)^{i+1} \binom{2k-1}{2i-1} M_{2(k-i)} \frac{2^{2i} (2^{2i-1})}{2^i} |B_{2i}| A^{2i} c \\
&\quad [1 - (1/2) e^{-T_0/T}]^{2i} \frac{e^{-2iT_0/T}}{1 - e^{-2iT_0/T}} \quad (3.93)
\end{aligned}$$

For a number of bits  $n$  and a sampling rate  $f_s$ , the PCM signal bit rate is,

$$f_0 = nf_s \quad \text{i.e.} \quad T_0 = T_s/n \quad (3.94)$$

Substituting eqs.(3.94) and (A5.3) into eq.(3.93) we finally get,

$$\begin{aligned}
M_{2k} &= \sum_{i=1}^k \binom{2k-1}{2i-1} (-1)^{i+1} M_{2(k-i)} \frac{2^{2i} (2^{2i-1})}{2^i} |B_{2i}| A^{2i} c \\
&\quad [1 - (1/2) e^{-4\pi i B/nf_s}]^{2i} \frac{e^{-4\pi i B/nf_s}}{1 - e^{-4\pi i B/nf_s}} \quad (3.95)
\end{aligned}$$

Knowing that  $M_0 = 1$ , all the higher order moments can be obtained via eq.(3.95).

The probability of error  $P_e$  in the presence of both ISI and white gaussian noise is given in ref.7, this is

$$\begin{aligned}
P_e &= (1/2) \operatorname{erfc}(A_c/2\sigma\sqrt{2}) + \\
&\quad e^{-(A_c/\sigma)^2/16} \sum_{j=1}^{+\infty} \frac{M_{2j}}{(2j)! \sigma^{2j}} H_{2j-1}(A_c/2\sigma\sqrt{2}) \quad (3.96)
\end{aligned}$$

where  $\sigma$  is the white gaussian noise rms and the  $H_j(x)$  are the Hermite polynomials

given by,

$$\begin{aligned}
 H_{n+1}(x) &= x H_n(x) - n H_{n-1}(x) \\
 H_0(x) &= 1 \\
 H_1(x) &= x
 \end{aligned}
 \tag{3.97}$$

The first term of eq.(3.96) is the  $P_e$  in the absence of ISI. Ref.7 pointed out that only the five first terms of the summation of eq.(3.96) suffice for the computation of  $P_e$ .

We let  $(A_c/\sigma)^2$  be the peak carrier to noise ratio CNR,

$$(A_c/\sigma)^2 = (S_c/N_c)
 \tag{3.98}$$

Knowing the moments  $M_{2k}$  and the Hermite polynomials, PCM output SNR in the presence of ISI can be computed through the following equation.

$$(S_0/N_0) = \frac{2^{2n} - 1}{1 + 4 P_e(2^{2n-1})}
 \tag{3.99}$$

Eq.(3.99) is plotted in Fig.3.12 for  $B = 40\text{MHz}$ ,  $f_s = 13.34\text{MHz}$  and  $n = 4, 5$ , and 6. In the same figure the curves of PCM SNR in the absence of ISI, for  $n = 5$ , and PWM SNR, for  $B = 40\text{MHz}$ , are given as well. These curves show that in the presence of ISI, PCM SNR can be worse than PWM SNR and this for  $\text{CNR} < 20\text{dB}$ .

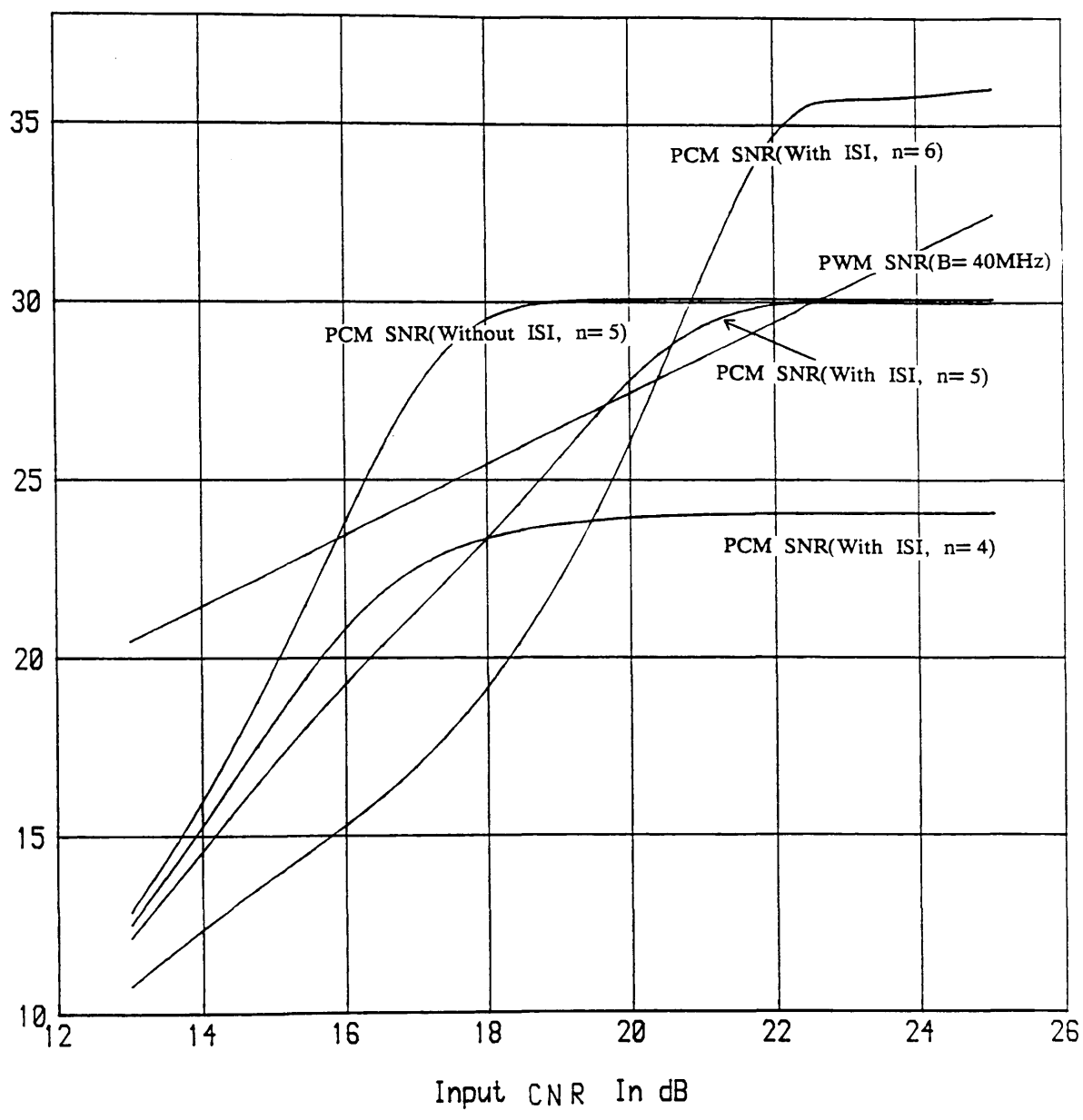


**Fig.3.12 Comparison Of PCM And PWM SNRs In Presence Of ISI.**

### 3.6 CONCLUSION

We showed in this chapter how the channel limitation bandwidth causes pulse distortion. The latter was computed for two types of modulating signals: one deterministic, the other random. For both types of signals, this distortion depended on  $B$  and  $M$ . In fact, it increases when  $M$  increases and decreases with increasing  $B$ . To keep the distortion low, we should either decrease  $M$  or increase  $B$ . Increasing  $B$  beyond the affordable value is a waste of bandwidth and makes the constraints on the receiver severe (short  $T_r$ ). An easy solution seemed to be a choice of a moderate  $M$ , but at the expense of a degradation in the output SNR, since the latter is proportional to the square of  $M$ . To make a compromising choice of these critical factors ( $M$ ,  $\gamma$ ,  $B$ , SNR,  $D_k$ ), curves taking into account all these parameters are given. Finally, to prove the feasibility of PWM with US systems, its SNR and PCM SNR were compared for a typical value of  $B$ . This comparison was found to be in favor of PWM for  $CNR < 20\text{dB}$  when the number of bits used,  $n$ , is less or equal than 5.

4.1 INTRODUCTION

Lightwave systems can be classified in terms of their evolution through four generations of technology. The first of these uses multimode fibers at an operating wavelength of about  $0.85\mu\text{m}$ . The second generation operates at a longer wavelength  $1.3\mu\text{m}$ . The shift to this wavelength permits greater separation between repeaters in a long distance transmission system. Most of the second generation systems use single mode fibers rather than multimode. The evolution beyond the second generation is unclear because the  $1.3\mu\text{m}$  systems are still relatively new. It seems probable, however, that the third generation will use a still longer wavelength,  $1.55\mu\text{m}$  where the attenuation of silica based fibers is at a minimum. Further improvement in lightwave systems beyond the third generation might come from the introduction of coherent optical techniques. Tab.4.1 summarises the characteristics of the four mentioned generations.

Generations	First	Second		Third	Fourth
Fiber type	multimode	few mul.mode	most sing.mode	sing. mode	sing. mode
Operating wavelength( $\mu\text{m}$ )	0.85	1.3		1.55	1.55
Sources	LEDs	LEDs	InGaAs	Ge LDs	LDs
	AlGaAs LDs		Ge LDs		
Detectors	Si PINs	InGaAs	PINs	InGaAsP	PINs
	Si APDs	Ge	APDs		
Loss (dB/Km)	2.5	0.6	0.4	0.25	<0.2
Disp._limited bit rate_dist. product (Gbit.Km/s)	0.01(step n)	4	250	17	900
	4(graded n)			300 <sup>(1)</sup>	

Tab.4.1 The four generations of lightwave technology.

(1) For single frequency lasers

## 4.2 FIBER STRUCTURE

An optical fiber is a cylindrical dielectric that operates at optical wavelengths. It consists of a core of refractive index  $n_1$ , covered by a thin cladding of a lower refractive index  $n_2$  covered by a buffer coating, see Fig.4.1.

Both the step index and graded index fibers can be further divided into single mode and multimode. Only three of them are of major importance: single mode step index, multimode step index, and multimode graded index. As the name implies a single mode fiber supports only one waveguide mode, whereas a multimode fiber supports hundreds of modes. For optical fibers there are three types of ray paths: central, meridional, and helical rays. Meridional rays pass through the center of the fiber undergoing total internal reflections and are confined to a single plane. For graded index fibers the rays follow smooth curves rather than the zig zag of the step index fibers. Skew rays are not confined to a single plane, instead, they tend to follow a helical path along the fiber. These rays travel longer distances than meridional rays but faster. Fig.4.3 shows typical sizes of single mode and multimode fibers along with the mentioned ray paths.

### 4.2.1 Fiber types

If the refractive index is uniform throughout the core and undergoes an abrupt change (step) at the cladding boundary, the fiber is called step index fiber. However, if the core refractive index is made to vary as a function of the radial distance from the center of the fiber, the latter is called graded index fiber. Both fibers types are illustrated in Fig.4.2.

### 4.2.2 Snell's law

To have total internal reflection the angle of incidence must be greater than the critical angle  $\theta_c$ , this is known as Snell's law. An illustration of this is given in Fig.4.4. The critical angle is,

$$\theta_c = \sin^{-1}(n_2/n_1) \quad (4.1)$$

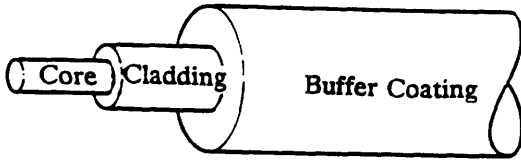


**Fig.4.1 Schematic Of The Fiber Structure.**

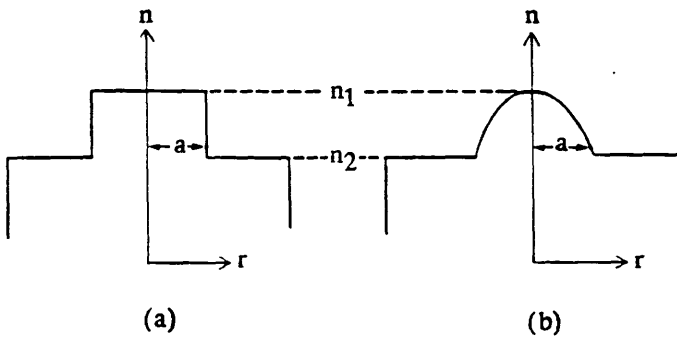


**Fig.4.2 Refractive Index Profiles For (a) Step Index And (b) Graded Index Fibers.**

Index Profile	Fiber Cross Section And Ray Paths	Typical Dimensions
	<p>Single Mode Step Index Fiber</p>	$125\ \mu\text{m}$ (Cladding) $8-12\ \mu\text{m}$ (Core)
	<p>Multimode Step Index Fiber</p>	$125-400\ \mu\text{m}$ (Cladding) $50-200\ \mu\text{m}$ (Core)
	<p>Multimode Graded Index Fiber</p>	$125\ \mu\text{m}$ (Cladding) $50\ \mu\text{m}$ (Core)

**Fig.4.3 Single Mode And Multimode Fibers Cross Sections And Ray Paths.**

The angle  $\gamma$  that the ray in the external medium makes with the normal to the end of the fiber is related to the internal angle  $\theta$  by Snell's law,

$$\sin\gamma = (n_1/n_0) \cos\theta \quad (4.2)$$

Fig.4.5 gives an illustration of a meridional ray as it enters a step index fiber. The maximum value that  $\gamma$  can take is determined by the minimum value of  $\theta$  which is  $\theta_c$ . This maximum angle is known as the fiber acceptance angle.

$$\sin\gamma_{\max} = (n_1\sqrt{2\Delta})/n_0 = NA/n_0 \quad (4.3)$$

where NA is known as the fiber numerical aperture and  $\Delta$  the index difference given by,

$$\Delta = (n_1 - n_2)/n_1 \quad (4.4)$$

The cladding refractive index  $n_2$  in terms of  $\Delta$  is,

$$n_2 = n_1(1-\Delta) \quad (4.5)$$

### 4.3 FIBER DISPERSION

Fiber dispersion causes the transmitted pulses to spread out and to overlap as they propagate, so they become indistinct at the receiver. As the bit rate increases, dispersive effects become more important. Dispersion manifests itself as a reduction in the high frequency of the transfer function of the fiber. An equaliser can be used, at the receiver, to boost the attenuated high frequency components. Along with the signal enhancement, however, comes an unavoidable increase in noise. By increasing the transmitter power we can compensate for the enhanced noise. This added transmitter power is called the dispersion penalty. To have a dispersion penalty of less than 1dB, the following condition should be satisfied,

$$\sigma_t B \ll 1/4 \quad (4.6)$$

where  $\sigma_t$  is the fiber impulse response rms width and B the bit rate.  $\sigma_t$  is expected to increase with the fiber length. The maximum fiber length that satisfies eq.(4.6) is called the dispersion-limited transmission distance. There are two types of dispersion: intramodal and intermodal.

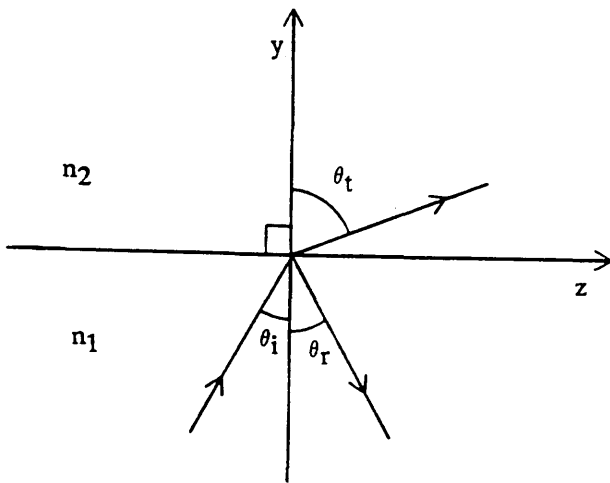


Fig.4.4 Illustration Of The Behavior Of A Light Ray Incident On The Junction Between Two Media With Refractive Indices  $n_1$  And  $n_2$ .

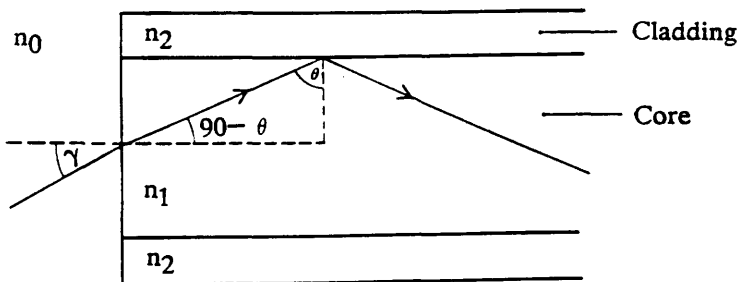


Fig.4.5 Illustration Of The Path Of A Meridional Ray As It Enters A Circular Step Index Waveguide.

### 4.3.1 Intramodal dispersion

It manifests itself as pulse spreading within a single mode. It is a result of the group velocity being a function of the wavelength. Hence, it increases with the spectral width  $\sigma_\lambda$  of the source.

The two main causes of intramodal dispersion are material and waveguide dispersions.

#### 4.3.1.1 Material dispersion

It occurs because the refractive index is a function of wavelength  $\lambda$ , hence, the various spectral components of the source will travel at different speeds. This dispersion is of importance in light emitting diodes (LEDs) systems (because LEDs have important spectral widths). After a pulse travel  $L$  Km through a fiber, it broadens to an rms width,

$$\sigma_t = D L \sigma_\lambda \quad (4.7)$$

where  $D$  is the material dispersion coefficient that can be determined, for silica-based fibers ( $\text{SiO}_2$ ), from Fig.4.6.

We should point out that material dispersion dominates at lower wavelengths and goes to zero at about  $1.3\mu\text{m}$  for silica-based fibers. This kind of dispersion can be reduced by either choosing sources with narrow spectral widths or by operating at higher wavelengths.

Substituting eq.(4.7) into eq.(4.6) we get the dispersion-limited bit rate-distance product,

$$B L \leq (4D \sigma_\lambda)^{-1} \quad (4.8)$$

#### 4.3.1.2 Waveguide dispersion

It occurs because the modal propagation constant  $\beta$  is a function of  $a/\lambda$  which is the ratio of the fiber core radius to the wavelength. For multimode fibers, waveguide dispersion is very small compared to material dispersion and can, therefore, be neglected. For single mode fibers, however, waveguide dispersion is of importance. Inspection of Fig.4.6 shows that at about  $1.3\mu\text{m}$  the material dispersion

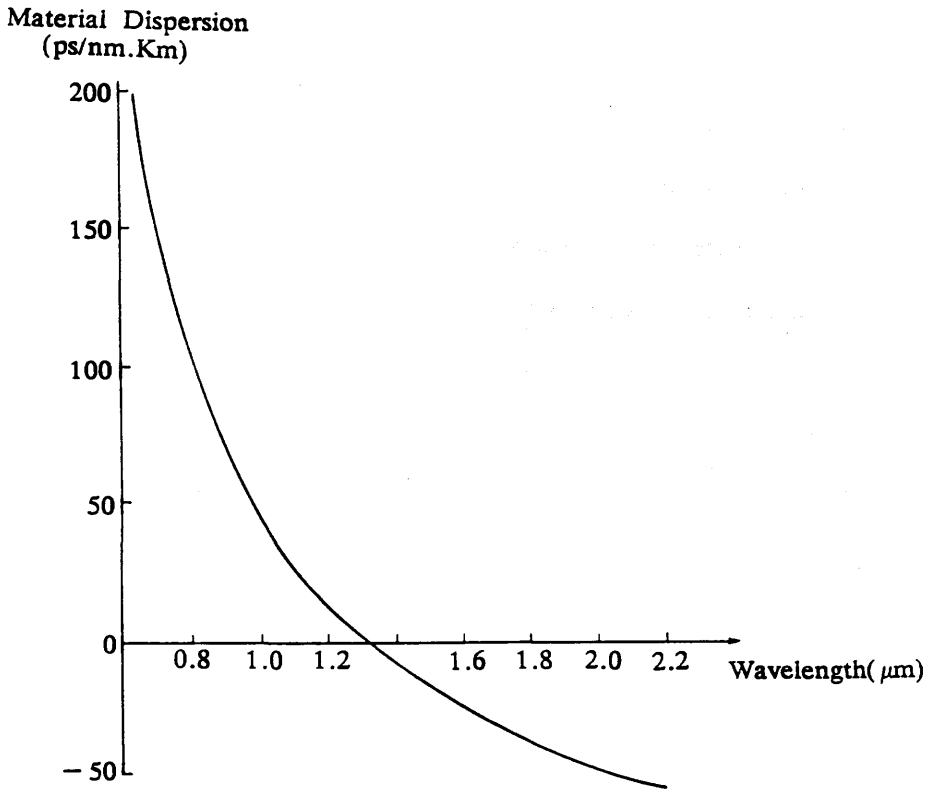


**Fig.4.6 Material Dispersion For Pure Silica(SiO<sub>2</sub>).**

coefficient D becomes zero, and above this value it has the opposite sign to the waveguide dispersion. It is, therefore, possible to obtain zero total dispersion in the region 1.3 to 1.8  $\mu\text{m}$  for specially designed single mode fibers. This region is also of interest since it is a low attenuation region.

#### 4.3.2 Intermodal dispersion

It is a result of different values of the group delay for each mode. The high order modes have a longer travel time than the low order modes, therefore, simultaneously launched rays will suffer dispersion on arrival. The steeper the angle of propagation of the ray, the higher is the mode and, therefore, the slower is the axial group velocity.

The rms full width of the broadened impulse due to the difference of time taken for the slowest and fastest modes to travel a distance L along a step index fiber is,

$$2\sigma_t = (Ln_1\Delta)/C = L(NA)^2/(2Cn_1) \quad (4.9)$$

Substituting eq.(4.6) into eq.(4.9) we get the dispersion-limited bit rate-distance product,

$$B L \leq C/(2\Delta n_1) \quad (4.10)$$

Modal dispersion can be reduced in step index fibers by reducing the NA to allow only the dominant mode to propagate. Orders of magnitude reduction in modal dispersion can be obtained by using graded index fibers for which the effect is compensated for by the high order modes travelling further than low order modes but faster. Typically, a parabolic profile is used and rays which stay near the core center travel relatively slowly because they are in the region of high n. On the other hand, rays which make wide excursions toward the cladding traverse longer paths, but they travel faster for they spend more time in lower index material.

The variation in the refractive index, is often expressed in the form,

$$n(r) = \begin{cases} n_1[1 - 2\Delta(r/a)^\alpha]^{1/2} & 0 \leq r \leq a \\ n_1(1-2\Delta)^{1/2} \approx n_1(1-\Delta) & r > a \end{cases} \quad (4.11)$$

The parameter  $\alpha$  called the profile parameter determines the core index variations. Fig.4.7 shows the variation in modal dispersion in graded index fibers in terms of  $\alpha$ .

Mode Dispersion  
(ns/Km)

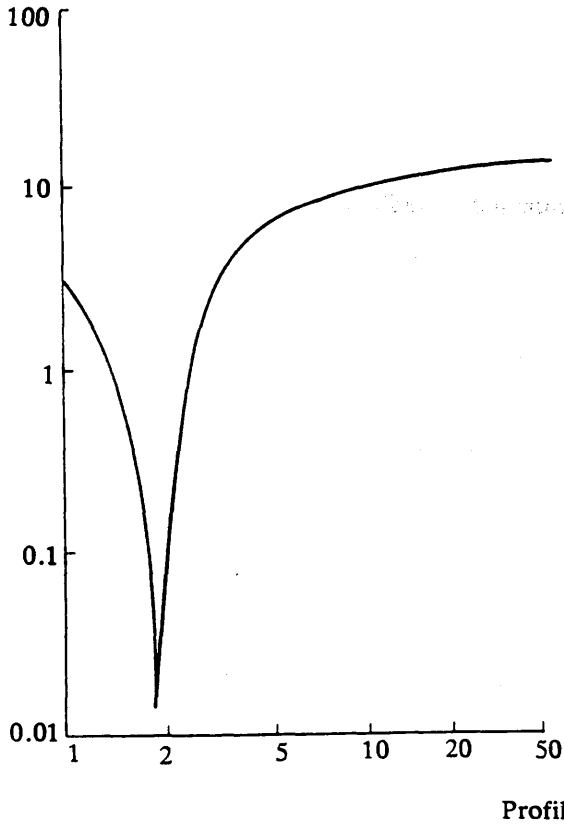


Fig.4.7 Intermodal Dispersion In A Graded Index Fiber As A Function Of The Profile Index  $\alpha$ .

This curve shows a very sharp minimum dispersion at a profile  $\alpha \approx 2$ . The graded index fibers show a pulse spreading quadratic in  $\Delta$  rather than the linear behaviour shown in eq.(4.9) for step index fibers.

$$\sigma_t = n_1 L \Delta^2 / (8C) \quad (4.12)$$

Substituting eq.(4.7) into eq.(4.12) we get the dispersion-limited bit rate-distance product,

$$B L \leq 2C / (n_1 \Delta^2) \quad (4.13)$$

#### 4.4 FIBER LOSSES

The knowledge of the fiber attenuation enables the determination of the maximum transmission distance. The power level at a distance  $L$  from the transmitter is,

$$P_r(L) = P_t 10^{-(AL/10)} \quad (4.14)$$

where  $A$  is the fiber attenuation given in dB.

There are two categories of fiber losses: those resulting from the distortion of the fiber from the ideal straight line configuration, radiative losses, and those which are inherent in the fiber itself, scattering and absorption losses.

##### 4.4.1 Radiative losses

They occur whenever a fiber undergoes a bend of finite radius of curvature. Fibers can be subject to bends having radii larger than the fiber radius, for example, when a fiber turns a corner, and to microbends of the fiber axis that can arise when the fibers are incorporated into cables, this kind of loss is called microbending loss. The microbendings are to be avoided because as the radius of curvature decreases the loss increases exponentially. This loss can be represented by an absorption coefficient  $\alpha_b$  given by,

$$\alpha_b = K e^{-R_c (NA)^2 / a} \quad (4.15)$$

where  $K$  is a constant,  $R_c$  the radius of curvature of the fiber bend see Fig.4.8.

#### 4.4.2 Scattering losses

They occur from the structural or compositional disorder of glasses. In structural disorder the same basic molecular units are present throughout the material but these are connected together in a random way. In compositional disorder, on the other hand, the exact chemical composition varies from place to place. Whichever of these types of disorder is present the net effect is a fluctuation in the refractive index occurring within the glass over distances small compared to the wavelength  $\lambda$ . This type of scattering is known as Rayleigh scattering, the loss associated with this scattering is,

$$A = 0.6/\lambda^4 \text{ dB/Km} \quad (4.16)$$

where  $\lambda$  is the free space wavelength in  $\mu\text{m}$ .

#### 4.4.3 Absorption losses

They are caused mainly by the presence of impurities particularly traces of transition metal ions ( $\text{Fe}^{3+}$ ,  $\text{Cu}^{2+}$ ) or hydroxyl ( $-\text{OH}$ ) ions. The latter have strong absorption peaks at 0.95, 1.24, and  $1.39\mu\text{m}$ . A plot of attenuation versus  $\lambda$  for a silica-based fiber is given in Fig.4.9.

### 4.5 OPTICAL SOURCES

There are two groups of light sources for optical communication:

- AlGaAs devices for the 800 – 900nm wavelength region.
- InGaAsP devices for the 1100 – 1600nm wavelength region.

The use of a specific light source is dictated by the type of application needed. LEDs present broad light spectra which set a limit to the bit rate because of the modal dispersion and wide beam divergence which causes a poor power coupling to the fiber. However, they have better drive current – output power linearity, smaller temperature dependence of the emitted power, they are inexpensive and easy to drive than laser diodes (LDs). The latter have much higher output power and narrower beam divergence which enable them to couple more power into the fiber than the LEDs. They are specially useful for small core diameter, and low NA

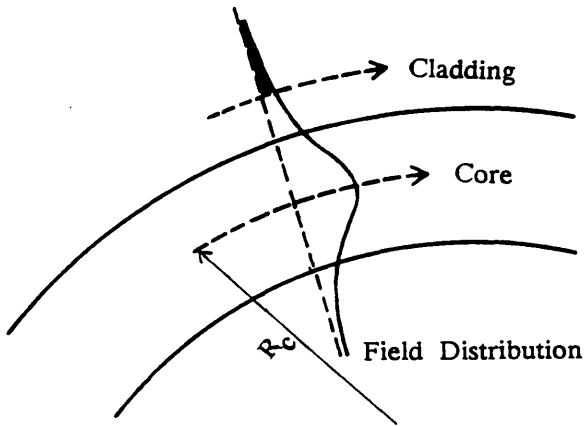


**Fig.4.8 Illustration Of The Electric Field Through A Bent Fiber.**

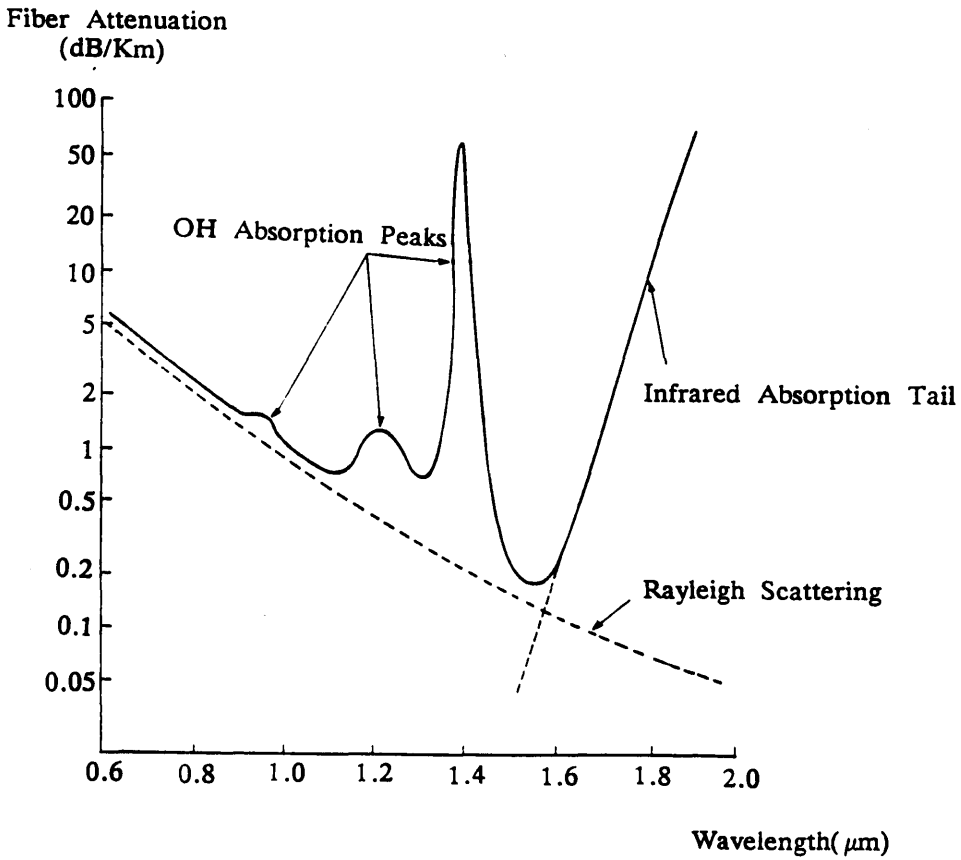


**Fig.4.9 Typical Attenuation Versus Wavelength Plot For A Silica-Based Fiber.**

fibers, in particular single mode fibers. Lasers modulation bandwidths are significantly larger than those of LEDs because the carriers recombination times are shortened appreciably by the action of stimulated emission. However, they are expensive and require high temperature control.

Eight

#### 4.5.1 LEDs response time

The factors that ultimately affect the modulation bandwidths of LEDs are the junction capacitance and the carriers' life time in the recombination region. Ref.11 shows that the LED frequency response can be written, in the case where the carrier life time is the dominating effect, as

$$R(f) = \frac{R(0)}{\sqrt{1 + 4\pi^2 f^2 \tau^2}} \quad (4.17)$$

where  $\tau$  is the minority carrier life time.

From eq.(4.17), the half power bandwidth is,

$$B_{3dB} = \sqrt{3}/(2\pi\tau) \quad (4.18)$$

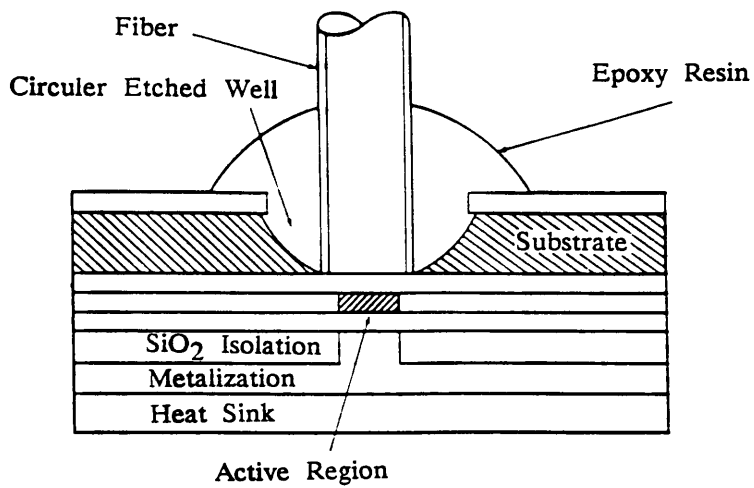
In GaAs LEDs a typical value of  $\tau$  would be 1ns, giving a half power bandwidth  $B_{3dB} = 300\text{MHz}$ .

In many sub 50Mbit/s applications LEDs are preferred to LDs. This tendency is even stronger for the 1100 – 1600nm LEDs wavelength region where silica-based fibers suffer least attenuation and glass dispersion can approach zero near 1300nm.

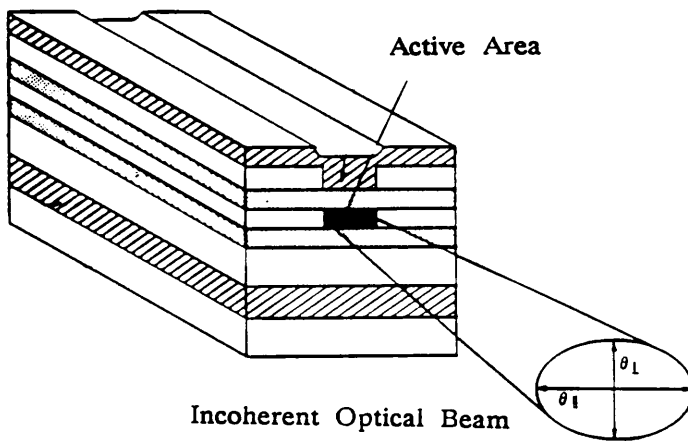
There are two types of LEDs: surface emitter and edge emitter.

#### 4.5.2 Surface emitter LEDs

In the surface emitters a well is etched through the GaAs substrate to enable the fiber end to be very close to the light emitting region, to couple as much power as possible to the fiber end. The fiber is held in position by the use of a transparent epoxy resin which also helps to reduce Fresnel losses.



(a)



(b)

**Fig.4.10 Schematic Of (a) A Surface Emitter And (b) An Edge Emitter LED s.**

### 4.5.3 Edge emitter LEDs

In the edge emitter the radiation is confined to a narrow channel. On emerging, the beam divergences tend to be narrower than those of the surface types. Thus for very thin active layers the emitted radiation half power beam width in the plane perpendicular to the junction is reduced to  $\theta_{\perp} = 30^{\circ}$ . Total optical power from edge emitters is several times smaller than from surface emitters, but the narrower beam divergence can give rise to more coupled power. For fibers with small NA ( $<0.2$ ) edge emitters are suitable, whereas for fibers with large NA, surface emitters are preferred. Fig.4.10 gives an illustration of the two types of LEDs.

## 4.6 PHOTODETECTORS

The two principal families of photodetectors are the PIN and the avalanche photodiodes (APD). The latter increase the sensitivity by internally multiplying the primary photocurrent before encountering the amplifier noise. The only <sup>i</sup>disadvantage of the APDs is their high operating voltage (up to 400v).

The main photodetectors materials used are:

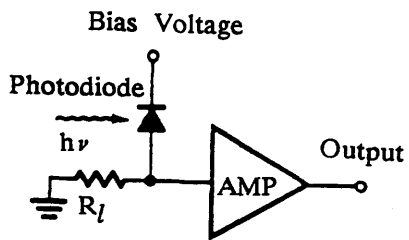
- Si photodetectors in the 800 – 900nm wavelength region.
- InGaAs and Ge photodetectors in the 1100 – 1600nm wavelength region.

### 4.6.1 Photodetectors response time

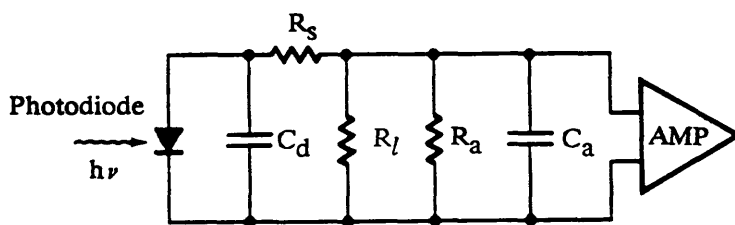
It depends mainly on three factors:

- The transit time of the photocarriers in the depletion region.
- The diffusion time of the photocurrent generated outside the depletion region.
- The RC time constant of the photodiode and its associated circuit.

The simplest model of a photodetector receiver along with its equivalent circuit are given in Fig.4.11. It consists of a photodiode having a series resistor  $R_s$ , a total capacitance  $C_d$  consisting of a junction and packaging capacitances, a load resistor  $R_l$  converting the photocurrent to a voltage and an amplifier having an input resistor  $R_a$  and a capacitance  $C_a$ .



(a)



(b)

**Fig.4.11 (a) Simple Model Of A Photodetector Receiver And (b) Its Equivalent Circuit.**

The limiting factor of the response time of this circuit is  $C_d$ . In general the photodetector receiver behaves like an RC low pass filter with a 3dB bandwidth given by,

$$B_{3dB} = 1/(2\pi R_T C_T) \quad (4.19)$$

where  $R_T = R_a \parallel R_l$  (neglecting  $R_s$ ) and  $C_T = C_a + C_d$ .

A fast response time can be obtained by decreasing  $R_l$ , but this sacrifices the SNR since a resistor's thermal noise current increases as the value of the load resistor decreases.

#### 4.6.2 Photodetectors quantum efficiency

The photodetector quantum efficiency  $\eta$  is defined as,

$$\eta = \frac{\text{number of electrons generated}}{\text{number of photons received}} = \frac{I_p/q}{P_o/h\nu} \quad (4.20)$$

where  $I_p$  is the primary average photocurrent generated by an average optical power  $P_o$ ,  $q$  the electron charge and  $h\nu$  the photon energy.

The ratio  $I_p/P_o$  is known as the responsivity  $R$ ,

$$R = I_p/P_o = \eta q/(h\nu) \quad (4.21)$$

$R$  specifies the photocurrent generated per unit optical power.

#### 4.6.3 Noises currents

The main noises currents of a photodiode are:

– Shot or quantum noise, arising from the statistical nature of photon – electron conversion. The mean square (ms) of this current is,

$$\langle i^2_q \rangle = 2qI_p G^2 F(G) B = 2qR P_o G^2 F(G) B \quad (4.22)$$

where  $F(G)$  is a noise figure associated with the random nature of the avalanche proces. From experimental results this figure is,

$$F(G) = G^x \quad (4.23)$$

where  $x$  ( $0 \leq x \leq 1$ ) depends on the material used.

– Dark current that continues to flow when no light falls on the photodiode. The ms of this current is,

$$\langle i^2_d \rangle = 2qI_d G^2 F(G) B \quad (4.24)$$

– Surface leakage current which depends on the surface defects, cleanliness, bias voltage and surface areas. The ms of this current is,

$$\langle i^2_l \rangle = 2qI_l B \quad (4.25)$$

The other most important noise source is the thermal noise current generated in the photodiode load resistor  $R_l$  and the amplifier input resistor  $R_a$ . The thermal noise current ms is,

$$\langle i^2_{th} \rangle = 4K_B T B F_t / R_{eq} \quad (4.26)$$

where  $K_B$  is Boltzmann's constant,  $T$  is the absolute temperature ( $^{\circ}K$ ),  $F_t$  is a noise figure of the amplifier and  $R_{eq} = R_l \parallel R_a$  ( $R_s$  being neglected).

Since all these noises are uncorrelated, the ms of the total noise is,

$$\begin{aligned} \langle i^2_n \rangle &= \langle i^2_q \rangle + \langle i^2_d \rangle + \langle i^2_l \rangle + \langle i^2_{th} \rangle \\ &= 2qR P_0 G^2 F(G) B + 2qI_d G^2 F(G) B + \\ &\quad 2qI_l B + 4K_B T B F_t / R_{eq} \end{aligned} \quad (4.27)$$

$\langle i^2_{th} \rangle$  can be reduced by increasing  $R_l$ , however, any increase in  $R_l$  causes a decrease in the receiver bandwidth. For PIN photodiodes  $F(G)$  and  $G$  are set to unity.

#### 4.7 POWER COUPLED FROM AN LED INTO A FIBER

The LEDs emitting areas are larger than the fiber core area. As a result a large coupling loss is incurred which, when added to the losses resulting from NA, make the total loss considerable.

##### 4.7.1 Power coupled into a step index fiber

The power coupled from an LED into a step index fiber, when the fiber core radius is less than the LED emitting area radius  $r_s$ , is given in ref.12. This is,

$$P_{step} = R(\pi a NA)^2 \quad (4.28)$$

where  $R$  is the LED radiance which is the optical power radiated into a solid angle per unit emitting area. It gives the spatial distribution of the optical power.

For Lambertian emission, and if we suppose that the emitting area is circular, the radiance R is given by,

$$R = P_{LED}/(\pi A_s) = P_{LED}/(\pi^2 r_s^2) \quad (4.29)$$

Substituting eq.(4.29) into eq.(4.28) we get the equation giving the power coupled into a step index fiber,

$$P_{step} = P_{LED} (aNA/r_s)^2 \quad (4.30)$$

#### 4.7.2 Power coupled into a graded index fiber

The power coupled from an LED into a graded index fiber is,

$$P_{grad} = 2\pi^2 R n^2_1 a^2 \Delta [1 - 2/(\alpha+2)] \quad (4.31)$$

For a parabolic profile (i.e.  $\alpha = 2$ ) and substituting eq.(4.29) into eq.(4.31) we get the equation giving the power coupled into a graded index fiber,

$$P_{grad} = R(\pi aNA)^2/2 = P_{LED} (aNA/r_s)^2/2 \quad (4.32)$$

We notice that for  $\alpha = 2$  and the same core diameter the power coupled into a step index fiber is twice that coupled into a graded index fiber.

#### 4.7.3 Power lost due to NA

The true amount of power coupled into a fiber depends on its NA. Since the fiber accepts only those rays contained within a cone whose maximum angle is determined by the critical angle  $\theta_c$ , an additional coupling loss will result if the angular emission cone of the source exceeds that defined by the NA of the fiber. This additional coupling loss is very often given in the LEDs used data sheets. Fig.4.12 gives an illustration of the power lost due to NA.

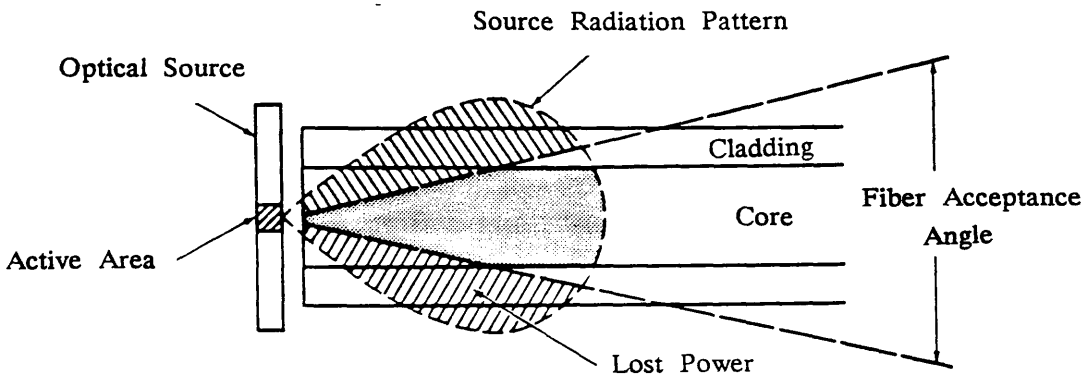


**Fig.4.12 Schematic Diagram Of An Optical Source Coupled To An Optical Fiber.**

## 5.1 INTRODUCTION

In this chapter we will investigate the performance of the whole PWM system. The choice of a light source, a fiber, a photodetector, the power budget, taking into account the various losses, the dependence of the system SNR on the received optical power and the rise time budget will all be discussed.

## 5.2 CHOICE OF THE OPTICAL SYSTEM

The optical system comprises a light source, a fiber and a photodetector. As we saw in chapter four, there are two types of light sources, fibers and photodetectors. The choice of the optical system is carried out in what follows.

### 5.2.1 Choice of a light source

The choice of a particular light source for a particular application determines first the electronic drive circuit needed to amplify the input signal to the required level to drive the light source and second the optical signal power available from the source for coupling to the fiber.

Since the main criterion of the choice of a system is cost and since the operating bandwidth is low ( $< 14\text{MHz}$ ) an edge emitter LED operating in the 800 – 900nm wavelength region will be suitable. The choice of an edge emitter LED is strongly recommended for low NA fibers (because of its power coupling efficiency).

### 5.2.2 Choice of a fiber

As far as fibers are concerned, multimode step index fibers are relatively inexpensive, have large NA but suffer from modal dispersion. Graded index fibers show reduced modal dispersion but have relatively small NA, therefore, the power coupled into them is half that coupled into step index fibers. Single mode fibers are subject only to material dispersion but because of their small core diameter, only lasers can be used to couple significant amount of power into them.

To use an LED – single mode fiber combination, we should either operate at longer wavelengths, where attenuation is at a minimum, or shorten the transmission distance. However, since the optoelectronics devices in the 1100 – 1600nm region are expensive and since any communication link for trunk routing of information involves long transmission distances, an LED – single mode fiber combination is to be avoided. A suitable combination would be an LED – multimode graded index fiber.

### 5.2.3 Choice of a photodetector

The choice of a photodetector depends mainly on the received optical power. For a large received optical power, an APD serves no advantage since the detector noise increases more rapidly with increasing gain  $G$  than the optical signal. Therefore, APDs can be used in applications where the received optical power is low and PIN photodiodes in applications where the received optical power is large. We assume that the received optical power is large enough so that we can use a PIN photodiode as a photodetector.

## 5.3 SCHEMATIC OF THE OPTICAL PWM SYSTEM

Thus, the optical system consists of an LED, a multimode graded index fiber and a PIN photodiode. The schematic of the whole optical PWM system is given in Fig.5.1.

### 5.4 LINK LOSSES

The optical power received by the photodetector depends on the amount of power coupled into the fiber and the losses occurring in the fiber, at the connectors and splices. Fig.5.2 gives an illustration of the various losses occurring in an optical link.

If we assume that only one splice is used, the total link loss is then,

$$l = 2l_c + Ll_f + l_s + l_{sf} + l_{NA} \quad (5.1)$$

where  $l_c$ ,  $l_f$ ,  $l_s$ ,  $l_{sf}$ ,  $l_{NA}$  are the connector, fiber, splice, source to fiber and NA

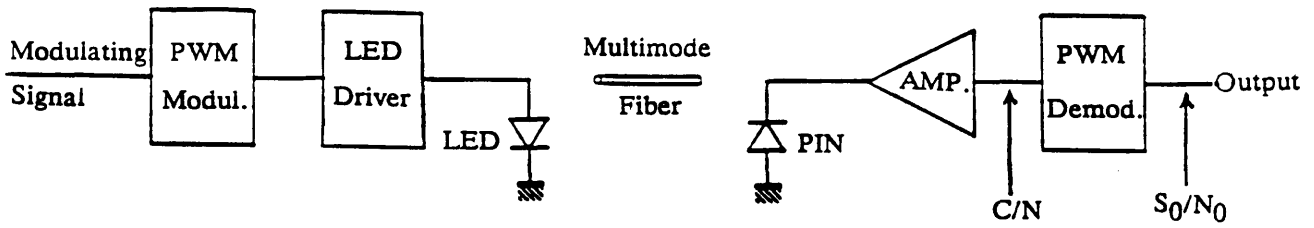


**Fig.5.1 Schematic Of The Optical PWM System.**

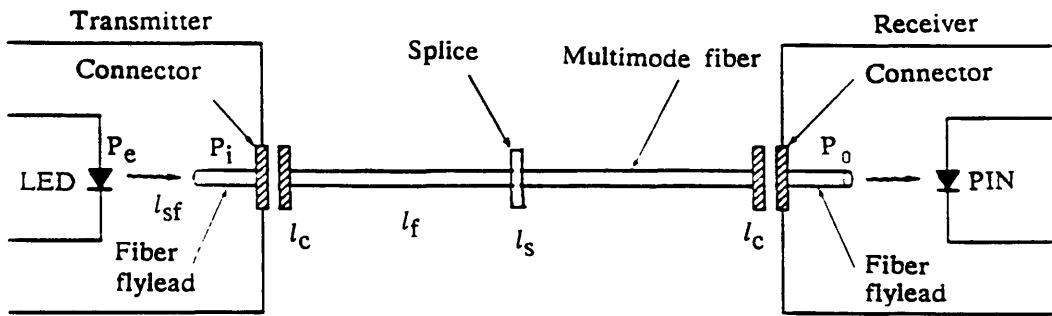


**Fig.5.2 The Various Losses Occuring In An Optical Link.**

losses respectively and L the fiber length.

In general, the connector and splice losses are equal to 0.5dB each.

The power  $P_0$  at the photodetector flylead, in terms of the LED output power  $P_e$ , is

$$P_0(\text{dB}) = P_e(\text{dB}) - (Ll_f + l_{sf} + l_{NA} + 1.5)\text{dB} \quad (5.2)$$

### 5.5 POWER BUDGET

We assume a multimode graded index fiber with parabolic profile  $\alpha = 2$ ,

NA = 0.2, a core diameter  $2a = 50\mu\text{m}$  and an attenuation  $A = 2.8 \text{ dB/Km}$  (at 850nm), an LED with an emitted power  $P_e$  into an aperture of diameter  $100\mu\text{m}$ , we further assume that the loss due to the NA of the fiber is  $l_{NA} = 0.3\text{dB}$ . The power available at the PIN photodiode is computed through eqs.(4.35) and (5.2). The power values at the fiber output are given, for various transmission distances, in Tab.5.1. A plot of  $P_0$  in terms of  $P_e$  is given in Fig.5.3.

	L = 0.5Km	L = 1Km	L = 1.5Km
$P_e(\text{mW})$	$P_0(\text{dBm})$	$P_0(\text{dBm})$	$P_0(\text{dBm})$
0.25	-32.2	-33.6	-35.0
0.5	-29.2	-30.6	-32.0
0.75	-27.4	-28.8	-30.2
1.0	-26.2	-27.6	-29.0
1.25	-25.2	-26.6	-28.0
1.5	-24.4	-25.8	-27.2
1.75	-23.8	-25.2	-27.2
2.0	-23.8	-25.2	-26.6
2.25	-22.7	-24.1	-25.5

**Tab.5.1 Fiber output power values for various transmission distances.**

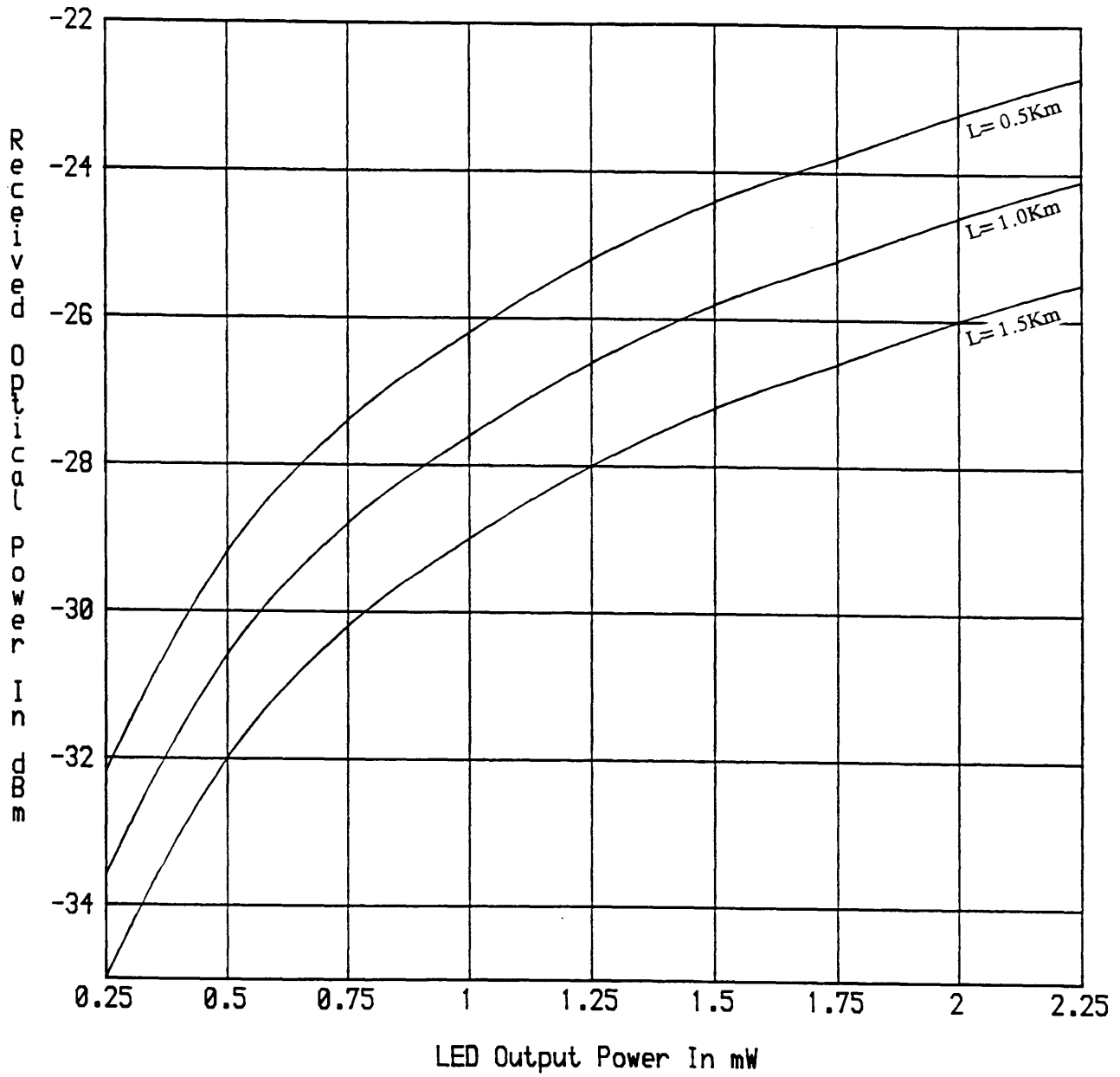


Fig.5.3 Received Optical Power Versus LED Output Power For Various Transmission Distances.

## 5.6 OPTICAL PWM SYSTEM SNR

In chapter three, we derived the PWM SNR for a white gaussian noise, but we did not precise the sources of this noise. In what follows, we will derive this SNR taking into account the various noises associated with the optical transmitter and receiver.

### 5.6.1 Optical signal generated current ms

We assume a rectangular power pulse  $p_s(t)$  of amplitude  $P_{\max}$ , falling on the PIN photodiode of responsivity  $R$ , a cosinusoidal modulating signal of amplitude  $A$  and a peak positive modulation, that is

$$s(kT_s) = A = MT_s/2 \quad (5.3)$$

The optical signal average power is,

$$P_o = \langle p_s(t) \rangle = (1/T_s) \int_0^{T_s/2+s(kT_s)} P_{\max} dt$$

$$= (P_{\max}/T_s)(T_s/2 + MT_s/2) = P_{\max} (1+M)/2 \quad (5.4)$$

The generated photocurrent is,

$$i_s(t) = R p_s(t) \quad (5.5)$$

The ms value of  $i_s(t)$  is,

$$\langle i^2(t) \rangle = R^2 \langle p_s^2(t) \rangle = (R^2/T_s) \int_0^{T_s/2+M \cdot T_s/2} P_{\max}^2 dt$$

$$= R^2 P_{\max}^2 (1+M)/2 \quad (5.6)$$

Substituting eq.(5.4) into eq.(5.6) we get the ms value of the signal current,

$$\langle i_s^2(t) \rangle = 2R^2 P_o^2 / (1+M) \quad (5.7)$$

### 5.6.2 Total noise current ms

We gave in chapter four the different noises currents associated with the optical receiver, but we did not give the noise current associated with the LED. The effect of the LED incoherence is to give rise to an additional noise called beat noise whose current ms is,

$$\langle i_b^2(t) \rangle = 2(RP_o)^2 B [1 - B/(2W)] / (JW) \quad (5.8)$$

where  $W$  is the LED spectral width and  $J$  the number of the spatial modes. The product  $JW$  is, in general, very large ( $10^{15}$ Hz) rendering thus the beat noise current  $i_{ms}$  negligible.

The other noises currents  $i_{ms}$  are evaluated not at  $P_0$  but rather at  $P_{max}/2$  because the latter is the expected value of the signal when the threshold crossing is to occur. Substituting  $P_0$  by  $P_{max}/2$  and  $F(G) = G = 1$  into eq.(4.27) we get the total noise current  $i_{ms}$ ,

$$\langle i_n^2 \rangle = qRP_{max}B + 2qI_dB + 2qI_lB + 4K_BTF_tB/R_{eq} \quad (5.9)$$

Substituting eq.(5.4) into eq.(5.9) we get,

$$\langle i_n^2 \rangle = 2qP_0RB/(1+M) + 2qI_dB + 2qI_lB + 4K_BTF_tB/R_{eq} \quad (5.10)$$

Finally, the CNR is,

$$\begin{aligned} (C/N) &= \frac{\langle i_s^2 \rangle}{\langle i_n^2 \rangle} \\ &= \frac{2R^2P_0^2}{2q[RP_0/(1+M) + I_d + I_l + 2K_BTF_t/(qR_{eq})](1+M)B} \end{aligned} \quad (5.11)$$

If we assume that the noise current  $i_n(t)$  is a gaussian random process, neglect the leakage current and substitute eq.(5.11) into eq.(3.68) we get the PWM system SNR,

$$\begin{aligned} (S_0/N_0) &= (\pi^2M^2/16)(B/f_s)^2(C/N) \\ &= (\pi^2M^2/16)(B/f_s)^2 \\ &\quad \frac{2R^2P_0^2}{2q[RP_0 + I_d(1+M) + 2K_B\Gamma(1+M)F_t/(qR_{eq})]B} \end{aligned} \quad (5.12)$$

Eq.(5.12) is computed in terms of  $P_0$  for various modulation indices  $M$  for

$R = 0.5A/W$ ,  $I_d = 2nA$ ,  $R_{eq}/F_t = 10K\Omega$ ,  $q = 1.6 \times 10^{-19}C$ ,  $K_B = 1.38 \times 10^{-23}J/^{\circ}K$ ,  $B = 40MHz$  and  $f_s = 13.34MHz$ . The results are given in Tab.5.2, and a plot of eq.(5.12) is given in Fig.5.4.

	M=0.4	M=0.6	M=0.8
$P_0$ (dBm)	$S_0/N_0$ (dB)	$S_0/N_0$ (dB)	$S_0/N_0$ (dB)
-45	6.8	9.7	11.7
-40	16.8	19.7	21.7
-35	26.7	29.7	31.7
-30	36.5	39.5	41.5
-25	45.9	49.0	51.0
-20	54.5	57.7	59.9
-15	61.8	65.1	67.4
-10	67.8	71.3	73.7

**Tab.5.2 PWM optical system SNR values for various M.**

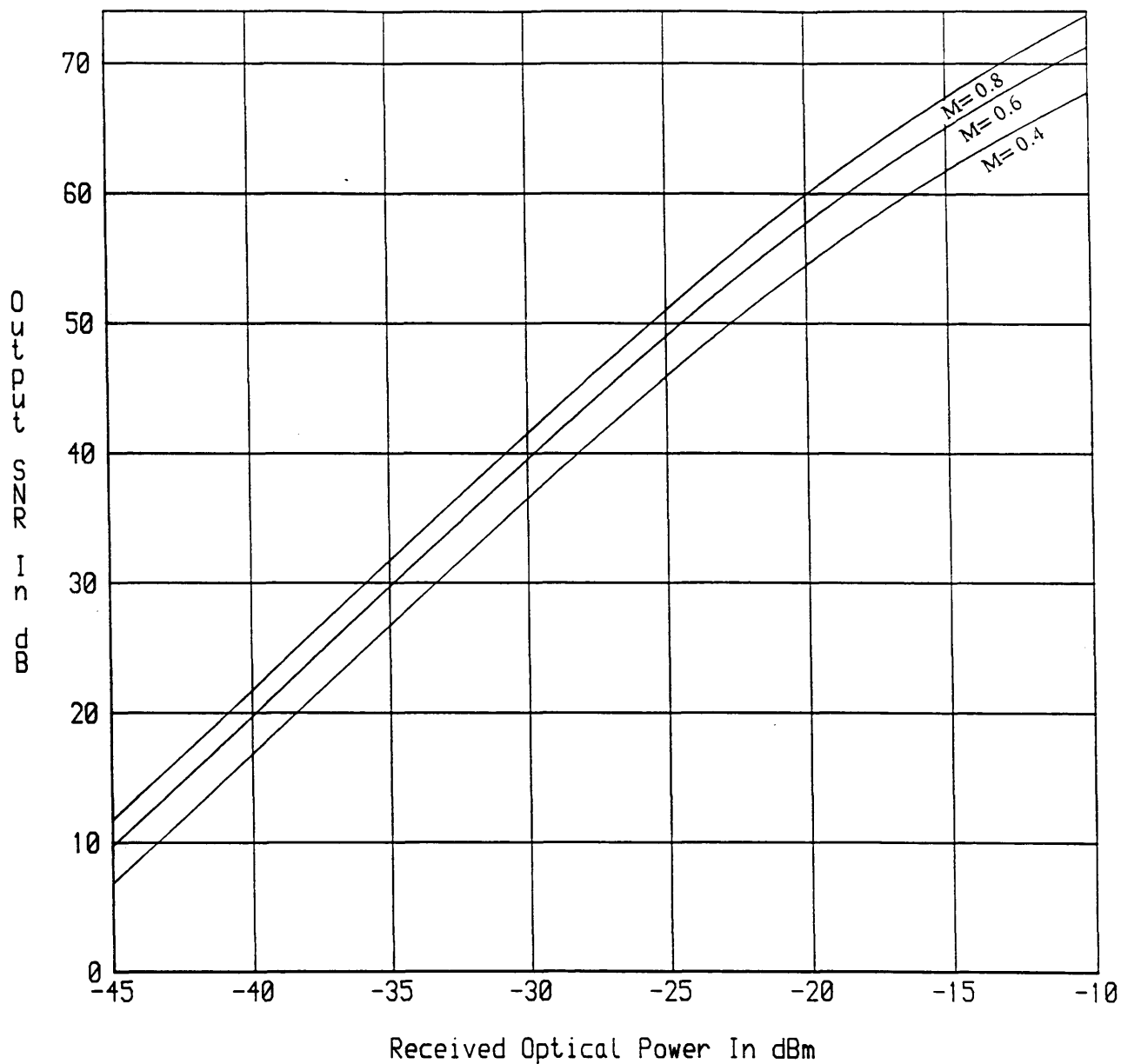


**Fig.5.4 PWM Output SNR Versus Received Optical Power For Various Modulation Indices.**

## 5.7 RISE TIME BUDGET

To be able to find the system total rise time  $T_r$ , we assume that the PWM pulses are gaussian, this is not true but gives a good approximate value of  $T_r$ . The latter is given in ref.12 by,

$$T_r = [T_t^2 + T_{rec}^2 + T_{mat}^2 + T_{mod}^2]^{1/2} \quad (5.13)$$

where  $T_t$ ,  $T_{rec}$  are the transmitter and receiver rise times respectively and  $T_{mat}$ ,  $T_{mod}$  the material and modal dispersion related rise times respectively.

The fiber bandwidth resulting from modal dispersion is inversely proportional to the cable length. The empirical relation of this bandwidth is given, in ref.12, by

$$B_M(L) = B_0/L^{0.7} \quad (5.14)$$

where  $B_0$  is the bandwidth of a 1-Km fiber length.

To find the relationship between the fiber rise time and its 3dB bandwidth, we assume that the fiber power impulse response is gaussian, this is the case for long fibers.

$$g(t) = \frac{1}{\sigma\sqrt{2\pi}} e^{-t^2/2\sigma^2} \quad (5.15)$$

where  $\sigma$  is the rms pulse width.

The FT of eq.(5.15) is the transfer function of the fiber,

$$G(f) = e^{-2\pi^2 f^2 \sigma^2} \quad (5.16)$$

If we define  $t_{fwhm}$  as the full width of the fiber impulse response at half maximum value, then

$$t_{fwhm} = 2(2\ln 2)^{1/2} \sigma = 2.35 \sigma \quad (5.17)$$

The 3dB optical bandwidth from eq.(5.16) is,

$$B_{3dB} = 0.188/\sigma \quad (5.18)$$

Substituting eq.(5.17) into eq.(5.18), we get the relationship between  $t_{fwhm}$  and  $B_{3dB}$ ,

$$t_{fwhm} = 0.44/B_{3dB} \quad (5.19)$$

Letting  $t_{fwhm}$  be the rise time resulting from modal dispersion and substituting eq.(5.14) into eq.(5.19) we get,

$$T_{mod} = 0.44/B_M = 0.44 L^{0.7}/B_0 \quad (5.20)$$

The material dispersion related rise time is given in chapter four, this is,

$$T_{\text{mat}} = D \sigma_{\lambda} L \quad (5.21)$$

Finally, the system rise time is,

$$T_r = [T_t^2 + T_{rc}^2 + (0.44 L^{0.7}/B_0)^2 + (D \sigma_{\lambda} L)^2]^{1/2} \quad (5.22)$$

If we assume a fiber with a 3dB bandwidth  $B_0 = 430\text{MHz.Km}$ ,  $T_t = 10\text{ns}$ ,

$T_{rc} = 12\text{ns}$  and an LED with spectral width  $\sigma_{\lambda} = 35\text{nm}$  (at  $\lambda_0 = 820\text{nm}$ ) and with material dispersion coefficient  $D = 0.09\text{ns/nm.Km}$ , then the system rise time for a 1-Km link is  $T_r = 16.0\text{ns}$ . This value of  $T_r$  limits  $M$  to 0.57.

## 5.8 CONCLUSION

Through this chapter, we have motivated the choice of optoelectronic devices for the optical PWM system. Because of cost, we have chosen devices operating in the 800 – 900nm wavelength region where optoelectronic devices are cheaper. The optical system consisted of an LED and its drive circuitry in the transmitter, a multimode graded index fiber, and a PIN photodiode in the receiver. Taking into account all the possible link losses, we found that, for typical devices values, if the LED delivers 1mW optical power into an aperture of  $100\mu\text{m}$  in diameter, then the PIN received power would be  $P_0 = -28\text{dBm}$  for 1-Km link. This would give an SNR, depending on the value of  $M$  used, in the range  $40 < \text{SNR} < 50\text{dB}$ . Finally, based on the assumption that the PWM are gaussian, we found that, for 1-Km link, the system rise time is  $T_r = 16\text{ns}$ . This value of  $T_r$  would limit the modulation index  $M$  to 0.57.

## CONCLUSIONS

The objective of the project was to investigate the feasibility of two PWM systems, PWM with uniform and natural sampling, for low cost transmission via an optical fiber. The latter was chosen as transmission medium because it is a very wideband medium, lighter, cheaper to install and free from interference than its coaxial equivalent. PWM was chosen as modulation technique because it offers, along with PPM, the ideal blend of analogue and digital modulation and because the transmitter and receiver design would be relatively simple. The transmitted signal is of two discrete states, this means that modulation of semiconductor sources, and demodulation can be achieved easily. It is true that PFM presents better SNR performance than PPM and PWM do, but the SNR is not the only consideration in choosing one or the other scheme. The question of multiplexing must be taken into account. PPM and PWM lend themselves easily to time multiplexing, whereas PFM does not. Frequency multiplexing can be used in PFM systems but at the expense of high constraint on the sampling rates and modulation indices. PWM was preferred over PPM because it is easier to demodulate PWM signals than PPM ones. The latter being synchronous require a clocking stage for demodulation.

The electronic aspect of the two PWM systems was examined in chapter two. We saw how easily modulation and demodulation can be achieved. It was shown that PWM with natural sampling (NS) demodulator consisted of only a low pass filter. The simplicity of this demodulator was at the expense of a limitation on the modulation index ( $M < 0.1$ ), since for high  $M$  the signal to interference ratio (SIR) is smaller than the quoted value (i.e. 36dB). The disadvantage of having low  $M$  is a degradation in the output signal to noise ratio (SNR) since the latter is proportional

to the square of  $M$ . A relaxation of the constraint on  $M$  can be obtained by increasing the sampling rate  $f_s$ . We showed that for  $f_s > 28\text{MHz}$  the permissible  $M$  could be as high as 0.7. However, such sampling rates would require, in turn, the use of very fast components to obtain pulses with short rise times. For a sampling rate  $f_s = 28\text{MHz}$ , the usable time slot is 35ns. If the permissible modulation index is 0.7, then 25ns are used for modulation and 10ns for rise and fall times, this corresponds to a bandwidth  $B = 100\text{MHz}$ . We should point out that components that allow 5ns rise time are very expensive and their use defeats one of the main choice criterion which is cost. PWM with uniform sampling (US) seemed attractive because it allows the use of modulation indices as high as 1.0 for frequencies covering the whole video band (up to 5.5MHz). The only limitation on  $M$  comes from the circuitry used. As far as the bandwidth required for the transmission of PWM signals is concerned, this was found to be equal to half the reciprocal of the allowable rise time. We concluded the chapter by comparing PCM and PWM SNRs in the absence of intersymbol interference (ISI), that is in the case where the receiver bandwidth is  $n \times f_s$  (for an  $n$ -bit transmission). This comparison was obviously in favor of PCM even for a 4-bit transmission.

The distortion due to the receiver bandwidth limitation was investigated in chapter three for two kinds of modulating signals, one deterministic, the other random. For both types of signals, the distortion depended on  $M$  and  $B$ . In fact it increases with increasing  $M$  and decreases with increasing receiver bandwidth  $B$ . To keep it low we should either increase  $B$  or decrease  $M$ . Increasing  $B$  is a waste of bandwidth and makes the constraint on the receiver more severe (short rise times). Decreasing  $M$  sacrifices the output SNR since the latter is proportional to the square of  $M$ . To make a compromising choice of parameters ( $M$ ,  $\gamma$ ,  $B$ , SNR,  $D_k$ ), curves taking into account all these parameters were given. For instance for  $M = 0.6$  and  $B = 40\text{MHz}$  the distortion was found to be equal to  $-40\text{dB}$  which is an acceptable level. For this same receiver bandwidth, PWM and PCM SNRs were compared in

the presence of ISI, that is in the case where  $B$  is not equal to  $n \times f_s$  (for an  $n$ -bit transmission) but equal to 40MHz. For the computation of PCM SNR, we used a method giving the probability of error ( $P_e$ ) in terms of the first  $2k$  moments of the ISI. It was shown that PWM with US presented better performance in SNR than PCM does and this for CNRs  $< 20$ dB and a number of bits less or equal than 5 ( $n \leq 5$ ).

Chapter five was devoted to the investigation of the optical PWM system. As far as the latter is concerned, devices operating in the 800 – 900nm wavelength region, where optoelectronic devices are cheaper, were used. The optical system consisted of an edge emitter LED and its drive circuitry in the transmitter, a multimode graded index fiber, and a PIN photodiode in the receiver. Having made use of typical devices data, we showed that if the LED delivers 1mW power into an aperture of  $100\mu\text{m}$  in diameter, then the PIN photodiode received power would be  $-28$ dBm ( $1.6\mu\text{W}$ ) for a 1-Km transmission distance. This would give an SNR in the range 40 to 50dB.

Finally, having assumed that the PWM pulses are gaussian in shape, and for transmitter and receiver allowing 10 and 12ns rise times respectively, we showed that the system  $T_r$  was approximately 16ns, and this would limit the modulation index  $M$  to 0.57.

The aim of this project was to prove, theoretically, two PWM systems experimental results found in ref.14. The theoretical results found in this project are extremely close to the experimental ones, and thus the systems have been proven to perform in the manner predicted by experimental work.

## LIST OF REFERENCES

1. Black, H.S., " Modulation Theory ", D. Van Nostrand Company, Inc., Princeton, N.J., 1953.
2. Panter, P.F., " Modulation, Noise and Spectral Analysis ", McGraw-Hill Book Company, New York, 1965.
3. Schwartz, M., " Information, Transmission, Modulation and Noise ", Third Ed., McGraw-Hill Book Company, New York, 1980.
4. Stremler, F.G., " Introduction to Communication Systems ", Second Ed., Adison Wesley Publishing Company, Inc., Madison, 1982.
5. Rowe, H.E., " Signals and Noise in Communication Systems ", D. Van Nostrand Company, Inc., Princeton, N.J., 1965.
6. Russel, M.G., " Modulation and Coding in Information Systems ", Prentice-Hall International, London.
7. Ho, E.Y., and Yeh, Y.S., " A New Approach for Evaluating the Error Probability in the Presence of Intersymbol Interference and Additive White Gaussian Noise ", B.S.T.J., 1970, 49, pp.2249- 2265.
8. Abramowitz, M., and Stegun, I.A., " Handbook of Mathematical Functions ", Dover, 1972.
9. Personick, S.D., " Baseband Linearity and Equalisation in Fiber Optic Digital Communication Systems ", B.S.T.J., 1973, 52, pp.1175- 1194.

10. Henry, P.S., " Lightwave Primer ", IEEE Journal of QE, 1985, 21, pp.1862-1879.
11. Wilson, J., and Hawkes, J.F.B., " Optoelectronics an Introduction ", Prentice-Hall International, Inc., Englewood Cliffs, N.J., 1983.
12. Keiser, G., " Optical Fiber Communications ", McGraw-Hill International Book Company, Tokyo, 1983.
13. Heatly, D.J.T., " Video Transmission in Optical Fiber Local Networks Using Pulse Time Modulation ", 9<sup>th</sup> ECOC, Geneva, Switzerland, 1983, pp.343-346.
14. Berry, M.C., and Arnold, J.M., " Video Pulse Width Modulation for Optical Fiber Transmission ", University of Nottingham, England, 1983.
15. Suh, S.Y., " Pulse Width Modulation for Analogue Fiber Optic Communications", J. Lightwave Technology, 1987, LT-5, pp 102-112.

## APPENDICES

To determine the necessary bandwidth for pulse systems, we assume that the transmission medium is an ideal low pass filter of bandwidth  $B$  to which a rectangular pulse of width  $\tau$  is injected.

The filter output is given in ref.3, to be

$$g(t) = (1/\pi) \text{Si}[2\pi B(t+\tau/2)] - (1/\pi) \text{Si}[2\pi B(t-\tau/2)] \quad (\text{A1.1})$$

where,

$$\text{Si}(x) = \int_0^x \frac{\sin t}{t} dt \quad (\text{A1.2})$$

A sketch of  $g(t)$  is given in Fig.A1.1 for different values of  $B$ . These curves bear out the following filter bandwidth - pulse width relationships:

- If  $B \ll 1/\tau$ , the filter output is a grossly distorted version of the input.
- If  $B = 1/\tau$ , the output is a recognisable pulse, roughly  $\tau$  seconds in width.
- If  $B \gg 1/\tau$ , the output resembles the input and has roughly the same width.

If we define the rise time  $T_r$  as the time taken by a pulse to rise from 0 to its maximum (1.09), then

$$B = 0.8/T_r \quad (\text{A1.3})$$

If  $T_r$  is defined as the time taken by a pulse to rise from 0.1 to 0.9 of its peak amplitude, then

$$B = 0.5/T_r \quad (\text{A1.4})$$

To summarise, if the object is merely to produce an output pulse which has about the same width as the input pulse, with fidelity unimportant, as is the case for PAM systems, then the required filter  $B$  is approximately the reciprocal of the pulse width,

$$B = 1/\tau \quad (\text{A1.5})$$

If fidelity is required,  $B$  must be at least several times the reciprocal of  $\tau$ , and is actually determined by rise time consideration through eqs.(A1.3) or (A1.4), depending on the adopted  $T_r$  definition. This is the case for PWM and PPM systems where the instants of arrival of each pulse must be known exactly.

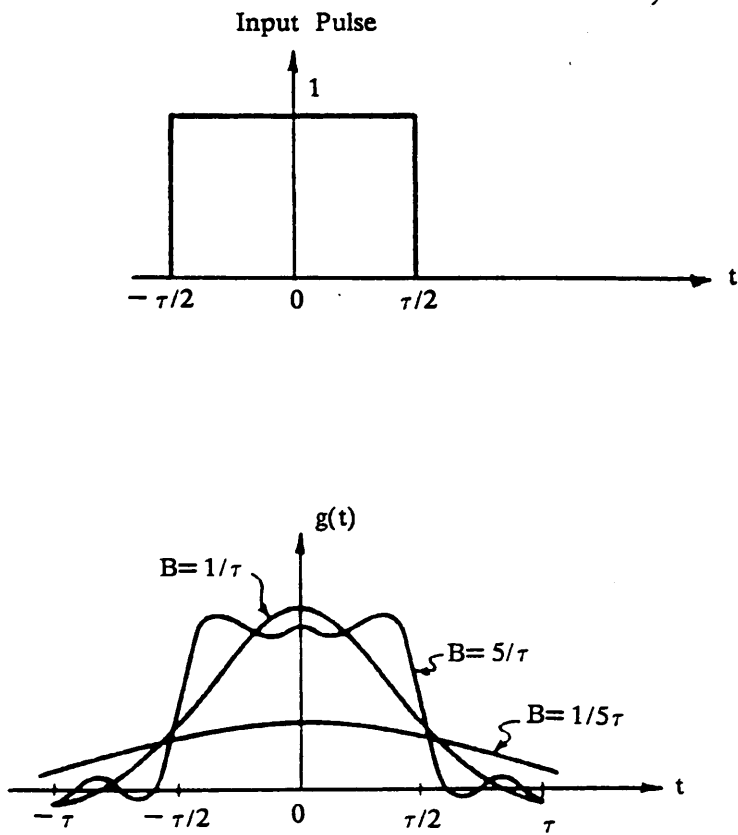


Fig.A1.1 Response Of An Ideal Low Pass Filter To A Rectangular Pulse.

We seek to determine the RC filter output when a rectangular pulse is injected to its input, see Fig.A2.1. The input signal can be decomposed into the difference of two step functions:

$$v_i(t) = A u(t) - A u(t-T_0) \quad (A2.1)$$

where,

$$u(t) = \begin{cases} 1 & t > 0 \\ 0 & t < 0 \end{cases} \quad (A2.2)$$

The time response of the RC filter to the input pulse  $v_i(t)$  is,

$$v_o(t) = v_i(t)*h(t) = \int_{-\infty}^{+\infty} h(t')v_i(t-t')dt' \quad (A2.3)$$

where  $h(t)$  is the RC filter impulse response given by,

$$h(t) = (1/RC) e^{-t/RC} u(t) \quad (A2.4)$$

Let  $T$  be the time constant  $RC$ ,

$$T = RC \quad (A2.5)$$

Since the RC filter is a causal filter, the integration is only from 0 to  $+\infty$ , and eq.(A2.3) becomes,

$$\begin{aligned} v_o(t) &= (A/T) \left[ \int_0^{+\infty} e^{-t'/T} u(t-t')dt' - \int_0^{+\infty} e^{-t'/T} u(t-t'-T_0)dt' \right] \\ &= (A/T) \left[ \int_0^t e^{-t'/T} dt' - \int_0^{t-T_0} e^{-t'/T} dt' \right] \end{aligned} \quad (A2.6)$$

To solve eq.(A2.6) we envisage two cases:

- If  $0 < t < T_0$ , the second term of eq.(A2.6) disappears because the limits of integration are negative, and we get what we call the charging of C.

- If  $T_0 < t < \infty$ , the limits of integration of both terms are positive and we get the discharging of C.

$$v_o(t) = \begin{cases} A (1-e^{-t/T}) & 0 < t < T_0 \\ A (1-e^{-T_0/T}) e^{-(t-T_0)/T} & T_0 < t < +\infty \end{cases} \quad (A2.7)$$

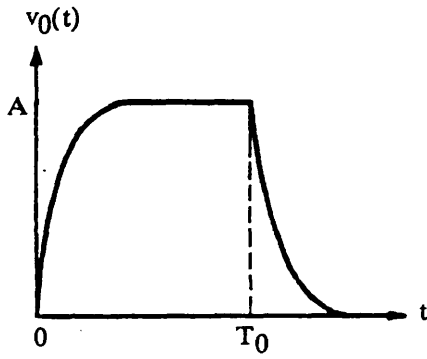
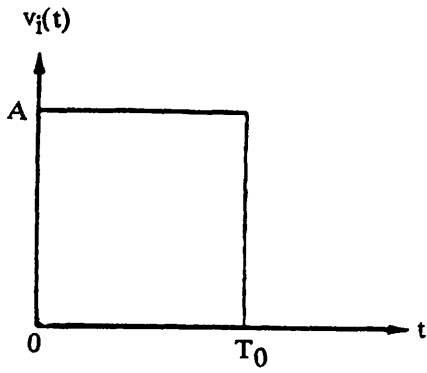


Fig.A2.1 RC Low Pass Filter Input And Output Pulses.

Suppose that a function  $g(t)$  has a simple, single zero at  $t = t_0$ ,

$$g(t_0) = \begin{cases} 0 & g(t)/(t-t_0) \neq 0 \\ \neq 0 & t \neq t_0 \end{cases} \quad (\text{A3.1})$$

Hence,

$$\delta[g(t)] = \delta(t-t_0)/|g'(t)| = \delta(t-t_0)/|g'(t_0)| \quad (\text{A3.2})$$

In the special case of the function,

$$g(t) = t - kT_s - s(t) \quad (\text{A3.3})$$

its zeros are,

$$t_k = kT_s + s(t) \quad (\text{A3.4})$$

Using the property given by eq.(A3.2) for  $g(t)$ , we have,

$$\delta[g(t)] = \delta[t - kT_s - s(t)] = \delta(t-t_k)/|g'(t)| \quad (\text{A3.5})$$

Taking the derivative of  $g(t)$  and substituting it into eq.(A3.5) we get,

$$\delta(t-t_k) = |1-s'(t)| \delta[t - kT_s - s(t)] \quad (\text{A3.6})$$

If  $s'(t) < 1$ , then eq.(A3.6) becomes,

$$\delta(t-t_k) = [1-s'(t)] \delta[t - kT_s - s(t)] \quad (\text{A3.7})$$

A4.1 FT OF AN IMPULSE TRAIN

Let  $c_\delta(t)$  be an impulse train of period  $T_s$ , as shown in Fig.A4.1,

$$c_\delta(t) = \sum_{-\infty}^{+\infty} \delta(t - kT_s) \quad (\text{A4.1})$$

$c_\delta(t)$  is periodic, it can therefore, be expanded into a Fourier series,

$$c_\delta(t) = \sum_{-\infty}^{+\infty} \delta(t - kT_s) = \sum_{-\infty}^{+\infty} C_n e^{2\pi j n f_s t} \quad (\text{A4.2})$$

where the Fourier coefficients  $C_n$  are given by,

$$\begin{aligned} C_n &= (1/T_s) \int_{-T_s/2}^{T_s/2} c_\delta(t) e^{-2\pi j n f_s t} dt \\ &= (1/T_s) \int_{-T_s/2}^{T_s/2} \delta(t) e^{-2\pi j n f_s t} dt = 1/T_s \end{aligned} \quad (\text{A4.3})$$

Substituting eq.(A4.3) into eq.(A4.2) we get,

$$c_\delta(t) = (1/T_s) \sum_{-\infty}^{+\infty} e^{2\pi j n f_s t} \quad (\text{A4.4})$$

The FT of eq.(A4.4) is,

$$\begin{aligned} c_\delta(t) &= (1/T_s) \int_{-\infty}^{+\infty} \sum_{-\infty}^{+\infty} e^{2\pi j n f_s t} e^{-2\pi j f t} dt \\ &= (1/T_s) \sum_{-\infty}^{+\infty} \int_{-\infty}^{+\infty} e^{-2\pi j (f - n f_s) t} dt = (1/T_s) \sum_{-\infty}^{+\infty} \delta(f - n f_s) \end{aligned} \quad (\text{A4.5})$$

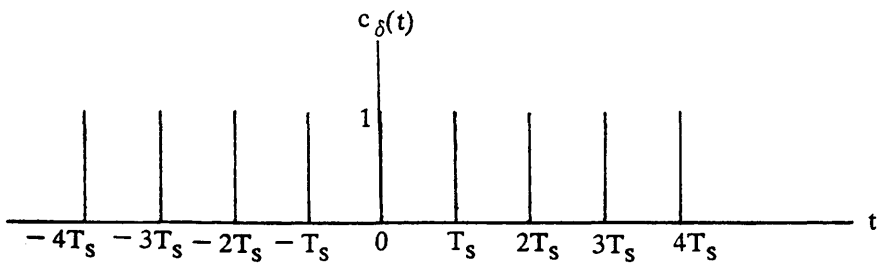
A4.2 FT OF A RECTANGULAR PULSE

Let  $f(t)$  be a rectangular pulse,  $\tau$  second wide and of amplitude 1.

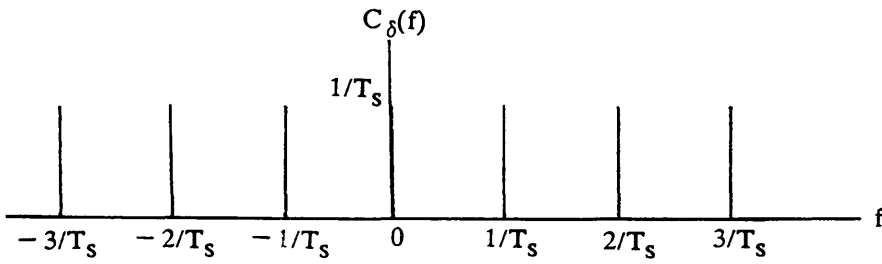
Its FT is,

$$F(f) = \int_{-\infty}^{+\infty} f(t) e^{-2\pi j f t} dt = \tau \sin(\pi f \tau) / (\pi f \tau) \quad (\text{A4.6})$$

A sketch of  $f(t)$  and its FT is given in Fig.A4.2.

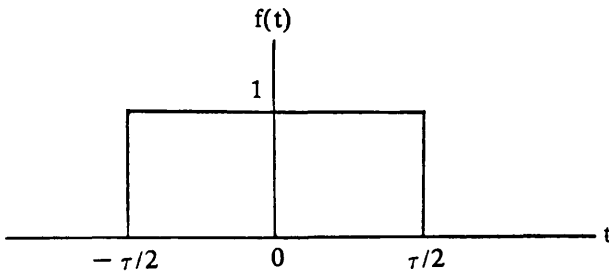


(a)

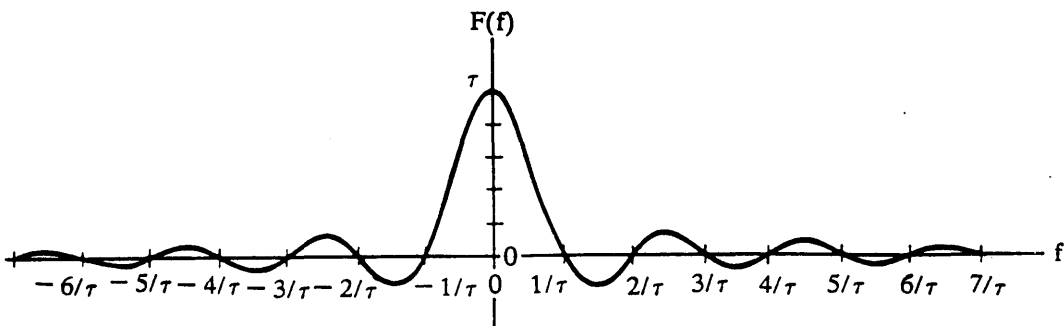


(b)

**Fig.A4.1 (a) An Impulse Train And (b) Its Fourier Transform.**



(a)



(b)

**Fig.A4.2 (a) A Rectangular Pulse And (b) Its Fourier Transform.**

The transfer function of the RC filter is,

$$H(f) = \frac{1}{1 + j2\pi RCf} \quad (A5.1)$$

The 3dB bandwidth is the frequency at which the maximum amplitude of  $H(f)$  falls by 3dB ( $1/\sqrt{2}$ ),

$$|H(f)| = |H(f)|_{\max}/\sqrt{2} = H(0)/\sqrt{2} = 1/\sqrt{2} \quad (A5.2)$$

Taking the modulus of  $H(f)$  we get,

$$|H(f)| = \frac{1}{\sqrt{1+(2\pi RC B_{3dB})^2}} = 1/\sqrt{2} \quad (A5.3)$$

Therefore,

$$B_{3dB} = 1/(2\pi RC) = 1/(2\pi T) \quad (A5.3)$$

APPENDIX A6 SIGNAL AVERAGE POWER - SPECTRAL DENSITY  
RELATIONSHIP

The variance of a function  $f(t)$  is defined as,

$$\sigma^2 = \langle f^2(t) \rangle - \langle f(t) \rangle^2 \quad (A6.1)$$

where  $\langle f^2(t) \rangle$  is called the ms and designates the power dissipated in a  $1-\Omega$  resistor. It is equal to the autocorrelation function of  $f(t)$  at the point  $\tau = 0$ ,

$$\langle f^2(t) \rangle = R_f(0) \quad (A6.2)$$

Since,

$$R_f(\tau) = \int_{-\infty}^{+\infty} G_f(f) e^{2\pi j f \tau} df \quad (A6.3)$$

therefore,

$$R_f(0) = \langle f^2(t) \rangle = \int_{-\infty}^{+\infty} G_f(f) df = R_f(0) \quad (A6.4)$$

If  $\langle f(t) \rangle = 0$ , then the average power of  $f(t)$  is equal to the variance,

$$\sigma^2 = \langle f^2(t) \rangle = R_f(0) \quad (A6.5)$$

The autocorrelation function of a periodic signal  $f(t)$  is,

$$R_f(\tau) = \sum_{-\infty}^{+\infty} |C_n|^2 e^{2\pi j n f_0 \tau} \quad (\text{A7.1})$$

where the Fourier coefficients  $C_n$  are given by,

$$C_n = (1/T_s) \int_{-T_s/2}^{+T_s/2} f(t) e^{-2\pi j n f_0 t} dt \quad (\text{A7.2})$$

If  $f(t)$  is the dirac impulse train, its autocorrelation function is,

$$R_{C\delta}(\tau) = \sum_{-\infty}^{+\infty} |C_n|^2 e^{2\pi j n f_s \tau} = (1/T_s^2) \sum_{-\infty}^{+\infty} e^{2\pi j n f_s \tau} \quad (\text{A7.3})$$

Its FT, called spectral density, is

$$\begin{aligned} G_{C\delta}(f) &= \int_{-\infty}^{+\infty} R_{C\delta}(\tau) e^{-2\pi j f \tau} d\tau = (1/T_s^2) \sum_{-\infty}^{+\infty} \int_{-\infty}^{+\infty} e^{-2\pi j (f - n f_s) \tau} d\tau \\ &= (1/T_s^2) \sum_{-\infty}^{+\infty} \delta(f - n f_s) \end{aligned} \quad (\text{A7.4})$$

We assume a white gaussian noise at the input of a sampler.

The sampler output is then,

$$n_{\delta}(t) = n_e(t)c_{\delta}(t) \quad (\text{A8.1})$$

Since we are dealing with noise, which is a random process, instead of using FTs we should use spectral densities.

The autocorrelation function of eq.(A8.1) is,

$$R_{n_{\delta}}(\tau) = R_{n_e}(\tau)R_{c_{\delta}}(\tau) \quad (\text{A8.2})$$

Taking the FT of eq.(A8.2) and substituting into it eq.(A7.4) we get,

$$\begin{aligned} G_{n_{\delta}}(f) &= G_{n_e}(f)*G_{c_{\delta}}(f) = \int_{-\infty}^{+\infty} G_{n_e}(f')G_{c_{\delta}}(f-f')df' \\ &= (1/T^2_s) \sum_{-\infty}^{+\infty} \int_{-\infty}^{+\infty} G_{n_e}(f')\delta(f-f'-nf_s)df' \\ &= (1/T^2_s) \sum_{-\infty}^{+\infty} G_{n_e}(f-nf_s) \end{aligned} \quad (\text{A8.3})$$

If this noise passes through the ideal low pass filter of eq.(2.13) we get,

$$\begin{aligned} G_{yn_{\delta}}(f) &= |H(f)|^2 G_{n_{\delta}}(f) = (1/T^2_s) |H(f)|^2 \sum_{-\infty}^{+\infty} G_{n_e}(f-nf_s) \\ &= \begin{cases} \sum_{-\infty}^{+\infty} G_{n_e}(f-nf_s) & |f| < f_s/2 \\ 0 & |f| > f_s/2 \end{cases} \end{aligned} \quad (\text{A8.4})$$

## IN THE PRESENCE OF ISI

C THIS PROGRAM CALCULATES THE PCM OUTPUT SNR IN PRESENCE OF  
 C ISI. IT FIRST CALCULATES THE PROBABILITY OF ERROR IN THE CASE  
 C OF A PCM SIGNAL IN PRESENCE OF WHITE GAUSSIAN NOISE AND ISI.  
 C IT MAKES USE OF A NEW METHOD FOR THE COMPUTATION OF  
 C THIS PROBABILITY OF ERROR.

C THE ROUTINE S15ADF CALCULATES THE Erfc(x).

```

    DIMENSION XS(40),A(40),AA(40),P(40),PP(40),PPP(40),G(40),
    .T(40),TT(40)

    COMMON/VAL/W,NB

    DOUBLE PRECISION XS,A,AA,P,PP,PPP,W,S15ADF,S14AAF,HAM,MOM,G,S
    .,X,T,TT
  
```

C READ IN THE INPUT CNR VALUES XS(decimal).

```

    READ(3,*)(XS(I),I= 1,26)
  
```

C READ IN THE NUMBER OF BITS USED NB.

```

    READ(3,*)NB
  
```

C READ IN THE RECEIVER BANDWIDTH W.

```

    READ(3,*)W
  
```

```

    DO 1 I= 1,26
  
```

```

    S= .0
  
```

```

    A(I)= .5*S15ADF(.5*DSQRT(.5*XS(I)),1)
  
```

```

    AA(I)= DEXP(-.0625*XS(I))
  
```

```

    DO 3 J= 1,5
  
```

```

    X= 2.*J+ 1.
  
```

```

    S= S+ (XS(I)**J)*HAM(2*J- 1,DSQRT(XS(I))/(2.*DSQRT(2.D+ 0)))
  
```

```

    .*MOM(J+ 1)/S14AAF(X,1)
  
```

3 CONTINUE

```

    G(I)= AA(I)*S
  
```

PPP(I)= A(I)+ G(I)

PP(I)= (2.\*\* (2.\*NB)- 1.)/(1.+ 4.\*PPP(I)\*(2.\*\* (2.\*NB)- 1.))

TT(I)= (2.\*\* (2.\*NB)- 1.)/(1.+ 4.\*A(I)\*(2.\*\* (2.\*NB)- 1.))

P(I)= 10.\*DLOG10 (ABS (PP(I)))

T(I)= 10.\*DLOG10 (ABS (TT(I)))

1 CONTINUE

WRITE(4,\*)('THESE RESULTS ARE OBTAINED FOR NB EQUAL TO')

WRITE(4,\*)NB

WRITE(4,\*)( 'W EQUAL TO')

WRITE(4,\*)W

WRITE(4,\*)('AND THE INPUT CNR XS EQUAL TO: ')

WRITE(4,26)(XS(I),I= 1,26)

26 FORMAT(10(F5.1,2X))

WRITE(4,\*)(G(I),I= 1,26)

WRITE(4,\*)('THE OUTPUT SNR IN dB IN PRESENCE OF ISI ARE:')

WRITE(4,8)(P(I),I= 1,26)

8 FORMAT(8(F5.2,3X))

STOP

END

C HER(N,X) IS A FUNCTION GIVING THE HERMITE POLYNOMIALS OF  
C ORDER N AND ARGUMENT X.

DOUBLE PRECISION FUNCTION HER(N,X)

DOUBLE PRECISION Y,X

DIMENSION Y(40)

Y(1)= .0

Y(2)= 1.0

DO 4 I= 1,N

Y(I+ 2)= X\*Y(I+ 1)- (I- 1)\*Y(I)

II= I

4 CONTINUE

HER= Y(II+ 2)

RETURN

END

C MOM(N) IS A FUNCTION GIVING THE MOMENT OF ISI OF ORDER N.

C THE ROUTINE S14AAF(N) GIVES THE FACTORIEL OF (N-1).

DOUBLE PRECISION FUNCTION MOM(N)

DIMENSION B(40),C(40),F(40),A(40,40),S(40,40)

COMMON/VAL/W,NB

DOUBLE PRECISION A,B,C,F,S,W,S14AAF

C B(2), B(3), B(4), B(5), B(6) ARE THE B2, B4, B6, B8, B10 BERNOULLI

C NUMBERS.

B(2)= 1./6.

B(3)= 1./30.

B(4)= 1./42.

B(5)= 1./30.

B(6)= 5./66.

F(2)= 1.

DO 2 K= 2,N

S(2\*K,2)= 0.0

DO 3 J= 2,K

A(K,J)= S14AAF(2.\*K- 2.,1)/((S14AAF(2.\*J- 2.,1)\*S14AAF(2.\*(K- J)+ 1.

\*,1)))

C(J)= ((2.\*\* (2.\*J- 2.)- 1.)\*(2.\*\* (2.\*J- 2.)))/(2.\*J- 2.)

S(2\*K,2\*J)= S(2\*K,2\*J- 2)+ ((- 1.)\*\*J)\*F(2\*(K- J)+ 2)\*C(J)\*A(K,J)\*B(J)

.\*DEXP(- .942D0\*(J- 1)\*W/NB)\*((1.- .5\*DEXP(- .471D0\*W/NB))\*\*(2.\*(J- 1)))

./(1.- DEXP(- .942D0\*(J- 1)\*W/NB))

JJ= J

3 CONTINUE

F(2\*K)= S(2\*K,2\*JJ)

KK= K

2 CONTINUE

MOM= F(2\*KK)

RETURN

END